The classified or limited status of this document applies to each page thereof unless otherwise marked. Separate page printouts MUST be marked accordingly.

NASA CR 54817
AGC 8800-51

ANALYSIS AND EXPERIMENTAL VERIFICATION OF AXIAL THRUST ON THE M-1 LIQUID OXYGEN TURBOPUMP

By

J. J. Brunner

Prepared for

National Aeronautics and Space Administration

Contract NAS 3-2555

AEROJET-GENERAL CORPORATION

SACRAMENTO, CALIFORNIA

NASA CR-54817
AGC 8800-51

TECHNOLOGY REPORT

ANALYSIS AND EXPERIMENTAL VERIFICATION OF AXIAL THRUST ON THE M-1 LIQUID OXYGEN TURBOPUMP

Prepared for

NATIONAL AERONAUTICS AND SPACE ADMINISTRATION

April 15, 1966

CONTRACT NAS 3-2555

Prepared by:

AEROJET-GENERAL CORPORATION
LIQUID ROCKET OPERATIONS
SACRAMENTO, CALIFORNIA

AUTHOR: J. J. Brunner

APPROVED: W. E. Campbell
Manager
M-1 Turbopump Project

Technical Management:

NASA LEWIS RESEARCH CENTER
CLEVELAND, OHIO

TECHNICAL MANAGER: M. M. Bailey
K. L. Baskin
C. F. Zalabak

APPROVED: W. F. Dankhoff
M-1 Project Manager

ABSTRACT

Axial thrust characteristics of two oxidizer turbopump assemblies are presented and evaluated over a representative range of speed, flow, and suction pressure. Estimates of thrust changes resulting from impeller backvane modifications and thrust verification tests conducted with a three-eighths size subscale pump are discussed. All tests were conducted with liquid nitrogen as the pumping fluid and either gaseous nitrogen or gas generator (H_2O_2) turbine drive. The turbopump consists of a centrifugal pump directly driven by a single-stage impulse turbine. The shaft is supported in rolling contact, propellant cooled bearings. The 27,000 shp turbopump has a nominal head generating capability of 3400 ft. The 28.5-in. unshrouded impeller produced a maximum thrust of approximately 70,000 lb towards suction. Net thrust was measured using calibrated sleeve-mounted strain gages.

TABLE OF CONTENTS

TABLE OF CONTENTS (Cont.)

LIST OF TABLES

LIST OF FIGURES

LIST OF FIGURES (Cont.)

LIST OF FIGURES (Cont.)

BLANK PAGE

I. SUMMARY

The determination of shaft axial thrust received major emphasis during development testing of the M-1 oxidizer turbopump. Two test series totaling 24 tests were completed using two turbopump buildups. During these tests, thrust was measured and calculated as a function of speed, pump flowrate, pump suction pressure, turbine flowrate, turbine inlet pressure, and turbine pressure ratio.

The effect of speed upon axial thrust was evaluated up to the design speed of 3635 rpm, the flowrate effect from 40% to 160% of design flow at partial speed and 85% to 120% at design speed, as well as the suction pressure effect from 100 psig to 50 psig. Turbine reaction, pressure levels, and flowrates were varied; both gaseous nitrogen (off-design blade/jet speed ratio) and gas generator characteristics were evaluated. Axial thrust up to approximately 70,000 lb occurred toward pump suction.

Pump and turbine thrust were calculated separately by computing the frontside and backside pressure forces of each rotating element through the integration of pressure profiles. A comparison of calculated net thrust values with those measured by the strain gaged thrust measurement sleeves showed typical agreement within 10% for magnitudes in excess of 15,000 lb. Pump thrust at design speed was 26% to 42% higher, depending upon Q/N, than the predicted ideal thrust based upon low speed thrust data and affinity laws. This resulted from a decrease in fluid density caused by inefficiency heating of the fluid on the impeller backside.

Thrust control that affected the general thrust level was achieved for the second test series with a reduction in the length of the impeller backvanes by increasing the inlet diameter. This modification resulted in an increased pump thrust towards suction, which partially counterbalanced the relatively high turbine downstream thrust experienced under the off-design condition encountered with the gaseous nitrogen turbine drive. Estimates of thrust changes resulting from impeller backvane modifications and thrust verification tests conducted with the subscale pump are discussed in this report.

II. INTRODUCTION

All activities described herein were conducted by the Aerojet-General Corp. for the NASA Lewis Research Center, Cleveland, Ohio under Contract NAS 3-2555. The unit tested was the 27,000 horsepower liquid oxygen turbopump of the M-1 rocket engine. The turbopump assembly consisted of a single suction one-stage radial flow pump driven by a one-stage axial flow impulse turbine. Power was transmitted by a single shaft with bearings arranged between the two rotating elements (see Figure 1). Axial thrust was absorbed by a tandem set of two ball bearings through a series of two strain gage thrust measuring sleeves. The power transmission assembly was structurally designed to accommodate thrust loads up to 100,000 lb in either direction at shaft speeds up to 4000 rpm. It was predicted that the bearings would be capable of carrying 65,000 lb in the sharing direction and 35,000 lb in reverse.

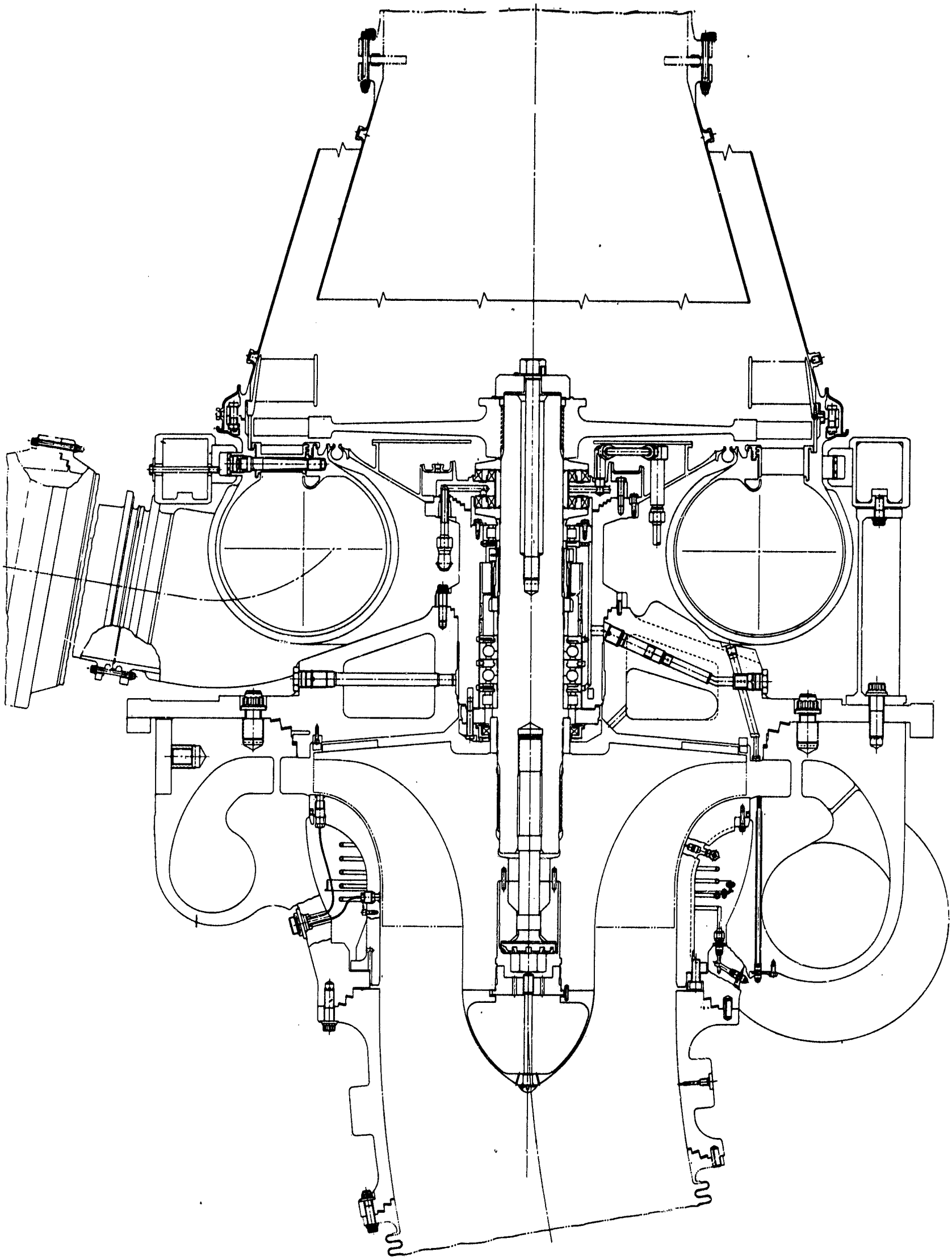

Figure 1

MODEL I OXIDIZER TURBOPUMP ASSEMBLY

Axial thrust was balanced by impeller radial backvanes used in combination with a backvane diffuser. This system was selected based upon performance (pressure profile), relative simplicity, and compliance with available space requirements. The backvane diffuser demonstrated the possibility of raising the hydraulic gradient beyond the capability of conventional backvanes.

The first test series conducted with the initial buildup pumping liquid nitrogen with gaseous nitrogen drive, consisted of 10 tests. Major emphasis was concentrated upon system checkout, demonstration of mechanical integrity, and determination of pump and turbine nominal as well as off-design performance. Test durations averaged 18 sec because of the on-stand fluid tankage limitations. The highest thrust value, 39,000 lb towards the turbine, was measured at the highest speed, 2450 rpm and 80% of nominal pump flowrate.

Following the initial test series, the impeller backvanes were modified for the purpose of decreasing the pressure rise capability of the backvanes, to reduce and possibly reverse thrust, raise the cavity pressure, and thereby avoid vapor formation on the impeller backside at lower pump suction pressures and high operating speed. A new backvane inlet diameter was determined and backvane performance verified with a three-eighths subscale pump.

The second test series with Buildup No. 2, which incorporated the backvane modification, consisted of 14 tests, including five acceleration tests, seven tests conducted with gas generator drive, and two torquemeter checkout tests. Again, the pumping fluid was liquid nitrogen. This test series was conducted for the purpose of determining mechanical integrity and performance characteristics of the turbopump at design speed (3635 rpm) under design and off-design flowrates with gas generator drive. The ability of the turbopump axial thrust to be balanced within the capability of the bearings was demonstrated during these tests.

Results of the first and second test series relating to axial thrust are discussed in this report.

III. TECHNICAL DISCUSSION

A. THRUST BALANCING SYSTEM

1. Objectives

The thrust balancing system, also referred to in this report as the backvane system, must be capable of producing a pressure force that is able to balance the hydraulic load of the impeller frontside and the turbine thrust so that the resulting net thrust can be maintained within the load capacity of the bearings. Thrust balance must be achieved at all operating points within the required flow and speed ranges and over the transients to steady-state operation. Because thrust cannot be accurately predicted (see Section III. C.) the system must be capable of reducing the excessive pressure force of the impeller backside as much as possible. This will enable the desired axial thrust to be achieved through simple component modification, such as trimming of the backvanes.

2. Description

The thrust balancing system (see Figure 2) consisted of 40 radial impeller backvanes and a backvane diffuser. The backvanes were integral with the pump impeller while the backvane diffuser vanes were part of a separate ring, which was attached to the pump backplate. For simplicity, the 31 diffuser vanes were machined straight with a vane inlet angle of 2 degrees (see Figure 3).

The clearance between the impeller backvanes and the backplate was the same as between the impeller and diffuser vanes (i.e., 0.088-in. on Buildup No. 1). Inspection of components after disassembly of Buildup No. 1 revealed a light rub at the tip of the impeller backvanes and between the backvane diffuser and the impeller disc. This rub was caused by rotor system axial vibration. The thrust loads alone were not great enough to cause the rub. As a result, the clearance was increased to 0.150-in. on Buildup No. 2 to avoid further rubbing at higher operating speeds (see Figure 4).

Backvane flow consisted of a mixture of bearing coolant and bypass flow (see Figure 2). The coolant flow was tapped off at the impeller discharge and directed through filters, pressure drop orifice combinations, and venturi meters to the bearings. The bypass flow was taken from the pump housing at the diffuser discharge and directed through external lines containing orifices and flowmeters back to the annular cavity in the backplate where it mixed with the coolant return flow. Flow entered the rear cavity behind the impeller through six 1/2-in. holes.

The backvane flowrate was dependent upon the hydraulic pressure gradient of the backvane system and the combined pressure drops of both the coolant supply and the bypass flow circuits. A bypass flow of 60 gpm at the nominal operating conditions was assumed for maintaining acceptable densities of the fluid through the backvanes. A decrease in fluid density as a result of a rise in fluid temperature increases thrust towards suction. A possible rise in fluid temperature was expected as a result of backvane inefficiency (disc friction) and added bearing heat input. Backvane flow amounted to approximately one-half percent of the pump flow. Thirty-three percent of this backvane flow was coolant flow.

The purpose of the backvane diffuser is to add to the static head generating ability of the backvanes and thereby increase the capability of the backvane system to balance axial thrust (see Figure 5).

3. Hydraulic Performance

In essence, the backvane system was a separate pump with a static discharge head controlled by the discharge pressure of the main pump impeller. The resulting inlet or cavity pressure depended upon the pressure generating ability of the system as well as pump suction pressure.

The backvanes operated at very low flowrates controlled by the fixed orifices in the bypass and coolant supply lines. Under these conditions, the fluid velocity at the backvane discharge was approximately equal to the tangential velocity,

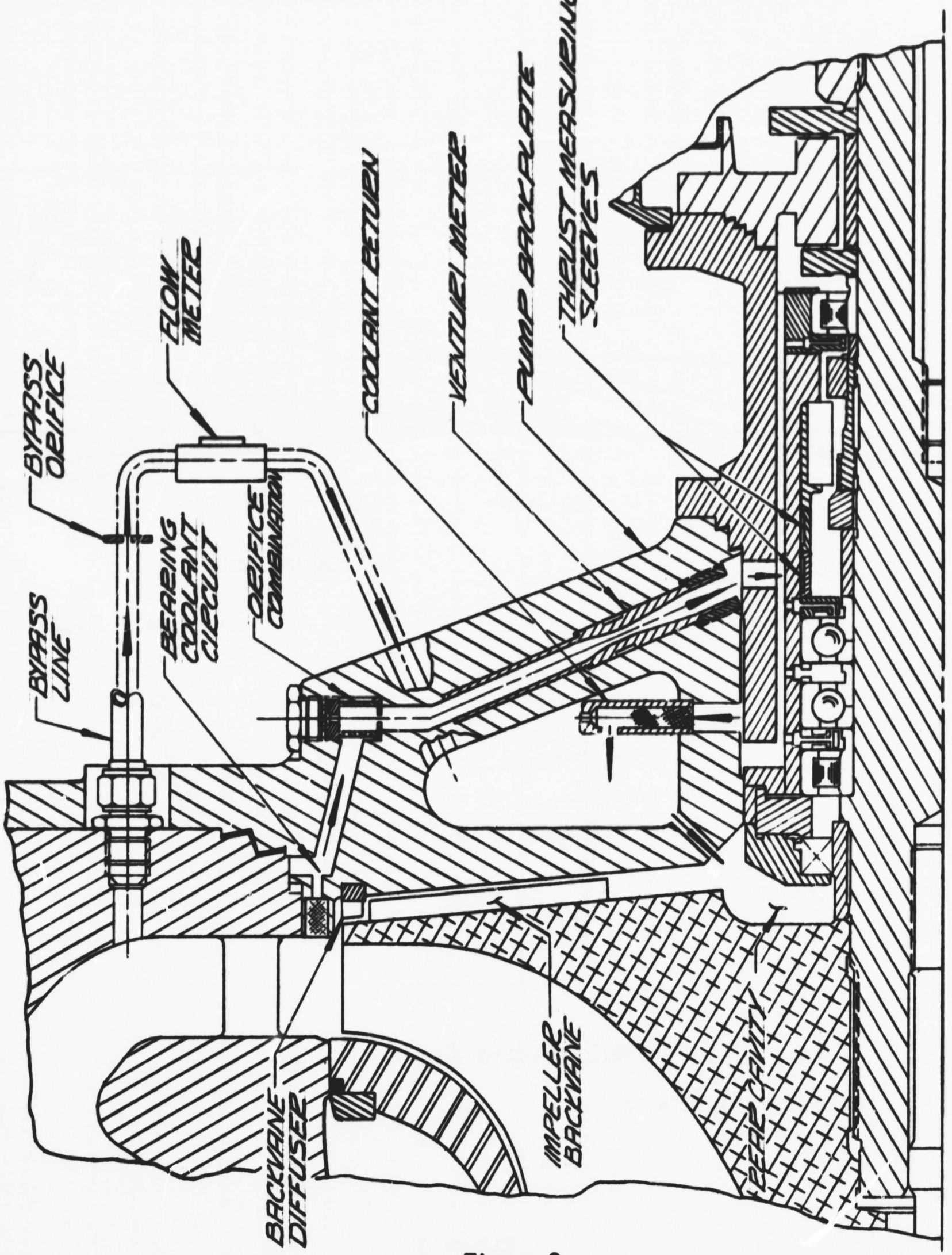

Figure 2

BACKVANE FEED SYSTEM

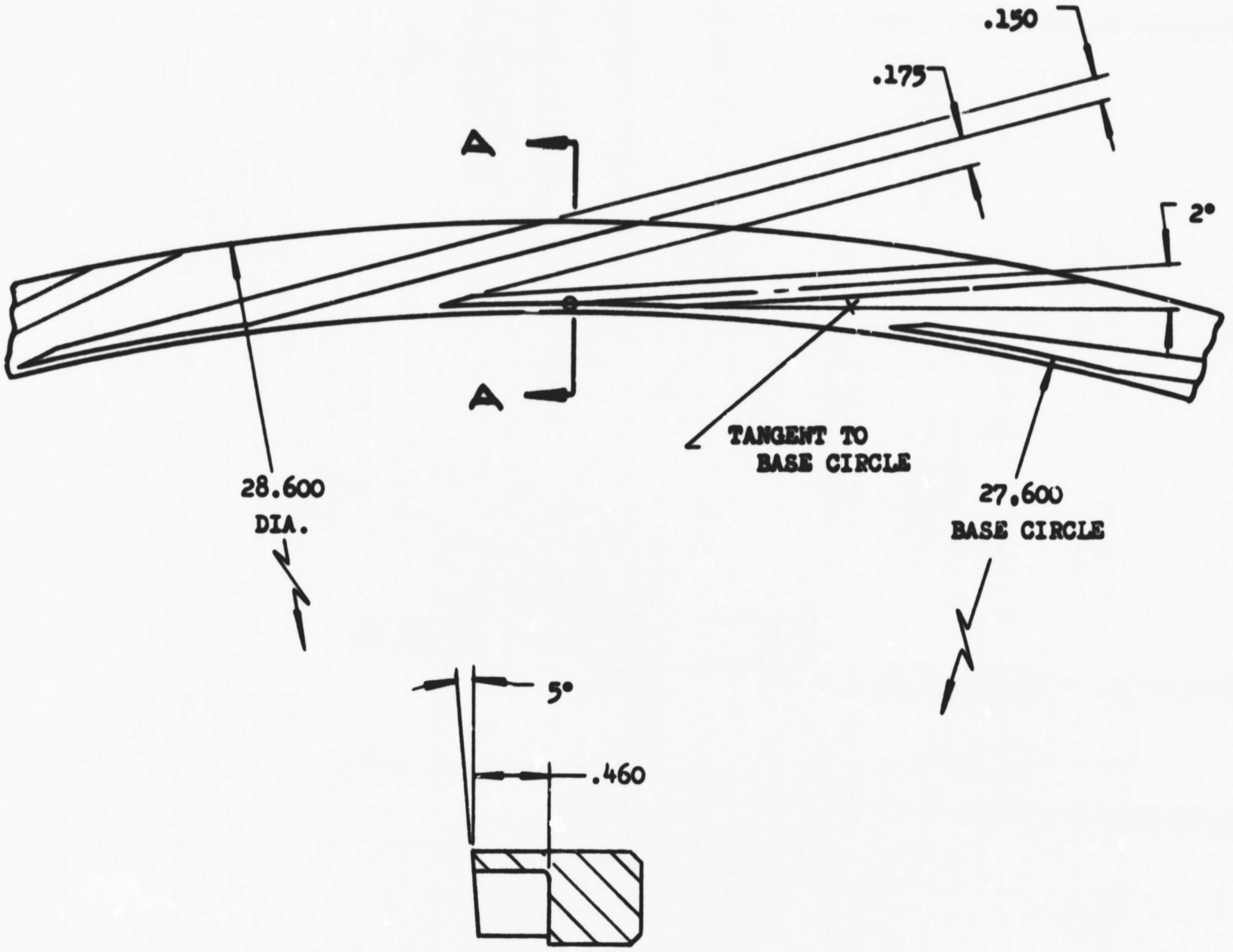

SECTION A-A

NUMBER OF VANES = 31

Figure 3

BACKVANE DIFFUSER

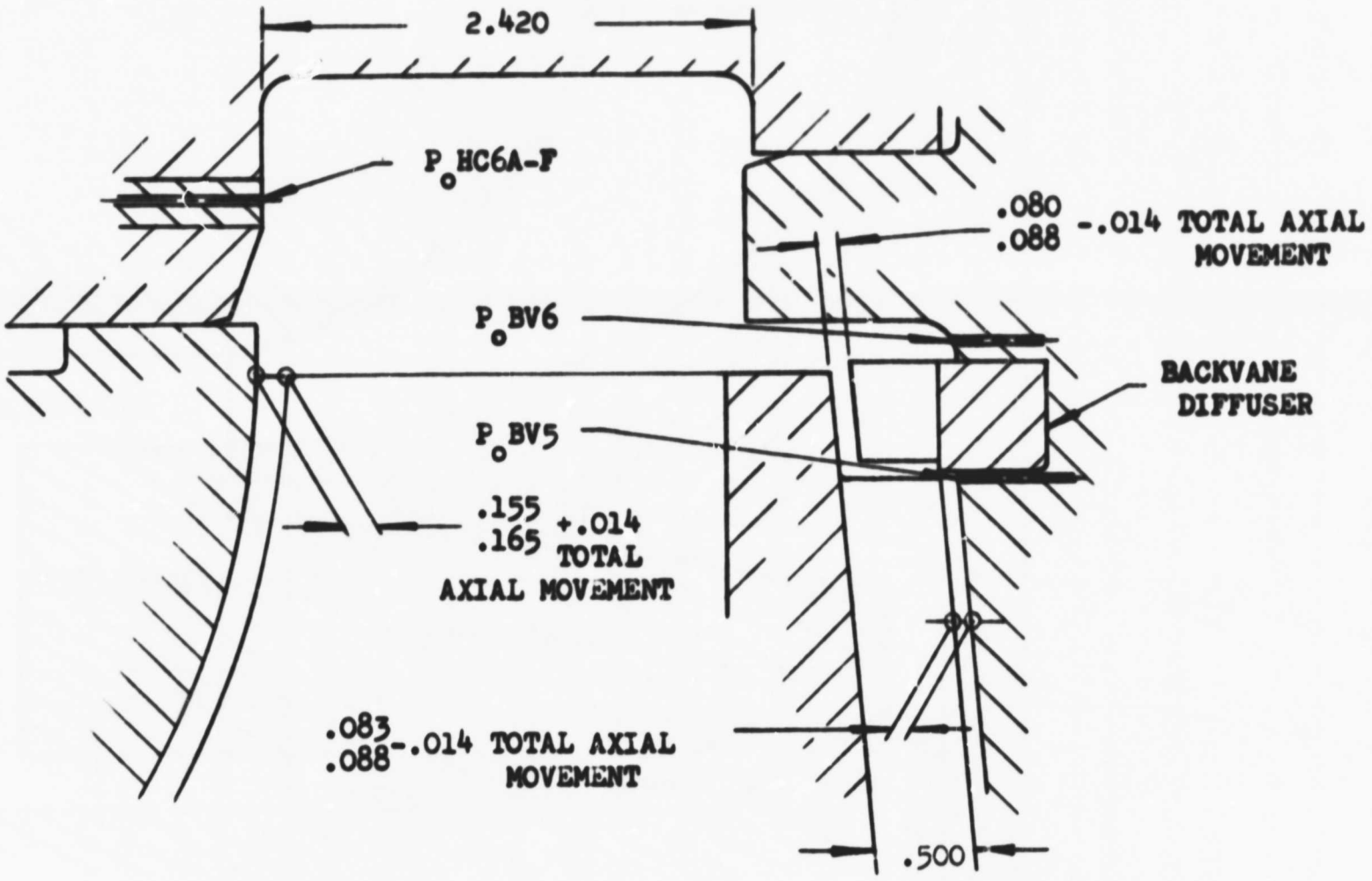

BUILDUP NO. 1

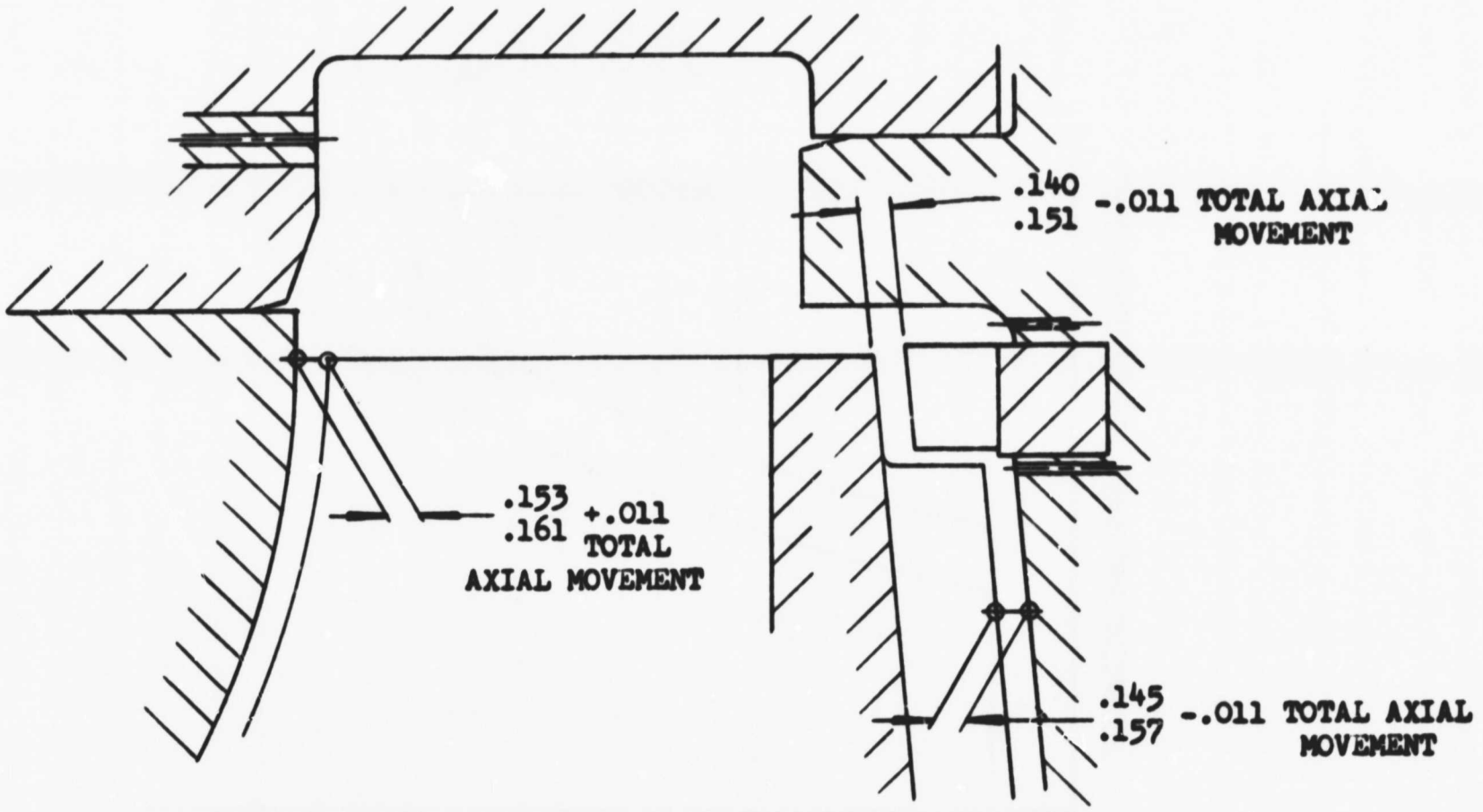

BUILDUP NO. 2

Figure 4

GEOMETRICAL RELATIONSHIP OF
PUMP COMPONENTS

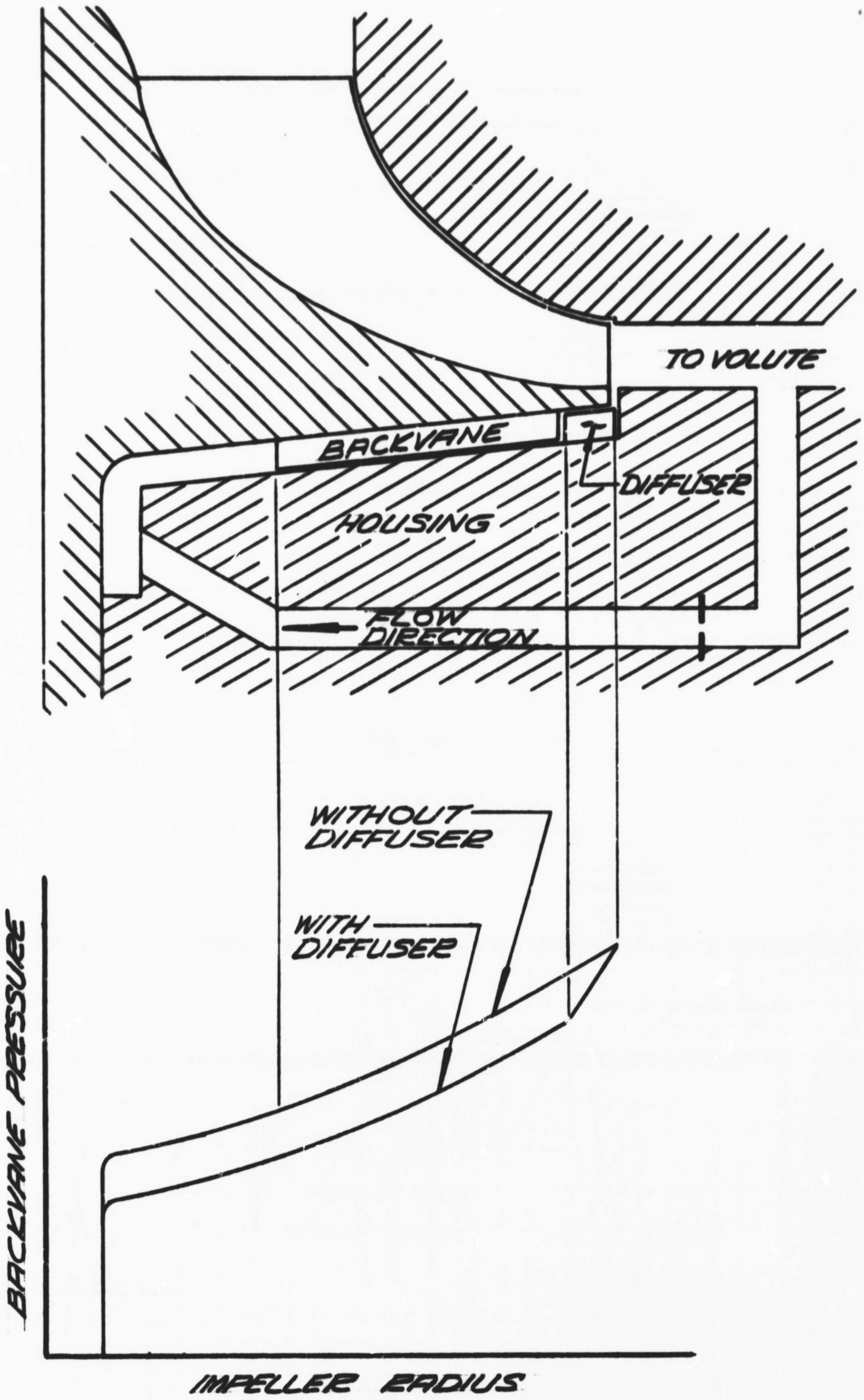

Figure 5

BACKVANE SYSTEM SCHEMATIC

u_{2BV}. The absolute fluid angle calculated was 5 min 18 sec and was constant for all speeds because flow varied linearly with speed as expected. Backvane performance and thrust were insensitive to backvane flow rate over a practical operating range.

A backvane pressure profile for a typical data point, as listed in Table I, is presented on Figure 6. The effect of the backvane diffuser upon the pressure profile is characterized by a distinct increase in slope starting at the diffuser inlet (pressure tap P_{OBV-5}).

The static headrise ceofficients defined as

$$\psi = 20{,}736 \frac{g}{\rho \omega^2} \cdot \frac{P_2 - P_1}{R_2^2 - R_1^2} \qquad \text{Equation (1)}$$

for all backvane pressure profile sections are summarized in Table II.

a. Fluid Density

The data scatter in calculated backvane static coefficients as shown in Figures 7 through 10 was mainly attributed to the temperature effect resulting from the inefficiency heating of the fluid. For reasons of consistency, all static head coefficients were based upon the density of the fluid in the cavity, because no temperatures other than the cavity temperature (TOBV-1), were measured on the backside of the impeller. Agreement could become more likely if head coefficients were calculated from appropriate fluid densities at each backvane station. Thus, even if perfect agreement in head coefficients could be achieved, pressures and thrust would still be affected by the pressure and temperature dependency of the fluid density.

b. Backvane Diffuser Efficiency

The efficiency of the open-type diffuser is rather low because of the high gap losses and the effect of the adjacent rotating disc. Further, at low capacities, the backvane diffuser is believed to operate in a stalled condition. For preliminary thrust estimates, a diffuser efficiency of 0.15 was applied. This value was determined from a similar but longer backvane diffuser tested under the NERVA pump development program.

The efficiency of the backvane diffuser at a typical data point can be verified from the following expression:

$$\eta_{BV} = \frac{288\, g\, \Delta P_{BV}}{\rho (V_{2BV}^2 - V_{4BV}^2)} \qquad \text{Equation (2)}$$

The discharge velocity is calculated by dividing the absolute discharge velocity V_{2BV} by the area ratio of the diffuser. For the typical data point (Table I) η_{BV} was 0.151.

TABLE I (Sheet 1 of 2)

PERFORMANCE DATA OF B/U 2 FOR A TYPICAL OPERATING POINT

Test 1.2-08-EHP-10, Time 10.400 to 10.900 sec

PUMP Pumping Fluid: Liquid Nitrogen

N	=	3652	rpm	
Q	=	18,992	gpm	$\frac{Q}{N} = 5.2$ (Design $\frac{Q}{N} = 5.18$)
Q_{BP}	=	73.9	gpm	(Bypass Flow)
Q_{BC}	=	36.6	gpm	(Coolant Flow)
Q_{BV}	=	110.5	rpm	($Q_{BC} + Q_{BF}$) (Backvane Flow)
P_{OS}	=	103.5	psia	(Suction Pressure)
P_{OD}	=	1173	psia	(Discharge Pressure)
$P_{OHC\ 1}$	=	136.5	psia	(Housing Contour Pressure)
$P_{OHC\ 2}$	=	156	psia	(Housing Contour Pressure)
$P_{OHC\ 3}$	=	255	psia	(Housing Contour Pressure)
$P_{OHC\ 4}$	=	569	psia	(Housing Contour Pressure)
$P_{OHC\ 5}$	=	810	psia	(Housing Contour Pressure)
$P_{OBV\ 1}$	=	193	psia	(Rear Cavity Pressure)
$P_{OBV\ 2}$	=	239	psia	(Backvane Pressure)
$P_{OBV\ 3}$	=	337	psia	(Backvane Pressure)
$P_{OBV\ 4}$	=	507	psia	(Backvane Pressure)
$P_{OBV\ 5}$	=	726	psia	(Backvane Discharge Pressure)
$P_{OBV\ 6}$	=	858	psia	(Backvane Diffuser Discharge Pressure)
T_{OS}	=	-308	°F	$\rho_{OS} = 48.5$ lb/ft^3 (suction)
T_{OD}	=	-299.7	°F	$\rho_{OD} = 48.6$ lb/ft^3 (discharge)

TABLE I (Sheet 2 of 2)

PERFORMANCE DATA OF B/U 2 FOR A TYPICAL OPERATING POINT

Test 1.2-08-EHP-10, Time 10.400 to 10.900 sec

PUMP	Pumping Fluid: Liquid Nitrogen			
$T_{OBV\ 1}$	=	-290.3	°F	$\rho_{BV1} = 45.5\ lb/ft^3$
$P_{OHC\ 6\ A}$	=	785.5	psia	(Circumferential Pressure, Impeller Dicharge)
$P_{OHC\ 6\ B}$	=	813	psia	(Circumferential Pressure, Impeller Discharge)
$P_{OHC\ 6\ C}$	=	814.5	psia	(Circumferential Pressure, Impeller Discharge)
$P_{OHC\ 6\ D}$	=	934.2	psia	(Circumferential Pressure, Impeller Discharge)
$P_{OHC\ 6\ E}$	=	827.7	psia	(Circumferential Pressure, Impeller Discharge)
$P_{OHC\ 6\ F}$	=	771.5	psia	(Circumferential Pressure, Impeller Discharge)
TURBINE	Drive Gas: Hydrogen-Oxygen			
$T_{OT\ 1}$	=	790	°F	(Inlet Temperature)
P_{GOTD}	=	65.7	psia	(Pressure, Rotor Disc, Upstream Side)
P_{TRET}	=	86.8	psia	(Pressure, Rotor Exit, Tip)
P_{TREH}	=	67.2	psia	(Pressure, Rotor Exit, Hub)
P_{GTDD-A}	=	73.2	psia	(Rake Pressure, Rotor Disc, Downstream Side)
P_{GTDD-B}	=	72.0	psia	(Rake Pressure, Rotor Disc, Downstream Side)
P_{GTDD-C}	=	69.1	psia	(Rake Pressure, Rotor Disc, Downstream Side)

TABLE II

STATIC HEADRISE COEFFICIENT Ψ AT VARIOUS BACKVANE STATIONS**

Pump B/U 2, Second Test Series

ϕ'_{BV} = 0.0024 to 0.0028

Density* (lb/ft^3)	Speed (rpm)	Ψ POBV 2-1 (Vaneless)	Ψ POBV 3-2 (Vaneless)	Ψ POBV 4-3 (Backvanes)	Ψ POBV 5-4 (Backvanes)	Ψ POBV 6-5 (Diffuser)
47.2	2061	0.115	0.245	0.441	0.443	0.657
47.0	2838	0.125	0.281	0.414	0.450	0.728
48.3	2080	0.1045	0.2565	0.443	0.465	0.674
47.5	3258	0.155	0.2875	0.410	0.462	0.703
46.1	2100	0.102	0 256	0.452	0.464	0.662
45.2	3650	0.152	0.290	0.416	0.444	0.682

* Based upon temperature measured in rear cavity.
** Figure 13 shows pressure tap locations for Stations 1 through 6.

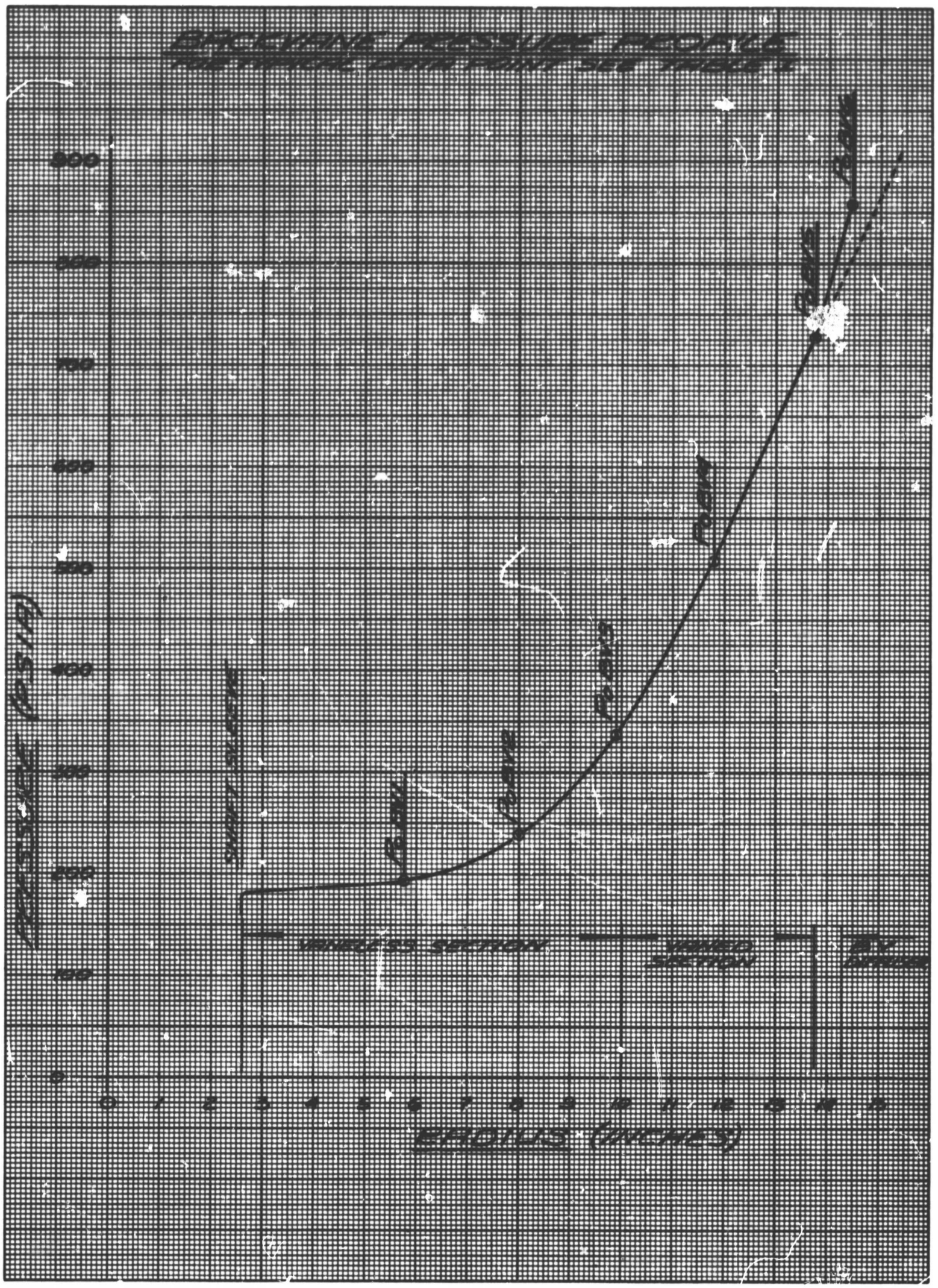

Figure 6

BACKVANE PRESSURE PROFILE

PUMP B/U #1, FLUID LN_2

TEST SERIES 6.0-04-EHP

SYMB.	TEST NO.	SPEED (RPM)
△	001	2303
△	001	1853
□	002	2086
○	003	2066
◇	004	2105
▷	005	2100
⬡	006	1044
⬡	006	2110
◁	007	1508
×	007	1514
+	007	1510
⊠	008	2096
⊕	009	2440
⊗	009	2332
●	010	2431

$\phi'_{BV} = .0483\ Q/N$

(NO BLOCKAGE
.095 NOM CLEARANCE)

$$\psi_{STATIC} = \frac{3 \times 10^5\ \Delta P}{S_{TOBV1}\ N^2}$$

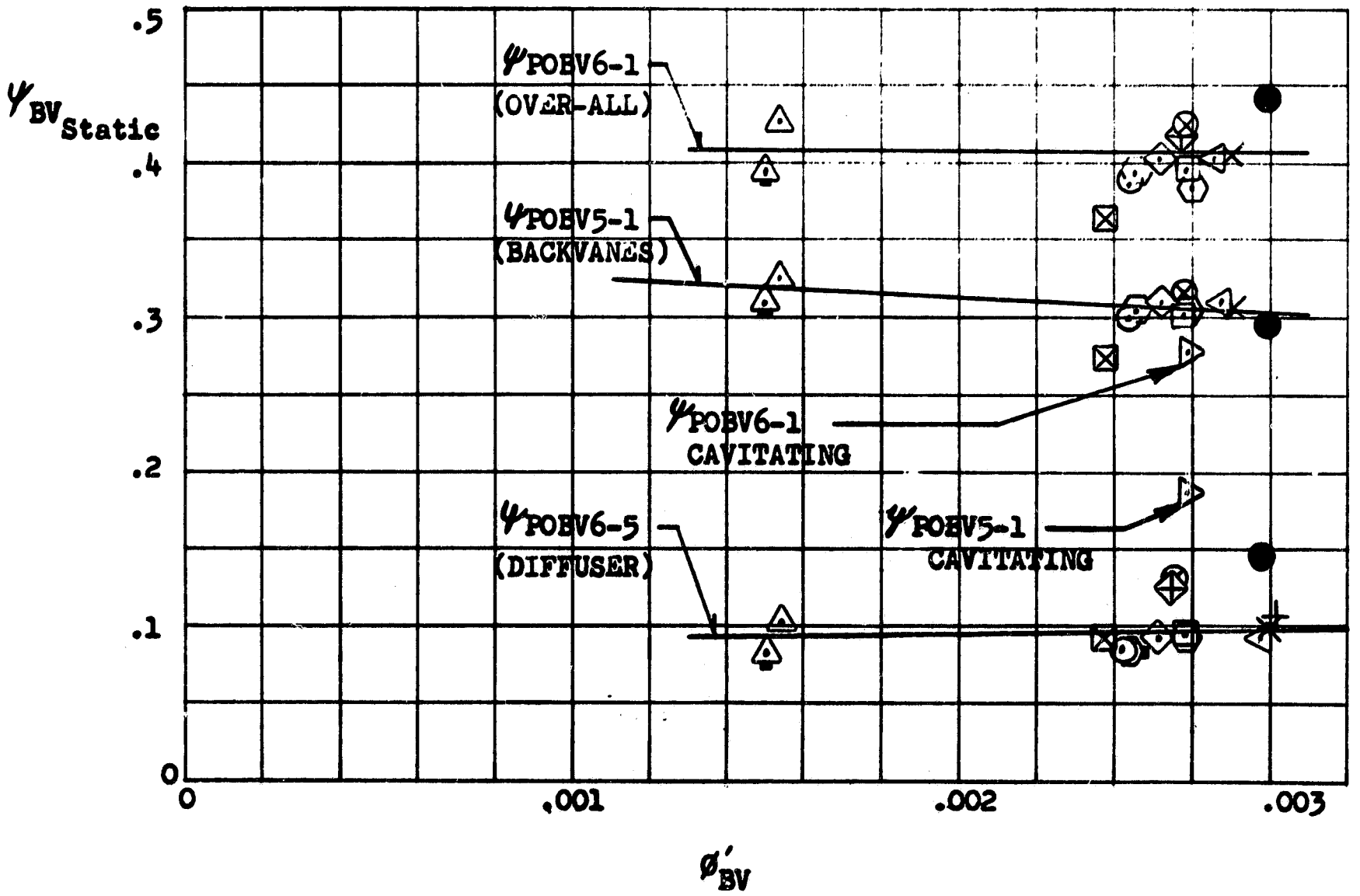

Figure 7

M-1 OTPA PERFORMANCE OF MODEL I PUMP BACKVANE STATIC HEAD COEFFICIENT VS BACKVANE FLOW COEFFICIENT, B/U 1

ϕ'_{BV} = .0015 to .0028

$\psi_{Static} = 3 \times 10^5 \frac{\Delta P}{\rho N^2}$

Pumping Fluid LN_2

R_2 = 14.25 In.

TEST SERIES 6.0-04-EHP

SYMB.	TEST NO.	SPEED (RPM)	TIME (SEC.)
△	001	2303	18.003
△	001	1853	12.918
□	002	2086	21.149
○	003	2066	17.062
◇	004	2105	15.002
▷	005	2100	12.038
⬡	006	1044	7.005
⬡	006	2110	16.521

SYMB.	TEST NO.	SPEED (RPM)	TIME (SEC.)
◁	007	1508	11.105
×	007	1514	20.223
+	007	1510	28.2-33.2
□	008	2096	12.22-17.0
◇	009	2440	7.088
○	0009	2332	11.027
●	0010	2431	11.41-16.41

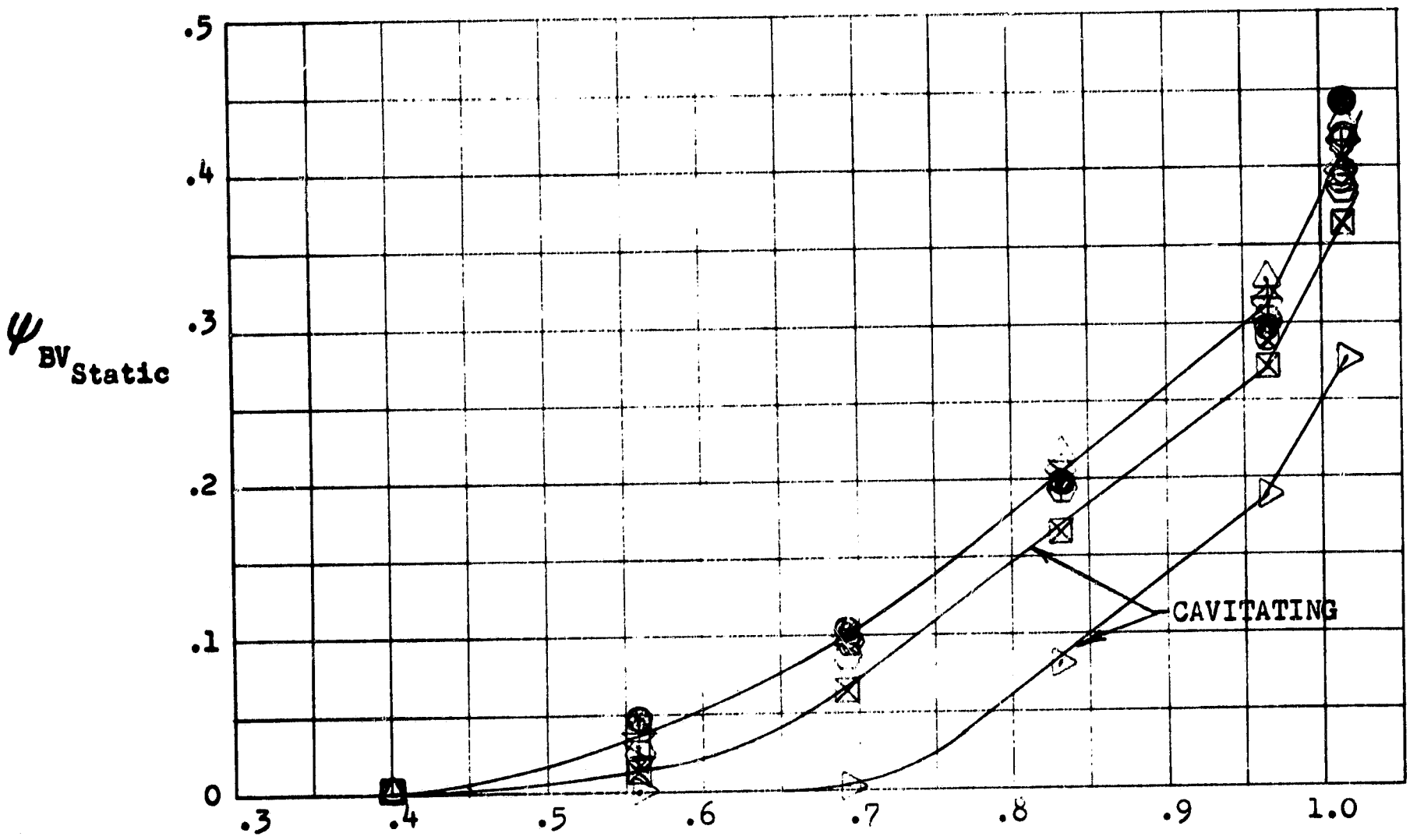

Figure 8

M-1 OTPA PERFORMANCE OF MODEL I PUMP BACKVANE STATIC HEAD COEFFICIENT VS RADIUS RATIO, BUILDUP NO. 1

PUMP B/U #2, FLUID LN_2

TEST SERIES 1.2-08-EHP

SYMB.	TEST NO.	SPEED (RPM)
⌂	001	2098
◇	002	2085
⬯	003	2061
◇	004	2098
⌂	005	2384
◺	006A	2061
◺	006B	2838
◺	007A	2062
◺	007B	3173
⬭	008A	2090
◇	008B	2918

SYMB.	TEST NO.	SPEED (RPM)
◆	009A	2080
◆	009B	3298
D	010A	2103
D	010B	3652
◇	011	2109
◆	012A	2101
◆	012B	2103
◆	012C	2100
U	013A	2100
U	013B	3577
○	014B	3697

$\phi'_{BV} = .0483\ Q/N$

(NO BLOCKAGE .095 NOM CLEARANCE)

$\psi_{STATIC} = \frac{3 \times 10^5\ \Delta P}{P_{TOBV1}{}^{N2}}$

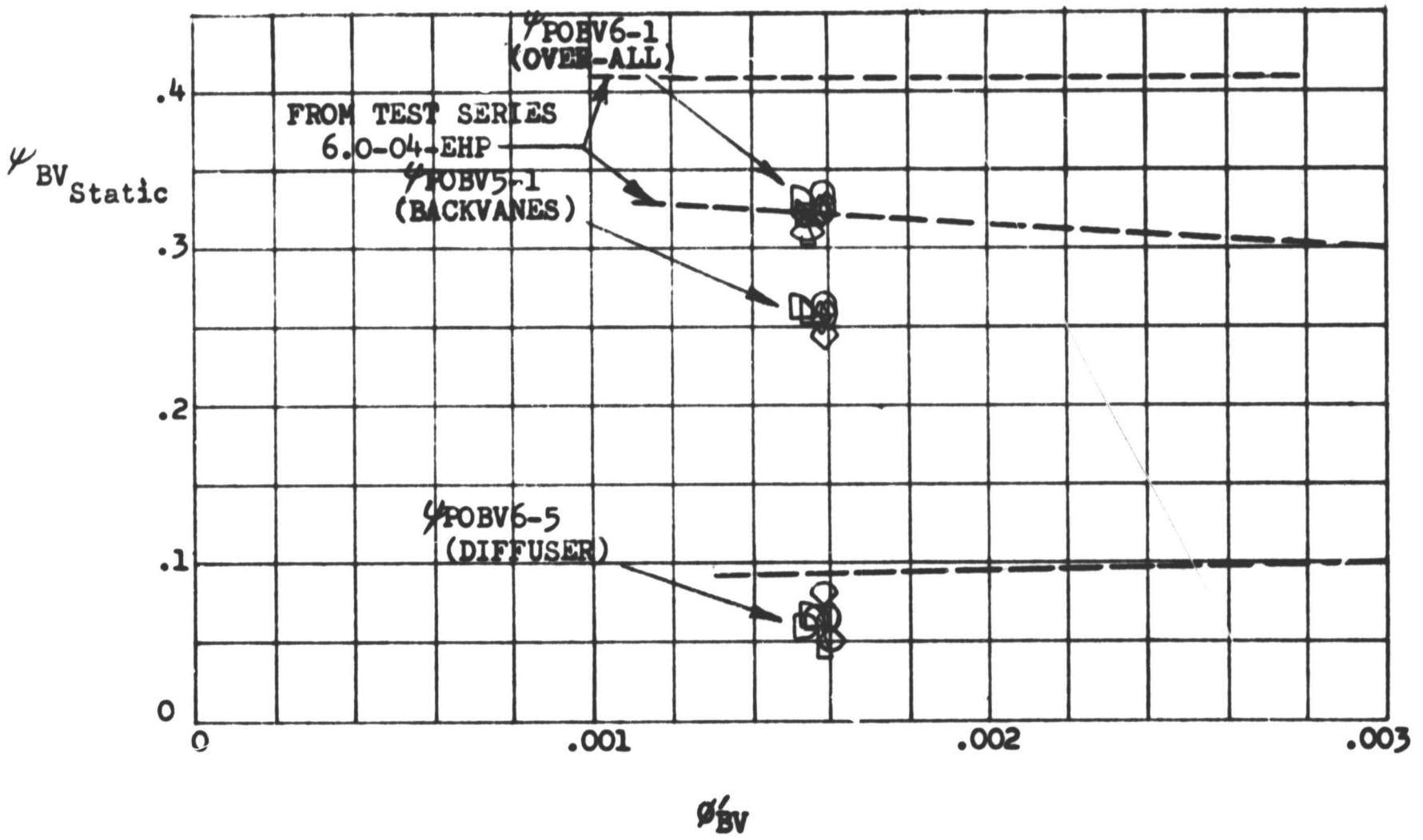

Figure 9

M-1 OTPA PERFORMANCE OF MODEL I PUMP BACKVANE STATIC HEAD COEFFICIENT VS BACKVANE FLOW COEFFICIENT, B/U 2

$\psi_{Static} = 3 \times 10^5 \frac{\Delta P}{\gamma N^2}$ Pumping Fluid LN_2

$\phi'_{BV} = .0015$ to $.0016$ $R_2 = 14.25$ In.

TEST SERIES 1.2-08-EHP

SYMB.	TEST NO.	SPEED (RPM)	SYMB.	TEST NO.	SPEED (RPM)
	001	2098		009A	2080
	002	2085		009B	3258
	003	2062		010A	2103
	004	2098		010B	3652
	005	2384		011	2109
	006A	2061		012A	2101
	006B	2838		012B	2103
	007A	2062		012C	2100
	007B	3173		013A	2100
	008A	2090		013B	3577
	008B	2918		014B	3697

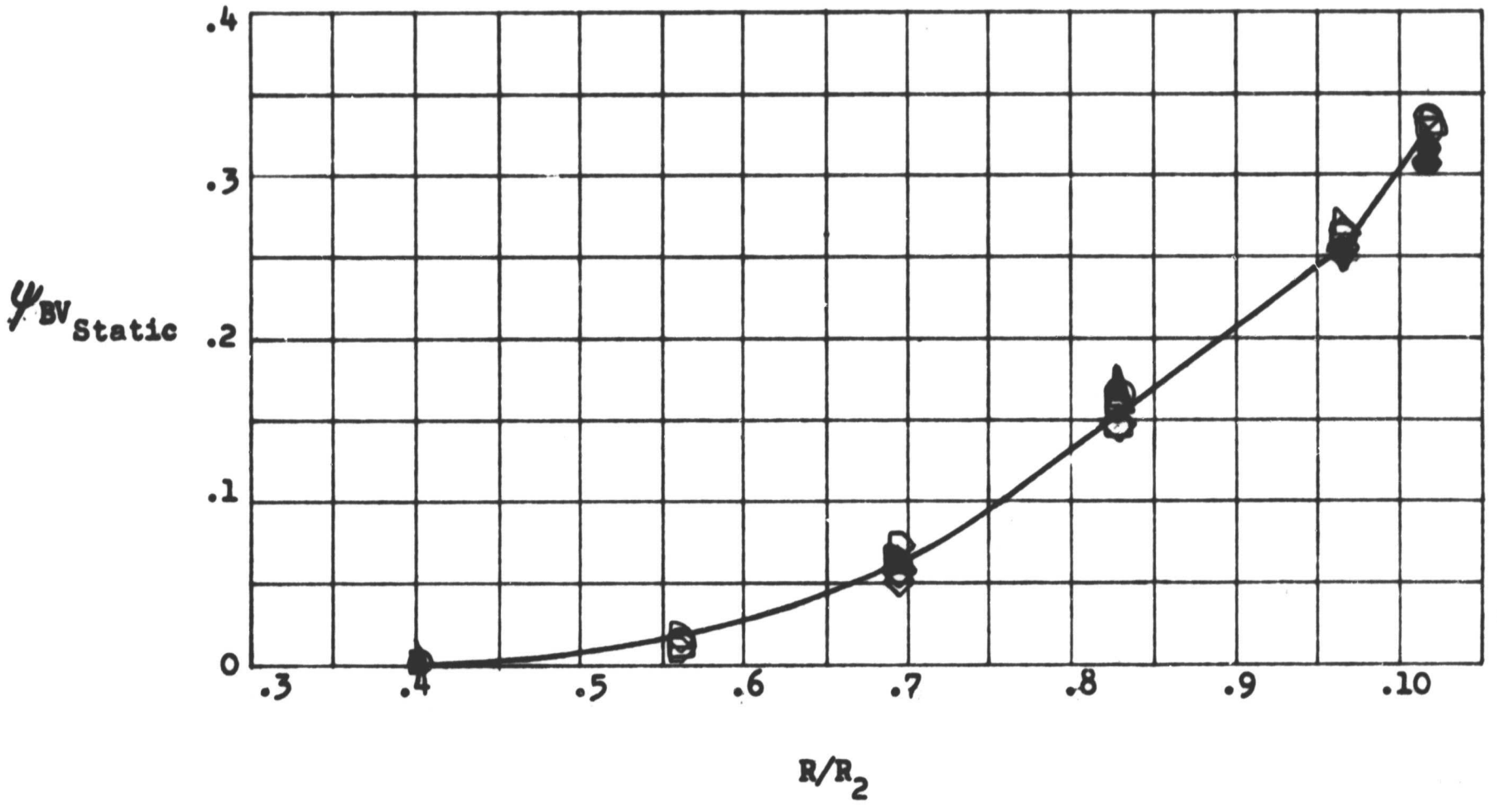

Figure 10

M-1 OTPA PERFORMANCE OF MODEL I PUMP BACKVANE STATIC HEAD COEFFICIENT VS RADIUS RATIO, BUILDUP NO. 2

Higher efficiencies of 0.21 to 0.23 were obtained with Buildup No. 1 operating with smaller vane-to-disc clearances. Other effects of blade clearance upon diffuser performance are discussed under gap sensitivity.

Efficiency alone is not a decisive criterion for selecting a backvane diffuser. The short diffuser of the oxidizer turbopump assembly was more effective than the relatively larger diffuser of the NERVA pump because it produced a comparatively higher yield in pressure per inch of radius (i.e., a higher static headrise coefficient Ψ). On the NERVA pump, the backvanes had to be appreciably shortened to accommodate the long diffuser and as a result, the anticipated total pressure gradient could not be achieved.

A useful performance parameter applicable for evaluation of backvane performance is the static head coefficient based upon rear cavity pressure P_{oBV-1} and the discharge diameter D_2 of the main pump impeller.

$$\psi_{BV} = \frac{H_{St,BV}}{u_2^2/g} = K \frac{\Delta P_{BV}}{\rho_{BV} N^2} \qquad \text{Equation (3)}$$

Where K (3×10^5) is an appropriate geometrical constant. This coefficient is plotted in Figures 7 through 10 to represent pressure rise across various sections of the backvanes.

c. Flow Sensitivity

Flow sensitivity of the backvane system is represented in Figures 7 and 9 for the first and second test series in terms of static head coefficients as a function of backvane flow coefficient ϕ_{BV}'. A grouping of data points at two different flow coefficients in Figure 7 indicates the change in feed-line orifices after the first test. Flow sensitivity was better demonstrated by scale pump tests[1] where backvane flowrates were varied from shut-off to magnitudes of up to ten times the nominal rate. A very minor decrease in head coefficient across the impeller backvanes with increasing backvane flow was offset by a small gain in pressure rise across the backvane diffuser. In summary, the backvane system was not flow sensitive within the test flow range indicated by the flow coefficients ϕ_{BV}' of 0.001 and 0.003.

d. Gap Sensitivity

Gap sensitivity of the impeller backvanes was investigated by comparing the static headrise coefficient, Equation (1), for the two different clearance/vane height ratios of 0.1825 in. for Buildup No. 1 and 0.289 in. for

---

(1) M-1 Oxidizer Scale Pump Performance with Initial and Interim Design Impellers, Aerojet-General Report No. TRP 0047, 15 April 1966.

Buildup No. 2. The difference of approximately 3% to 4% between the two groups of data was ascribed to an inaccurate estimate of cavity temperature, the measurements of which were considered invalid because of a defective thermocouple on Buildup No. 1.

A similar comparison was performed with the scale pump, which operated with clearance/vane height ratios of 0.169 and 0.243. The tests revealed no change in performance because of the difference in backvane clearance.

Performance of the backvane diffuser of Buildup No. 2 (see Figures 9 and 10) was approximately 32% below that of Buildup No. 1. Increased stator vane-to-disc clearance is the only known cause of this deficiency. The clearance/vane height ratio for the diffuser changed from 0.200 on Buildup No. 1 to 0.360 on Buildup No. 2. Based upon subscale and full size tests, it is believed that performance of an open backvane diffuser becomes significantly flow sensitive at clearance/vane height ratios in excess of 0.24.

B. THRUST MEASUREMENT

Net unbalanced axial thrust load is first resisted in the power transmission by two tandem ball bearings mounted as shown in Figure 2. The load is then transmitted from the bearing outer races to the housing through a series of spacers and coolant supply rings. The thrust transmitter (or load cell, which consists of a thin wall cylindrical Inconel spacer with eight strain gages bonded to the outer diameter, arranged in a self-temperature-compensating Wheatstone bridge, is incorporated into this spacer system (see Figures 2 and 11). The results of laboratory calibration tests performed on the transmitter showed that its output varied linearly with the load and that bending loads and temperature changes had little effect upon the axial loads. Total calibration data scatter was found to be approximately $\pm$ 4% (for all effects, including supply variations).

Because the thrust transmitter is basically a compression load cell which must sense load changes in both directions during turbopump operation, it was necessary to preload the transmitter into compression. The power transmission was structurally designed to accomodate thrust loads up to 100,000 lb in either direction. The preload was obtained by first tightening the retainer bolts to 24,600 lb load at ambient temperature and allowing differential thermal contractions to increase the load to 75,000 lb. Typical calibration curves obtained with the power transmission at ambient and cryogenic temperatures are shown in Figure 12. The ambient temperature calibration retains the linear properties demonstrated during laboratory calibration, but the calibration obtained at -320°F is nonlinear and exhibits considerable hysteresis. Apparently, the nonlinear properties of the cryogenic calibration are caused by radial interference or binding of the thrust transmitters, spacers, and coolant supply rings within the transmission housing.

Therefore, the calibration data available was not very useful for establishing safe malfunction shutdown limits because it was not possible to determine which side of the hysteresis loop would be active prior to the test. There is also some doubt as to whether the mechanically-induced nonlinear properties are present

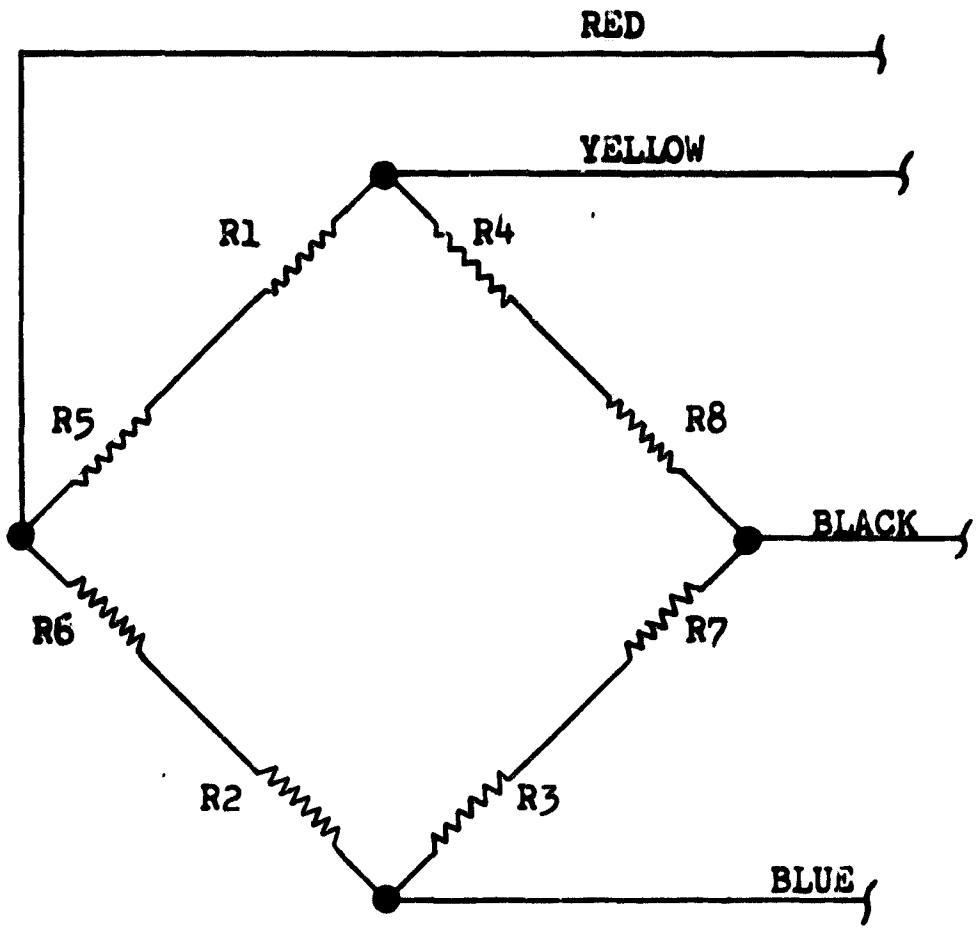

WIRING SCHEMATIC

R1 to R8 Are 260 Ω Strain Gages Bonded to Outside Diameter of Thrust Ring

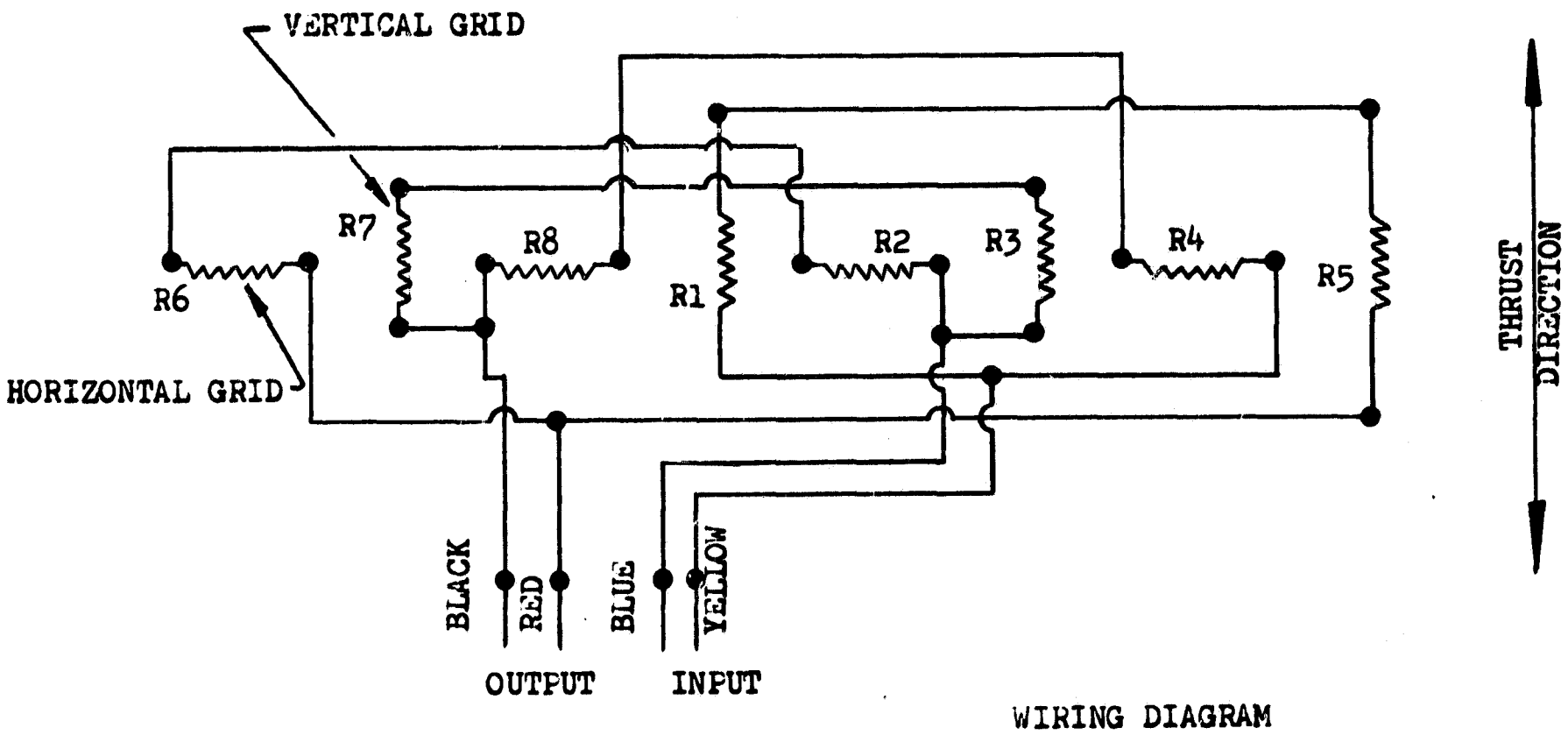

WIRING DIAGRAM

THRUST TRANSMITTER

Figure 11

THRUST TRANSMITTER, STRAIN GAGE
WHEATSTONE BRIDGE CIRCUIT

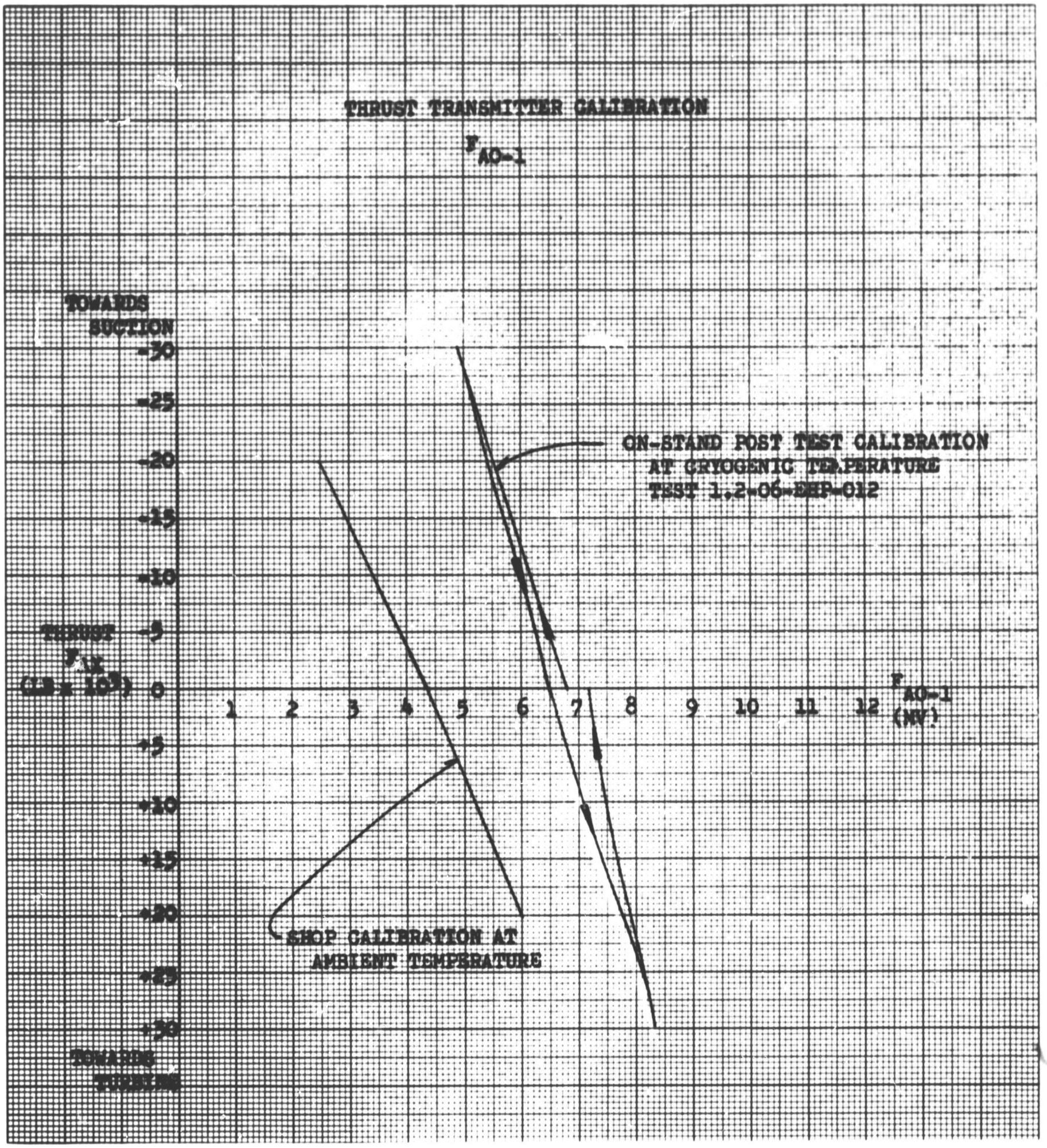

Figure 12

THRUST TRANSMITTER CALIBRATION

during turbopump operation when high energy vibrations are available to reduce the apparent coefficients of friction in the system. Knowledge of the post-test no-load transmitter output and the shape of the calibration curve allowed construction of an accurate calibration curve for each test and the measured values of thrust were determined upon that basis.

C. THRUST CALCULATION

1. Pump Thrust

The net axial pump thrust is equal to the difference between the total integrated frontside pressure force and the total backside force. The force resulting from the change in momentum of the flow passing through the impeller eye is often neglected because of its relatively minor effect upon the net thrust. The momentum force acts away from suction and if considered in calculations it must be added to the pressure load of the frontside.

The momentum force can be expressed as follows:

$$F_{Mt} = \frac{\dot{w}}{g} V_{m,1} \qquad \text{Equation (4)}$$

At the typical data point presented in Table I F_{Mt} is 1680 lb. This amounts to 2.7% of the thrust calculated by pressure integration.

During the first test series, pump thrust was determined by graphical integration of pressure profiles. The products of pressure and radius for each pressure tap location (see Figure 13) were plotted versus radius and the points for the frontside and backside were fitted with a smooth curve as shown in Figure 14. The shaded differential area of the two profiles was then determined with a planimeter and the thrust was calculated by applying the proper scale factor to convert square inches into pounds.

In equation form

$$F_{AX,pump} = 2\pi \left[\int_{R_{SH}}^{R_2} P_{BV}(r)\ r\ dr - \int_{o}^{R_2} P_{HC}(r)\ r\ dr \right]$$

(Thrust towards suction is considered positive.)

Because speed levels were increased during later tests and thrust values approached appreciable magnitudes, the need for a more rapid method of thrust computations became necessary for post-test evaluation and/or making quick decisions prior to retesting. The method devised is based upon straight line point-to-point pressure profiles. Frontside and backside forces were determined by numerical integration of the area elements. The procedure is set up in tabulated form and presented in Table III.

$$P_{BV}(r)\ r\ dr \quad ; \quad P_{HC}(r)\ r\ dr$$

TABLE III (Sheet 1 of 2)

PUMP THRUST CALCULATION BY NUMERICAL INTEGRATION OF STRAIGHT LINE PRESSURE PROFILES

INPUT DATA

Parameter	Units	Test No. 9A	Test No. 9C	Test No. 10B
Time	sec	4.43	~ 8,500	10.400 10.900
POS 6	psia	111.7	102.0	103.5
POHC 1	psia	110.0	106.6	136.5
POHC 2	psia	118.0	132.5	156.6
POHC 3	psia	150.5	198.5	255.5
POHC 4	psia	261.0	465.7	569.0
POHC 5	psia	343.4	675.0	810.0
POBV 1	psia	125.1	154.5	193.0
POBV 2	psia	136.0	190.2	239.7
POBV 3	psia	166.0	270.0	337.3
POBV 4	psia	228.7	407.0	507.4
POBV 5	psia	308.3	596.0	726.3
POBV 6	psia	353.4	708.5	858.0
RPF 0 = 9.75 x POS 6	lb/in.	1090	994	1010
RPF 1 = 9.75 x POHC 1	lb/in.	1072	1040	1330
RPF 2 = 10.21 x POHC 2	lb/in.	1210	1353	1599
RPF 3 = 11.04 x POHC 3	lb/in.	1665	2190	2820
RPF 4 = 12.46 x POHC 4	lb/in.	3255	5800	7090
RPF 5 = 14.25 x POHC 5	lb/in.	4890	9630	11530
RPB 0 = 2.5 x POBV 1	lb/in.	312.5	387	483
RPB 1 = 5.75 x POBV 1	lb/in.	720.0	890	1100
RPB 2 = 8 x POBV 2	lb/in.	1089	1520	1915
RPB 3 = 9.9 x POBV 3	lb/in.	1643	2670	3340
RPB 4 = 11.8 x POBV 4	lb/in.	2700	4800	5980
RPB 5 = 13.75 x POBV 5	lb/in.	4240	8200	10000
RPB 6 = 14.42 x POBV 6	lb/in.	5090	10200	12400

TABLE III (Sheet 2 of 2)

PUMP THRUST CALCULATION BY NUMERICAL INTEGRATION
OF STRAIGHT LINE PRESSURE PROFILES

PROCEDURE

Equation	Test No.	9A	9C	10B
	Time	4.43	~ 8.500	10.400 10.900
FRONTSIDE FORCE, FF				
1. 4.875 RPF 0		5320	4850	4920
2. 0.23 (RPF 1 + RPF 2)		526	550	673
3. 0.415 (RPF 2 + RPF 3)		1193	1470	1830
4. 0.71 (RPF 3 + RPF 4)		3500	5660	7040
5. 0.895 (RPF 4 + RPF 5)		7280	13800	16680
6. Σ (1 to 5)		17819	26330	31143
7. FF = $2\pi\Sigma$(1 to 5) (lb)		112000	165500	195800
BACKSIDE FORCE, FB				
8. 1.625 (RPB 0 + RPB 1)		1680	2075	2570
9. 1.125 (RPB 1 + RPB 2)		2035	2710	3390
10. 0.95 (RPB 2 + RPB 3)		2590	3980	5000
11. 0.95 (RPB 3 + RPB 4)		4125	7100	8850
12. 0.975 (RPB 4 + RPB 5)		6760	12690	15580
13. 0.25 [0.746 (RPB 6 - RPB 5) + 2RPB 5]		2275	4470	5290
14. Σ (8 to 13)		19,465	33025	40680
15. FB = $2\pi\Sigma$(8 to 13) (lb)		122200	207500	255500
16. F_{AX} = FB - FF (lb)		10200	42000	59700

SYMBOL	R IN.
PoBV1	5.75
PoBV2	8.00
PoBV3	9.90
PoBV4	11.80
PoBV5	13.75
PoBV6	14.42

SYMBOL	R IN.
PoCH1	9.75
PoCH2	10.21
PoCH3	11.04
PoCH4	12.46
PoCH5	14.25
PoCH6	15.12

BACKVANE INLET RADIUS : R_{BV_4} = 8.00 IN FOR B/U #1
R_{BV_4} = 10.00 IN FOR B/U #2

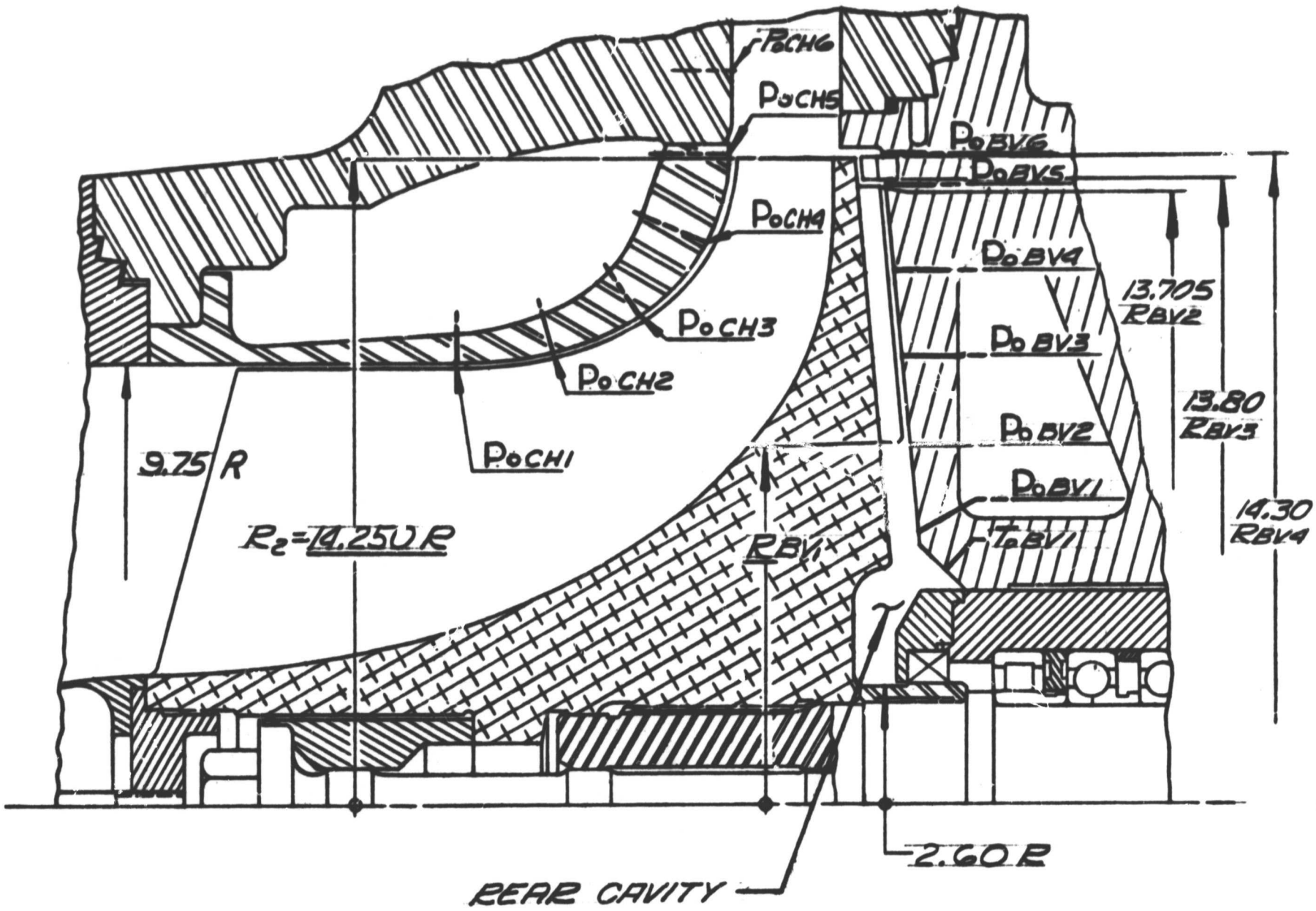

Figure 13

STATIC PRESSURE TAP LOCATION

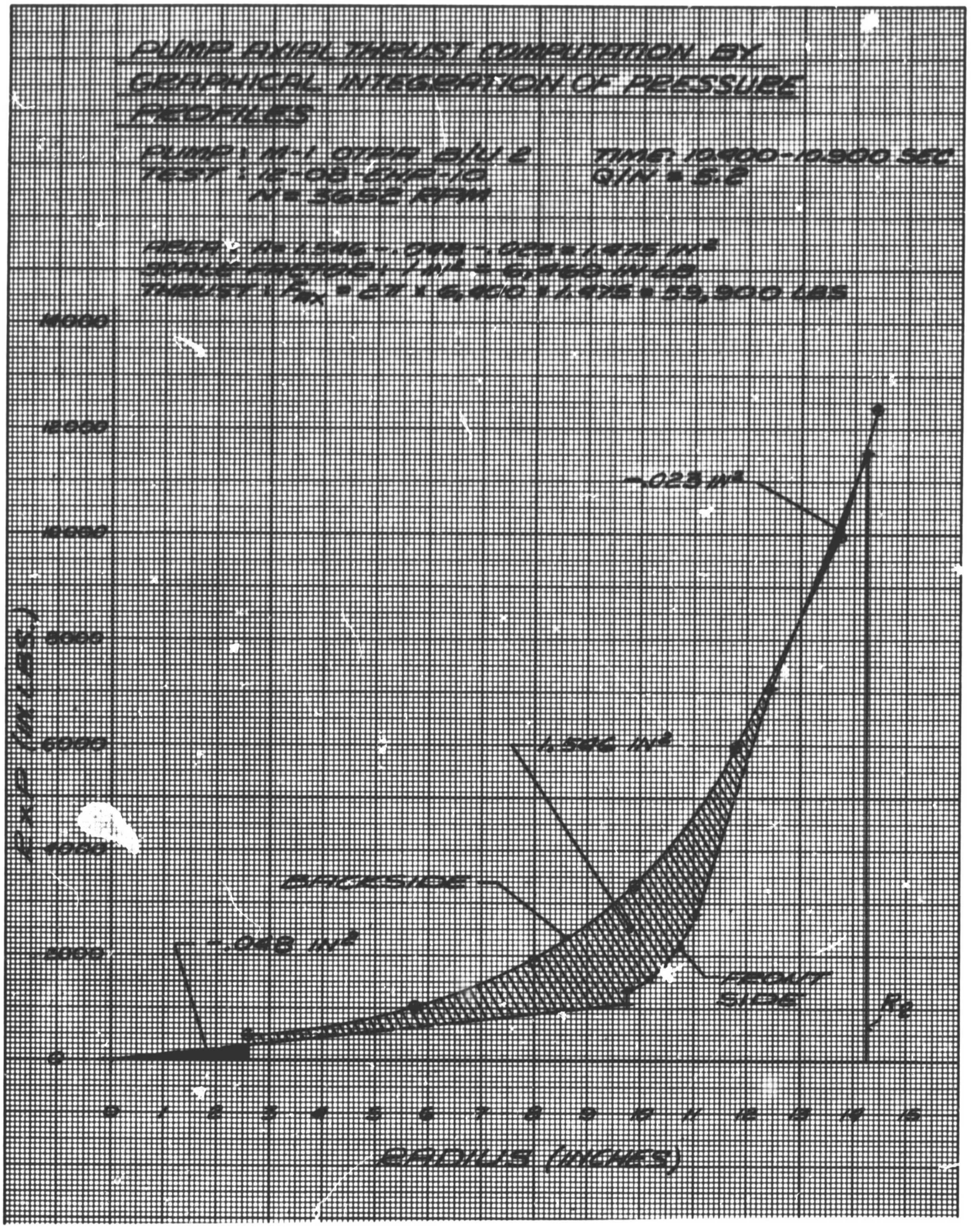

Figure 14

PUMP AXIAL THRUST COMPUTATION BY GRAPHICAL INTEGRATION OF PRESSURE PROFILES

A third and fourth method were derived from the above method to determine the effect of smoothed pressure profiles on axial thrust. Because curve fitting of the inflected frontside pressure profile by analytical methods is rather complex, the pressure force of the impeller frontside was calculated from straight line pressure profiles according to the second method. In the third method, the backside pressure force was calculated from a curve-fitted profile consisting of two parabolic sections for the vaned and vaneless sections. In the fourth method, the backvane pressure profile was based upon parabolic sections representing the theoretical hydraulic gradient between the measured pressures. All thrust data plotted was obtained from the computer program for data reduction. The computer method used for computation of axial thrust was based upon curve fitted frontside and backside pressure profiles. The procedures and results of the various methods are summarized in Table IV.

The lower magnitudes obtained with the third and fourth methods reflect the combination of curve fitted backside and straight line frontside pressure profiles. Results of the first, second, and fifth methods fall within 2.6% of their average value.

2. Turbine Thrust

Turbine thrust is dependent upon inlet pressure, turbine flow rate, pressure ratio, and the properties of the drive gas. In general, axial thrust of an impulse turbine is relatively low at design conditions. However, under off-design conditions, as in the case of this turbine operating with gaseous nitrogen drive, thrust magnitudes can be significant.

Turbine thrust was computed from pressure forces on both sides of the rotor disc. The thrust caused by gas friction in the rotor blades was neglected because it was in all cases smaller than 1000 lb for gas generator (hydrogen-oxygen) drive and smaller than 500 lb for gaseous nitrogen drive.

a. Thrust with Gaseous Nitrogen Turbine Drive

Test results from the first test series confirmed evidence of an expected rotor exit swirl, which caused large pressure losses in the exhaust cone and consequently, a lower than desired pressure ratio across the turbine. The swirl created a large pressure gradient behind the disc and thereby caused a thrust component downstream. This partly compensated for the decrease in turbine thrust caused by the decrease in pressure ratio. A similar exit swirl was experienced on the Model II scale turbine tested by NASA/LeRC. Test data indicated a large reduction in pressure towards the center of the exhaust side of the disc and a large thrust downstream. No provision was made during initial tests of the first series to measure such a pressure distribution; therefore, the representative pressure on the downstream side of the disc was determined from the pressure gradient measured on the scale turbine.

The pressure force acting on the inlet side of the rotor was estimated from the single pressure probe P_{GOTD} (Figure 15) in the hub area of the disc. Radial equilibrium was assumed at the nozzle exit and the nozzle discharge

TABLE IV

PUMP THRUST CALCULATIONS
COMPARISON OF METHODS AND RESULTS

PUMP: OIPA, B/U 2, N = 3652 rpm, Q/N = 5.2, P_S = 103.5 psia

Method	Procedure	Pressure Profiles	Frontside Force (lb)	Backside Force (lb)	Thrust[1] (lb)
1	Graphical Integration	Curve fitted frontside and backside.	--	--	59,900
2	Numerical Integration	Straight lines frontside and backside.	195,800	255,500	59,700
3	Numerical Integration	Straight lines on frontside, parabolic sections on backside.	195,800	252,847	57,047
4	Numerical Integration	Straight lines on frontside, curve fitted backside.	195,800	251,370	55,750
5	Computer Integration	Curve fitted frontside and backside.	--	--	61,500

(1) Momentum force neglected.
Pressure profiles to above data point are presented in Figure 14 in terms of radius times pressure.

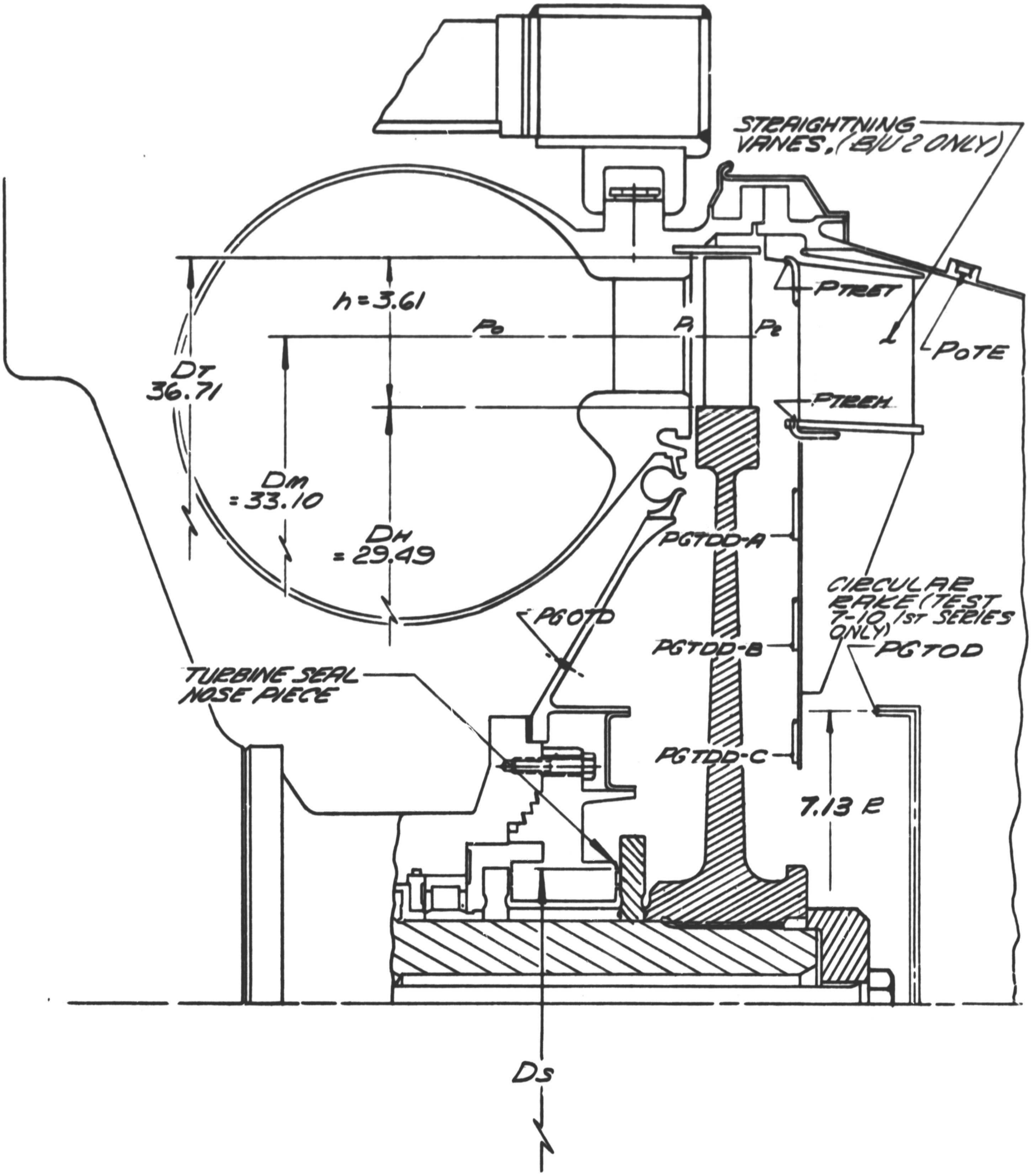

Figure 15

M-1 OTPA MODEL I TURBINE ROTOR MAIN DIMENSIONS AND INSTRUMENTATION LOCATIONS

pressure P_1 was calculated by multiplying the measured pressure P_{GOTD} with a radial equilibrium factor of 1.11. P_{GOTD} was considered representative of the mean pressure acting against the upstream side of the disc because the pressure tap is located close to the appropriate center of pressure.

The pressure force F_u towards the pump was determined for Test No. 1 through 6 of the first test series from the wall static pressure P_{OTE1} in the exhaust cone. The swirl effect was considered by multiplying the pressure force obtained by a correction factor K_{F_u} of 0.855 determined from NASA scale turbine data.

Pressure force towards the pump, uncorrected, $F_u' = A_2 P_{OTE1}$

Pressure force towards the pump, corrected for swirl effect, $F_u = K_{F_u} A_2 P_{OTE1}$

Pressure force towards the exhaust, $F_D = A_{1H} P_{1H} + A_B P_1$

Net turbine thrust = $F_u - F_D = K_{F_u} A_2 P_{OTE1} - A_{1H} P_{1H} - A_B P_1$

Whereby: (see Figure 15)

$A_{1H} = \pi/4 (D_H^2 - D_S^2) = 647.5$ in.^{2} (Hub area, inlet side)

$P_{1H} = P_{GOTD}$ (Rotor inlet pressure, hub, inlet side)

$P_1 = 1.11 P_{GOTD}$ (Rotor inlet pressure at the mean diameter)

$A_B = \pi D_{m\,h} = 375$ in.^{2} (blade area)

$A_2 = \pi/4 \; D_T^2 = 1060$ in.^{2} (Total area, exhaust side)

Test No. 7 through 10 of the first series were conducted with a circular rake installed on the exhaust side of the rotor hub with pressure pickups located on a 7.13-in. radius.

A linear pressure profile was assumed through P_{OTE}, and P_{GTOD} and the pressure force towards suction was then determined by integration of the profile.

$$F_{u2} = 2\pi \int rp(r)\, dr$$

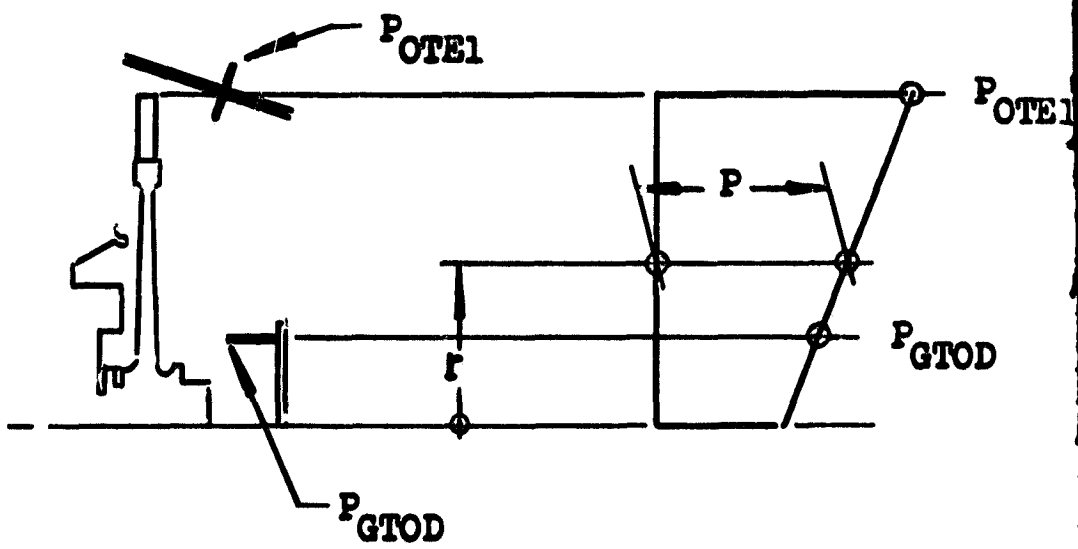

The pressure force towards suction for a specific case (Test 6.0-04-EHP-9) determined by the different methods described above compare as follows:

Pressure force towards suction, uncorrected.	F_u'	= 67,300 lb
Pressure force towards suction, corrected for swirl effect on the basis of NASA data.	F_{u_1}	= 57,500 lb
Pressure force towards suction, based upon circular rake data and wall static exhaust pressure.	F_{u_2}	= 54,000 lb

The correction factor K_{F_u}, applicable to this data was verified from the above results

$$K_{F_u} = \frac{F_{u_2}}{F_u'} = 0.805$$

When straightening vanes were installed on Buildup No. 2 to eliminate the exit swirl, additional static taps were provided to measure the pressure distribution on the downstream side of the disc. With these new instrumentation stations, the computation of the pressure force towards suction was greatly simplified and yielded more representative magnitudes. The force was calculated as follows:

$$F_u = A_{2H}\, P_{GTDD_{mean}} + 1/2\, A_B\, (P_{TRET} + P_{TREH})$$

Whereby: $A_{2H} = \pi/4\ D_{H_2}^2$ and $A_B = \pi\ D_m\ h$

Test results from the second test series showed no significant variation of the three pressure measurements P_{GTDD} behind the turbine disc. This indicated that the swirl was eliminated. Thus, the mean value of the three pressures P_{GTDD} was used for calculating turbine thrust. Turbine pressures are listed for a typical data point in Table I.

b. Thrust with Gas Generator (Hydrogen-Oxygen) Turbine Drive

The turbine operated with a pressure ratio of approximately 2.4 with gas generator drive and the small exhaust orifice (240-in.^{2}). A comparison of the mean exhaust pressure with the calculated inlet pressure based upon radial equilibrium indicated impulse conditions $P_1 = P_2$. Under those circumstances, thrust was directly computed from the pressure forces acting upon the turbine disc. Thrust resulting from some negative reaction at the disc and some positive reaction at the blade tip partly cancelled each other so that their difference was considered insignificant. The thrust equation was reduced to:

$$F_{AX} = A_{2H} P_{GTDD_{mean}} - A_{1H} P_{GOTD}$$

Under impulse conditions, thrust was always positive or directed towards the pump because of the effect of radial equilibrium upon the upstream side of the rotor.

Pressure ratios of approximately 3.5 were obtained with the large exhaust orifice of 314-in.^{2}. The rotor operated with some reaction because of the high pressure ratio. New radial equilibrium factors were calculated for the upstream side of the disc for gas generator Tests No. 13 and 14. A correction factor was obtained that was nearly identical to the one obtained for gaseous nitrogen turbine drive (1.11). Axial thrust was computed similar to the method derived for gaseous nitrogen drive.

$$F_{AX} = A_{2H} P_{GTOD_{mean}} + \frac{1}{2} A_B (P_{TRET} + P_{TREH}) - P_{GOTD} (A_{1H} + KA_B)$$

Whereby:

K = radial equilibrium factor.

3. Thrust Predictions

a. Initial Estimates

The thrust direction predicted for the interim impeller was towards the pump. However, for gaseous nitrogen turbine drive, a downward turbine thrust direction was expected. The net thrust of these two estimates was predicted to be towards the pump, even though downward thrust was possible at low pump speeds. A bearing orientation to give load sharing towards the pump was then chosen for the following reasons.

(1) Net thrust was predicted in a direction towards pump suction.

(2) Poor performance of the backvane diffuser would result in increased thrust towerds pump suction.

(3) Tests with gas generator drive as intended for this unit would have no turbine thrust, and, hence, net thrust toward the pump. At these higher speeds, thrust prediction errors would be better accommodated with the bearing orientation chosen.

b. The Ideal Pump Thrust

Pump thrust predictions for full speed operation (with gas generator turbine drive) were based upon thrust values established from low speed tests (with gaseous nitrogen turbine drive) and on the following assumptions:

(1) Affinity laws hold true (static headrise varies directly with speed squared; efficiency remains constant).

(2) Fluid Temperature remains constant (no change in friction losses).

(3) Fluid density is not dependent upon pressure.

(4) Reynolds number effects are negligible.

The idealized thrust was calculated from front and backside pressure forces derived as follows:

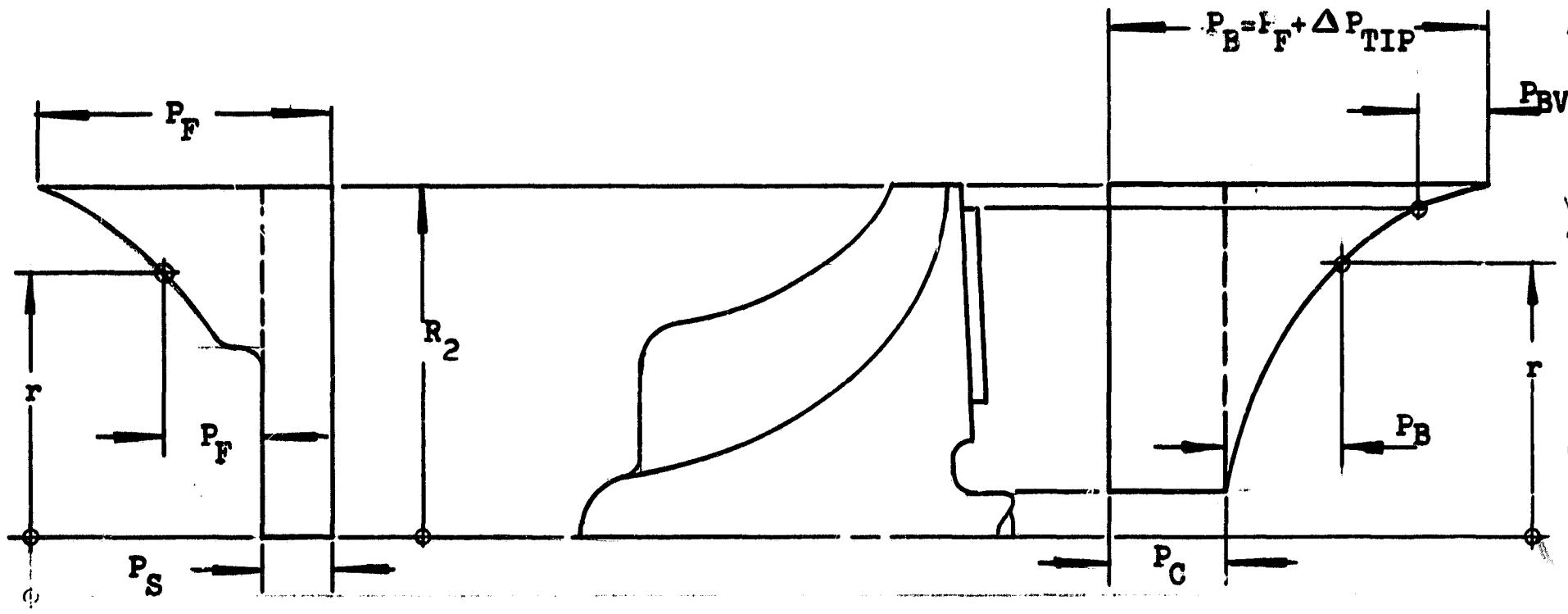

ΔP_{TIP} = Pressure Gradient Across Impeller Discharge = $(P_B - P_F)$

Frontside pressure force:

$$F_F = F_s + \Delta F_F = P_s A_F + K_{fF} N^2 \int_0^{R_2} \psi_F(r)\, r\, dr$$

Backside pressure force:

$$F_B = F_c + \Delta F_B = P_C A_B + K_{fB} N^2 \int_{R_{SH}}^{R_2} \psi_B(r)\, r\, dr$$

As explained in Section III.A. the cavity pressure P_c is equal to the suction pressure, plus the pressure rise of the frontside, plus the pressure difference at the discharge, and minus the pressure rise of the backside.

$$P_c = P_s + \Delta P_F + \Delta P_{TIP} - \Delta P_B$$

The pressure difference at the discharge $\Delta P_{TIP} = P_{OBV6} - P_{OHC5}$ is assumed to stay proportional with N^2.

Thus:

$$P_C = P_s + K_{p,F}\, \psi_F N^2 + K_{p,TIP}\, \psi_{TIP}\, N^2 - K_{p,B}\, \psi_B\, N^2$$

$$= P_s + N^2 (K_{p,F}\, \psi_F + K_{p,TIP}\, \psi_{TIP} - K_{p,B}\, \psi_B)$$

Substituting this expression into the equation for the backside pressure force:

$$F_B = \left[P_s + N^2 (K_{p,F}\, \psi_F + K_{p,TIP}\, \psi_{TIP} - K_{p,B}\, \psi_B) \right] A_B$$

$$+ K_{f,B}\, N^2 \int_{R_{SH}}^{R_2} \psi_B(r)\, r\, dr$$

Neglecting the momentum force

$$
\begin{aligned}
F_{AX} &= F_B - F_F \\
&= A_B \left[P_s + N^2 \left(K_{p,F}\ \Psi_F + K_{p,TIP}\ \Psi_{TIP} - K_{p,B}\ \Psi_B \right) \right. \\
&+ K_{f,B}\ N^2 \int_{R_{SH}}^{R_2} \Psi_B (r)\ r\ dr - P_s A_F - K_{f,F}\ N^2 \int_o^{R_2} \Psi_F (r)\ r\ dr \\
&= P_s\ (A_B - A_F) + N^2 \left[A_B \left(K_{p,F}\ \Psi_F + K_{p,TIP}\ \Psi_{TIP} - K_{p,B}\ \Psi_B \right) \right. \\
&+ K_{f,B} \int_{R_{SH}}^{R_2} \Psi_B (r)\ r\ dr - K_{f,F} \int_o^{R_2} \Psi_F (r)\ r\ dr \Big]
\end{aligned}
$$

Equation (5)

This equation shows that if $A_B = A_F$, the thrust is directly proportional to N^2 and suction pressure P_s cancels out. The thrust component caused by suction pressure F_{SH} can be expressed in terms of the shaft area $A_{SH} = A_F - A_B$.

Thus: $F_{SH} = P_s\ (A_F - A_B) = P_s\ A_{SH}$.

Thrust, F_{SH}, can be removed from Equation (5) so that the resulting expression becomes directly a function of speed squared.

$$F_{AX} + F_{SH} = F_{AX} + P_s\ A_{SH} = f\ (N^2)$$

Knowing F_{SH} and a thrust value at low speed, the ideal thrust at full speed can be calculated from the following relationship:

$$\frac{F_{AX2} + P_s\ A_{SH}}{F_{AX1} + P_s\ A_{SH}} = \left[\frac{N_2}{N_1} \right]^2$$

and

$$F_{AX2} = \left[\frac{N_2}{N_1} \right]^2 \left(F_{AX1} + P_s\ A_{SH} \right) - P_s\ A_{SH}$$

Equation (6)

The ideal pump thrust based upon actual measured or estimated values (F_{AX1}) at the prespin speed of 2100 rpm is plotted versus speed for 85%, 100%, and 120% of design Q/N on Figure 16. The characteristics shown are exponential curves $F_{AX} = N^n$ with (n) approaching 2 at high magnitudes of F_{AX}. This reflects the effect of the thrust component caused by suction pressure $P_S A_{SH}$, which becomes negligible at very high thrust values.

The scale factors to relate ideal thrust at full speed from thrust data at prespin (N_1 = 2100 rpm, N_2 = 3635 rpm, and constant suction pressure P_s = 115 psia) are:

$$F_{AX2} \text{ at } 85\% \text{ DES } Q/N = F_{AX1} \times \left[\frac{N_2}{N_1}\right]^{2.135} \qquad (F_{AX1} = 17{,}500 \text{ lb})$$

$$F_{AX2} \text{ at } 100\% \text{ DES } Q/N = F_{AX1} \times \left[\frac{N_2}{N_1}\right]^{2.17} \qquad (F_{AX1} = 14{,}000 \text{ lb})$$

$$F_{AX2} \text{ at } 120\% \text{ DES } Q/N = F_{AX1} \times \left[\frac{N_2}{N_1}\right]^{2.22} \qquad (F_{AX1} = 12{,}000 \text{ lb})$$

4. Accuracy

When calculating pump thrust, a very accurate analytical procedure could yeild an axial thrust value far from the value obtained experimentally. For example, if an axial balance of 30,000 lb towards the impeller eye is desired and a frontside force of approximately 230,000 lb is underestimated by as little as 3% and a backside force of approximately 260,000 lb is overestimated by 3%, the measured thrust could be off by 50% of the analytical estimate. This can also apply to turbine thrust, although pressure forces on the rotor are of much smaller magnitudes; however, they are acting upon larger areas.

The above is an example that perfect agreement between predicted and measured thrust is strictly incidental, especially if pressure distributions or thrust values at different operating points are unknown. For large pumps, where margins between nominal and maximum safe operating thrust loads result in lower percentages than with smaller size pumps, it becomes necessary to conduct a partial speed test to verify estimates before attempting full speed operation.

Variations in the magnitudes of pressure forces could result from circumferential pressure variations. As illustrated in Figures 17, 18, and 19, the pressures $P_{OHC\ 6\ A\ -\ F}$ along the impeller periphery show a variation of approximately $\pm$ 10%. However, it was believed that the thrust calculated from pressure forces is representative because the tip pressures $P_{OHC\ 5}$ and $P_{OBV\ 6}$ were measured in areas of average circumferential pressure (Figures 17 through 19).

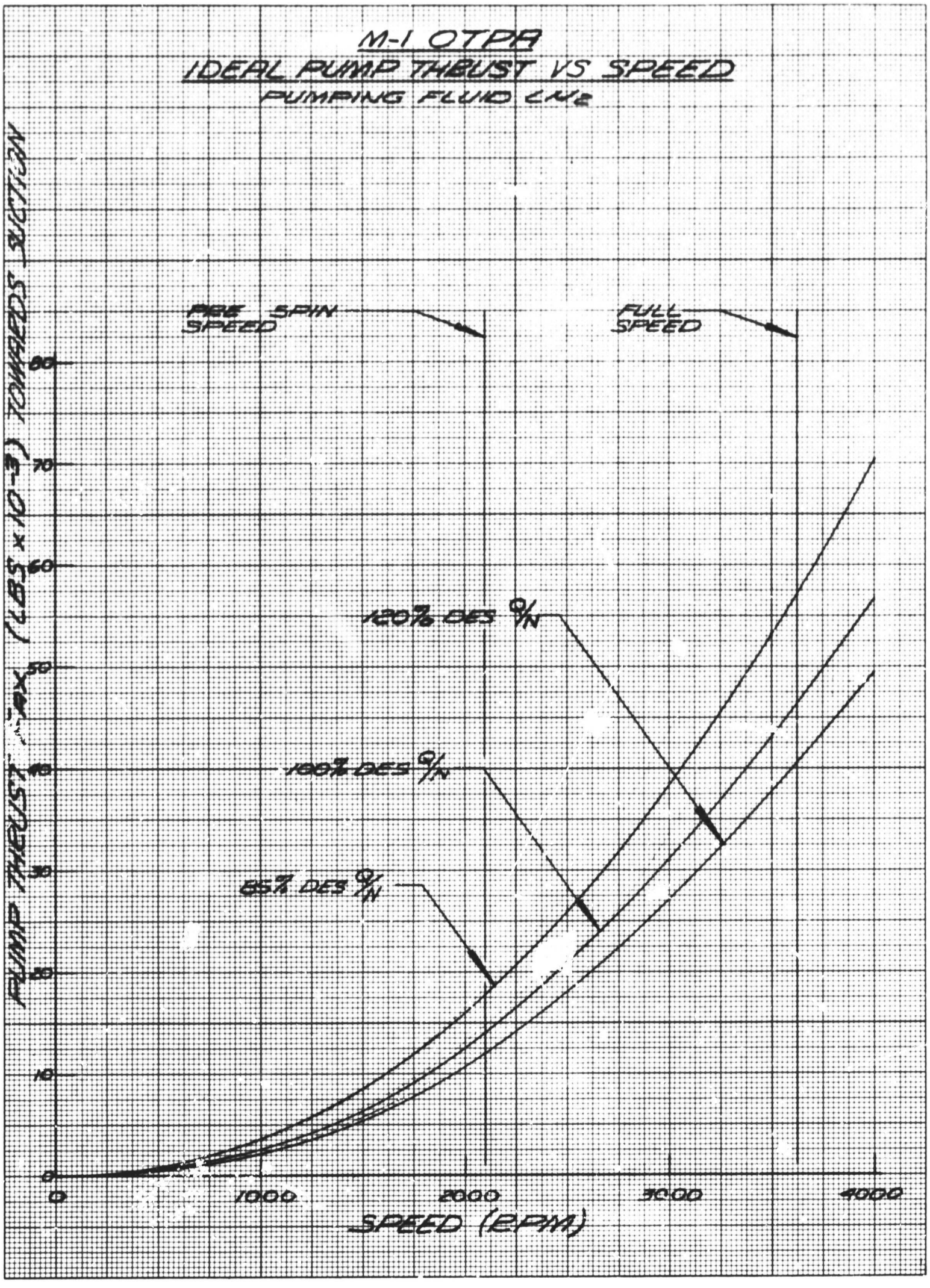

Figure 16

M-1 OTPA IDEAL PUMP THRUST VS SPEED

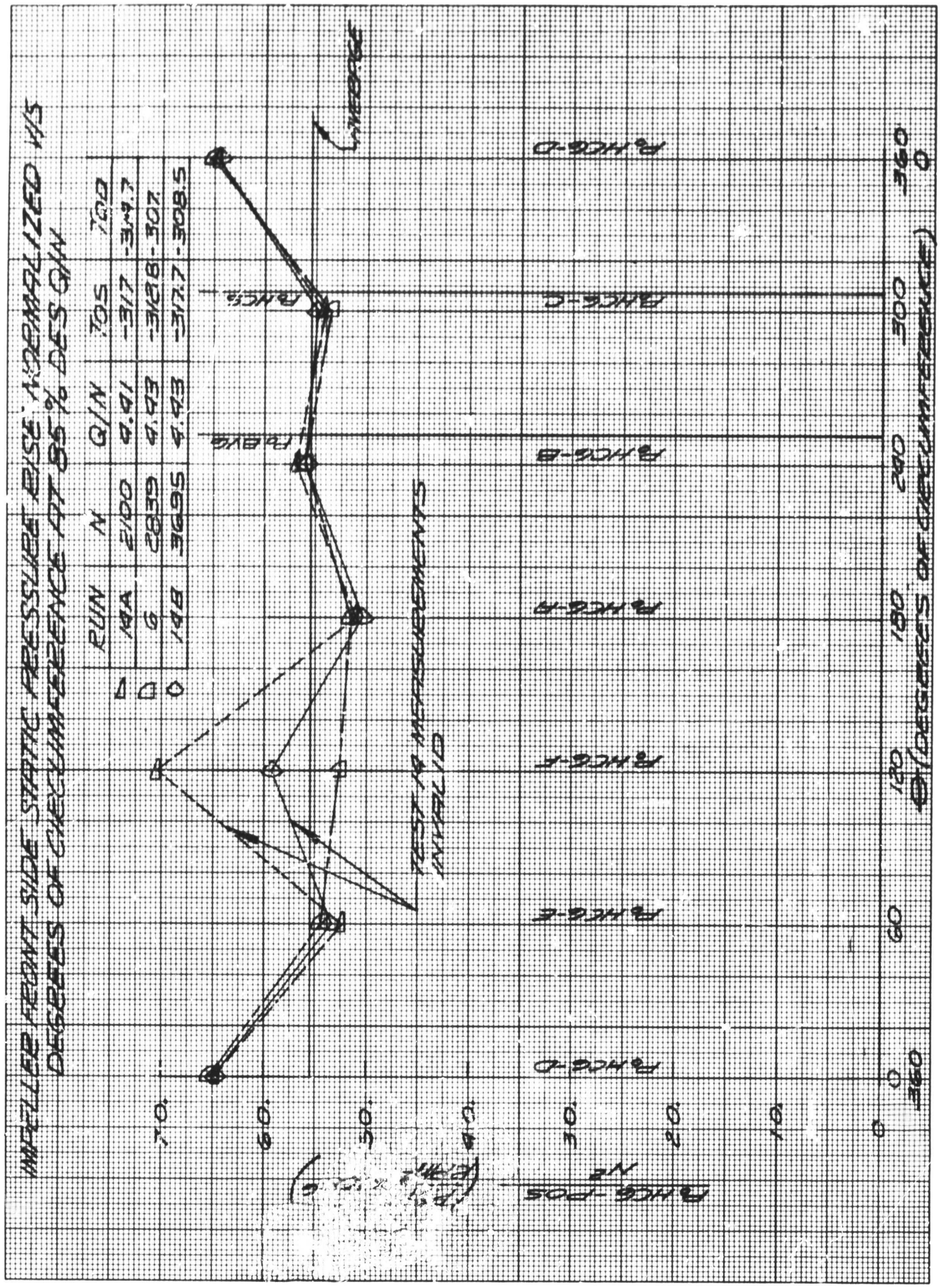

Figure 17

IMPELLER FRONTSIDE NORMAL STATIC PRESSURE RISE VS
DEGREES OF CIRCUMFERENCE AT 85% OF DESIGN Q/N

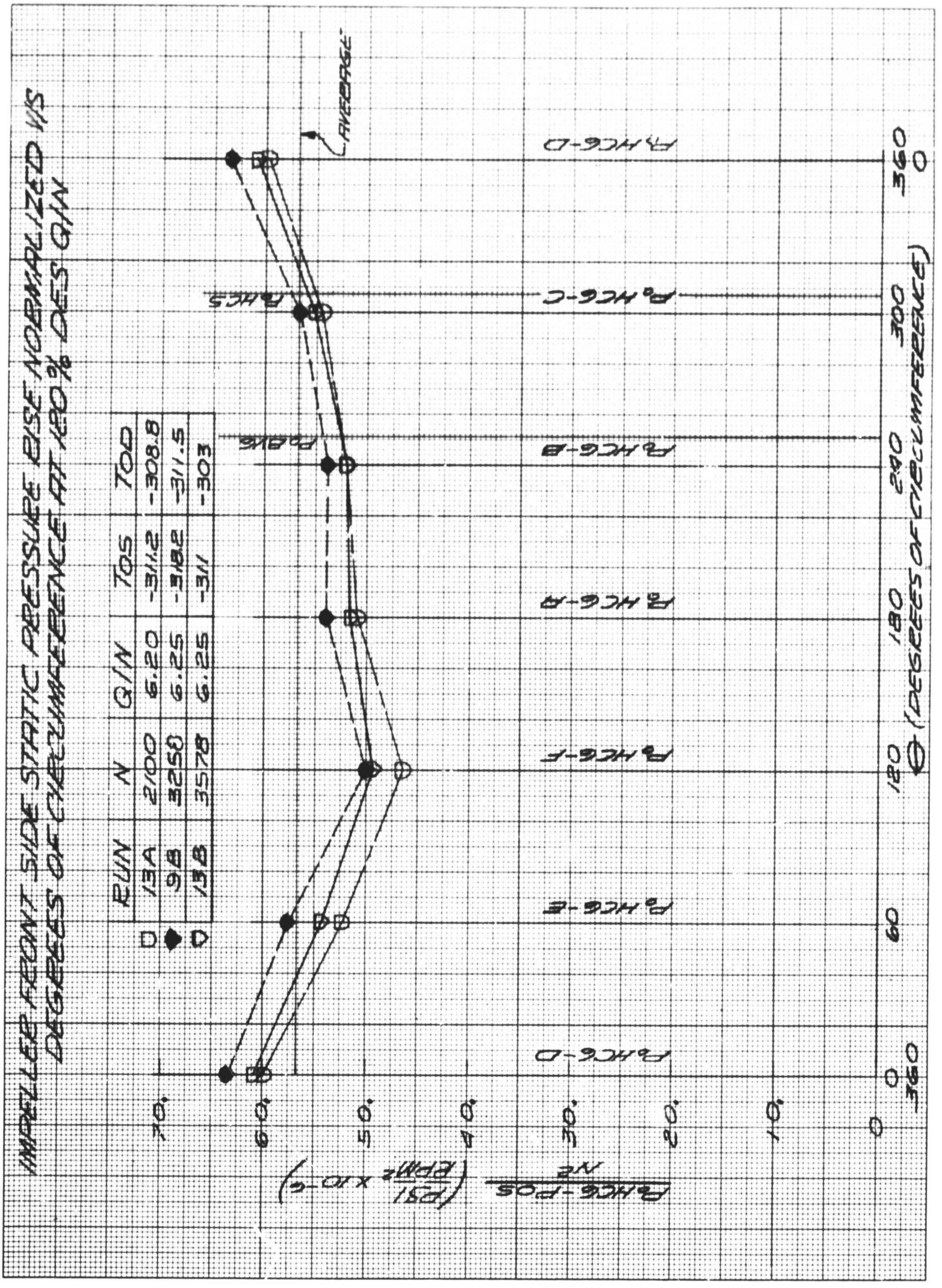

Figure 18

IMPELLER FRONTSIDE STATIC PRESSURE RISE NORMALIZED vs DEGREES OF CIRCUMFERENCE AT 120% OF DESIGN Q/N

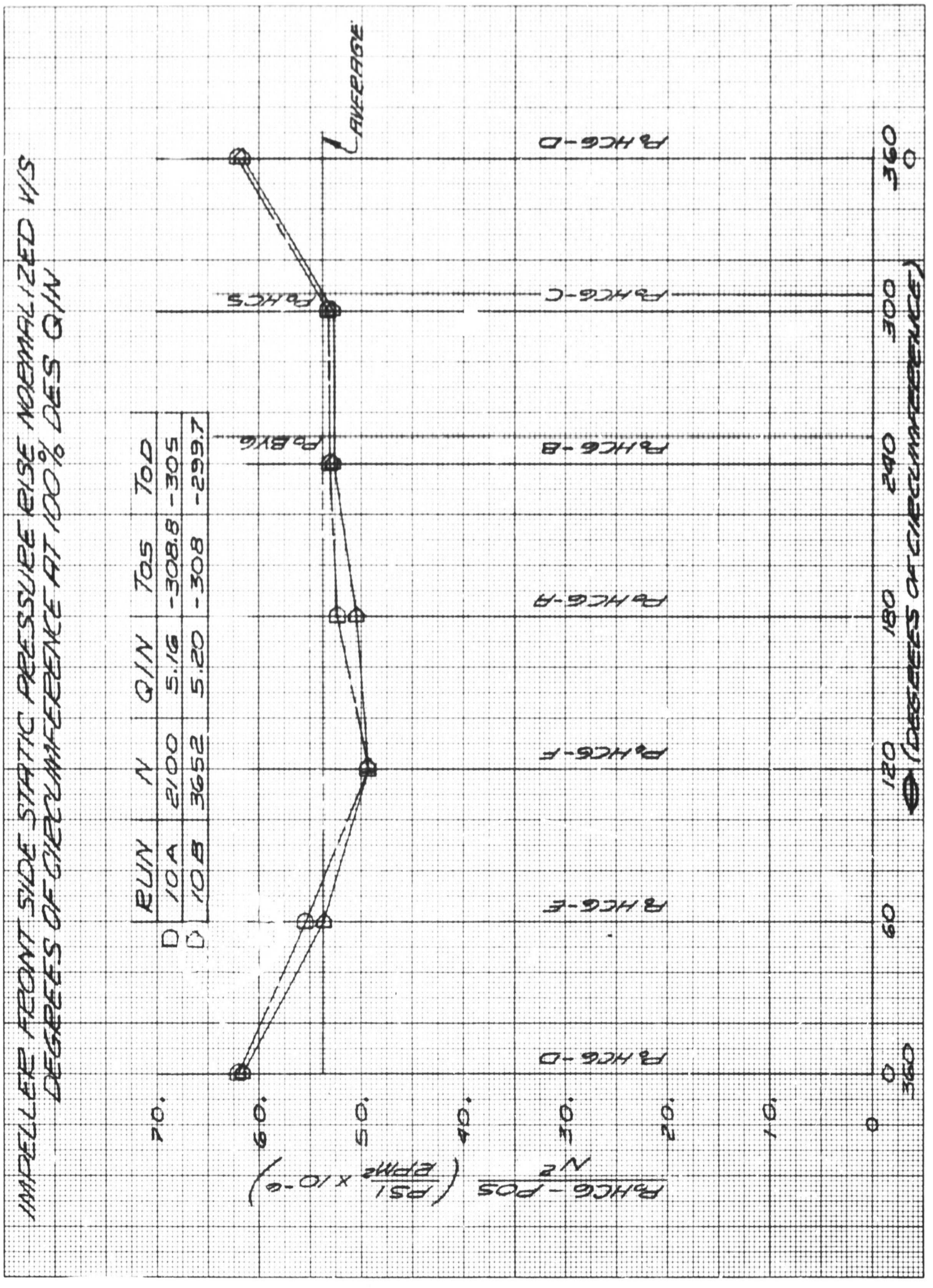

Figure 19

IMPELLER FRONTSIDE STATIC PRESSURE RISE NORMALIZED vs DEGREES OF CIRCUMFERENCE AT 100% OF DESIGN Q/N

D. THRUST CONTROL

1. Results of First Test Series

The first firm indication of axial thrust characteristics was obtained from the first partial speed test of Test Series No. 1. Both the pump and the turbine thrust components were directed downwards or towards the turbine. Pump thrust was higher in magnitude than estimated while turbine thrust was approximately 18% less than predicted. Test data confirmed evidence of a rotor exit swirl that produced large pressure losses in the exhaust cone, and consequently, a lower than desired pressure ratio across the turbine stage. The swirl created a large radial pressure gradient behind the disc, thereby causing a downstream thrust component directly towards the exhaust that partly compensated for the decrease in turbine thrust resulting from the decrease in pressure ratio.

Steady-state pump and turbine thrust of each test are summarized and compared with the measured thrust values in Table V. The relatively large scatter in thrust data presented in this table for similar operating conditions is believed to be caused by cavitation in the rear impeller cavity. Data analysis relative to thrust revealed the following:

a. The impeller was overbalanced. The pressure rise on the impeller backside was greater than on the impeller frontside ($\psi_B > \psi_F$). Mean values of static head coefficients obtained were: $\psi_B = 0.41$, $\psi_F = 0.29$.

b. At all operating points of equal suction pressure, the cavity pressure decreased with increasing speed (see Figure 20). At the higher speeds, the cavity pressure was limited by the vapor pressure of the fluid, or:

$$P_c = P_s + \frac{u_2^2 \rho}{144g} (\psi_{FB} - \psi_B) = P_{vapor} \qquad \text{Equation (7)}$$

(ψ_{FB} is introduced for simplicity and accounts for the pressure difference across the impeller discharge ($P_{BV6} - P_{HC5}$), ($\psi_{FB} = 3 \times 10^5 \frac{P_{BV6} - P_s}{\rho N^2}$).

c. Vapor pressure was attained in the cavity at high operating speeds or low suction pressures (48 psia) and/or at higher than nominal flow-speed ratios. At nominal operating conditions (P_{os} 115 psia), a cavity pressure of 48.5 psia (approximately vapor pressure) was measured at 2377 rpm.

The speed required to produce vapor pressure in the cavity was calculated from Equation (7) for average head coefficients and nominal suction pressure. The value obtained amounted to approximately 2300 rpm. While $P_c = P_{vap} \sim 50$ psia is, disregarding temperature changes, supposed to remain constant at higher operating speeds, the head coefficient ψ_B will decrease to maintain equality of Equation (7). The reduction in head coefficient occurs as the vapor level in the cavity increases to higher radii.

TABLE V

OTFA AXIAL THRUST SUMMARY

TFA B/U 1, FIRST TEST SERIES

Comparison of steady-state pump and turbine thrust with measured thrust.

Run No.	Speed (rpm)	Q/N (1)	Suction Pressure (psia)	F_{AX} - Pump Computer (lb) (4)	F_{AX} - Pump Graphic (lb) (4)	F_{AX} - Turbine (lb) (4)	F_{AX} - Net(2) (lb) (4)	F_{AX} - Measured (lb) (4)
001	1853	4.65	117	N/A	- 3400	- 2700(3)	- 6100	- 7500
002	2086	4.22	117	N/A	- 4100	- 6900	-11,000	-11,000
003	2066	6.53	110.6	N/A	- 6950	- 7900	-14,850	-16,800
004	2105	5.55	104.5	N/A	- 9800	- 5300	-15,100	-11,300
005	2100	8.3	77.6	N/A	- 2150	- 5100	- 7250	-17,500
006	1044	5.23	87	N/A	- 3400	850	- 2550	- 2250
006	2110	5.32	83.4	N/A	N/A	- 5300	N/A	N/A
007	1508	4.06	119	276	- 1550	- 2650	- 2374	- 2400
007	1514	3.09	121	1993	2250	- 2500	- 507	- 1900
007	1510	2.06	123	- 2300	- 400	- 1850	- 4150	- 1700
008	2096	5.1	47.8	2268	0	- 9000	- 6732	- 8000
009	2440	5.06	115	N/A	N/A	-18,600	N/A	N/A
009	2332	5.14	115	-16,637	-18,900	-19,200	-35,837	-35,800
010	2431	4.12	116.4	-20,337	-24,500	-18,900	-39,277	-39,500

(1) Design Q/N = 5.18.

(2) F_{AX} Net = F_{AX} - Pump Computer + F_{AX}-Turbine (where computer data available).

(3) Test 001 conducted with larger turbine exhaust orifice A_{exit} = 263 in.^{2}. A_{exit} for all other tests was 240 in.^{2}.

(4) Thrust directed towards suction is considered positive.

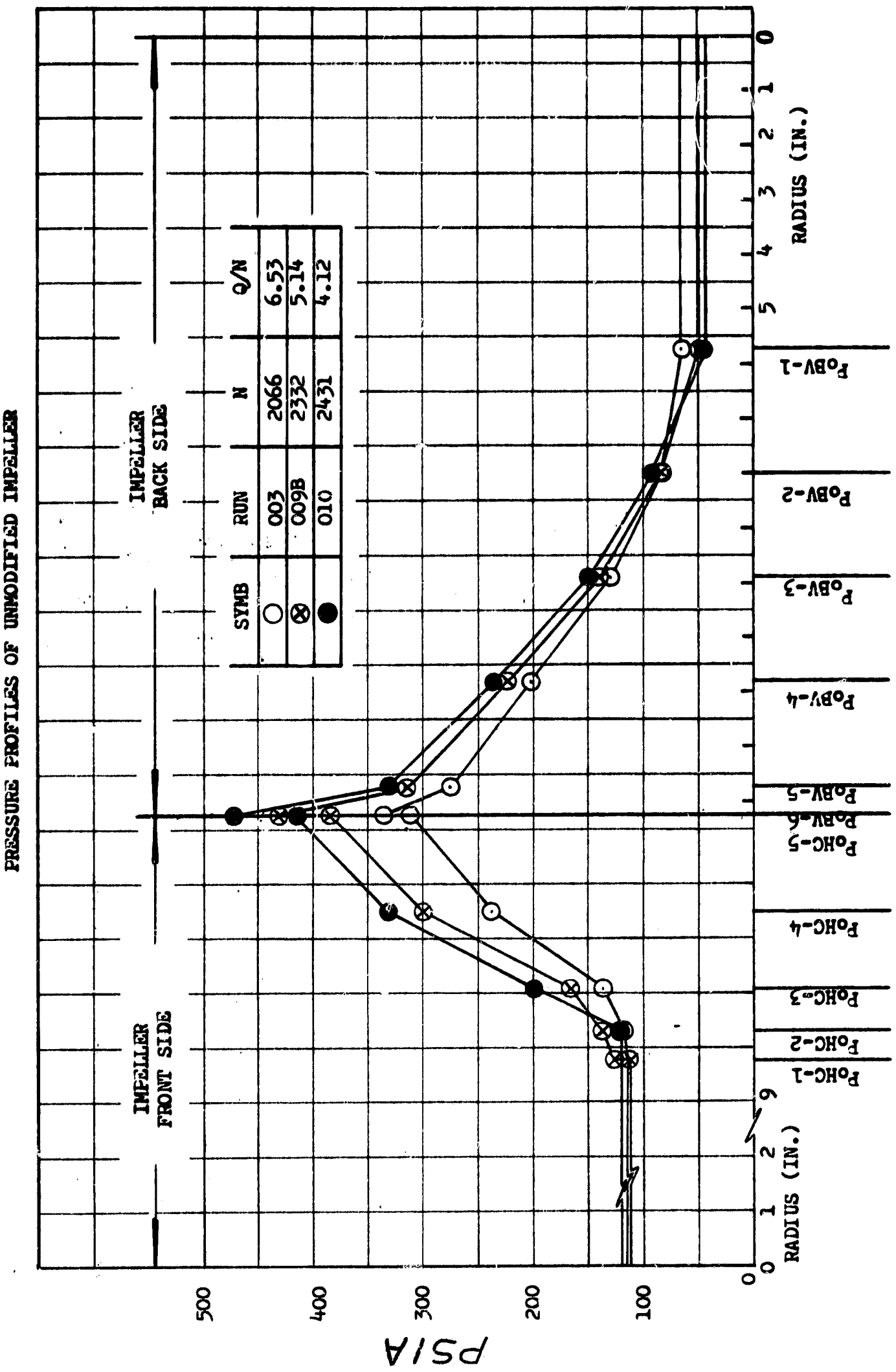

Figure 20

PRESSURE PROFILES OF UNMODIFIED IMPELLER

An estimated thrust characteristic of a pump impeller operating with cavitating backvanes is shown in Figure 21. With increasing speed, cavitation in the cavity or at the backvane inlet will tend to limit the down thrust as the backside pressure force increases more rapidly with decreasing head coefficient Ψ_B.

2. Purpose of Backvane Modification

Evaluation of the test data from Test Series 1 revealed the presence of vapor in the impeller near cavity at speeds in excess of 2300 rpm at nominal Q/N and suction pressure. Also, it was predicted that with increasing operating speeds cavitation would extend to larger radii and possibly penetrate into the annular cavity of the backplate. A build-up of a low pressure sink extending from the pump seal to the area of the bearing coolant return discharge would present the possibility for obtaining local vapor formations within the power transmission assembly which, in turn, could be detrimental to the operation of the bearings. Also cavitation or the presence of vapor in liquid oxygen would represent a potential explosion hazard. For these reasons, it was decided to eliminate cavitation during anticipated full speed liquid nitrogen and liquid oxygen tests by decreasing the pressure rise capability of the backvane system so that the resulting cavity pressure would always exceed the vapor pressure. The primary effect of such a backvane modification would be an increase in thrust towards suction.

Two possibilities considered for decreasing the pressure generating ability of the backvane system were:

a. Removal of the backvane diffuser and operation of the pump with a vaneless cavity at the discharge of the backvanes (vaneless backvane diffuser).

b. Reduction in the length of the backvanes to obtain a larger backvane inlet radius.

The following drawing shows pressure profiles for both possible approaches.

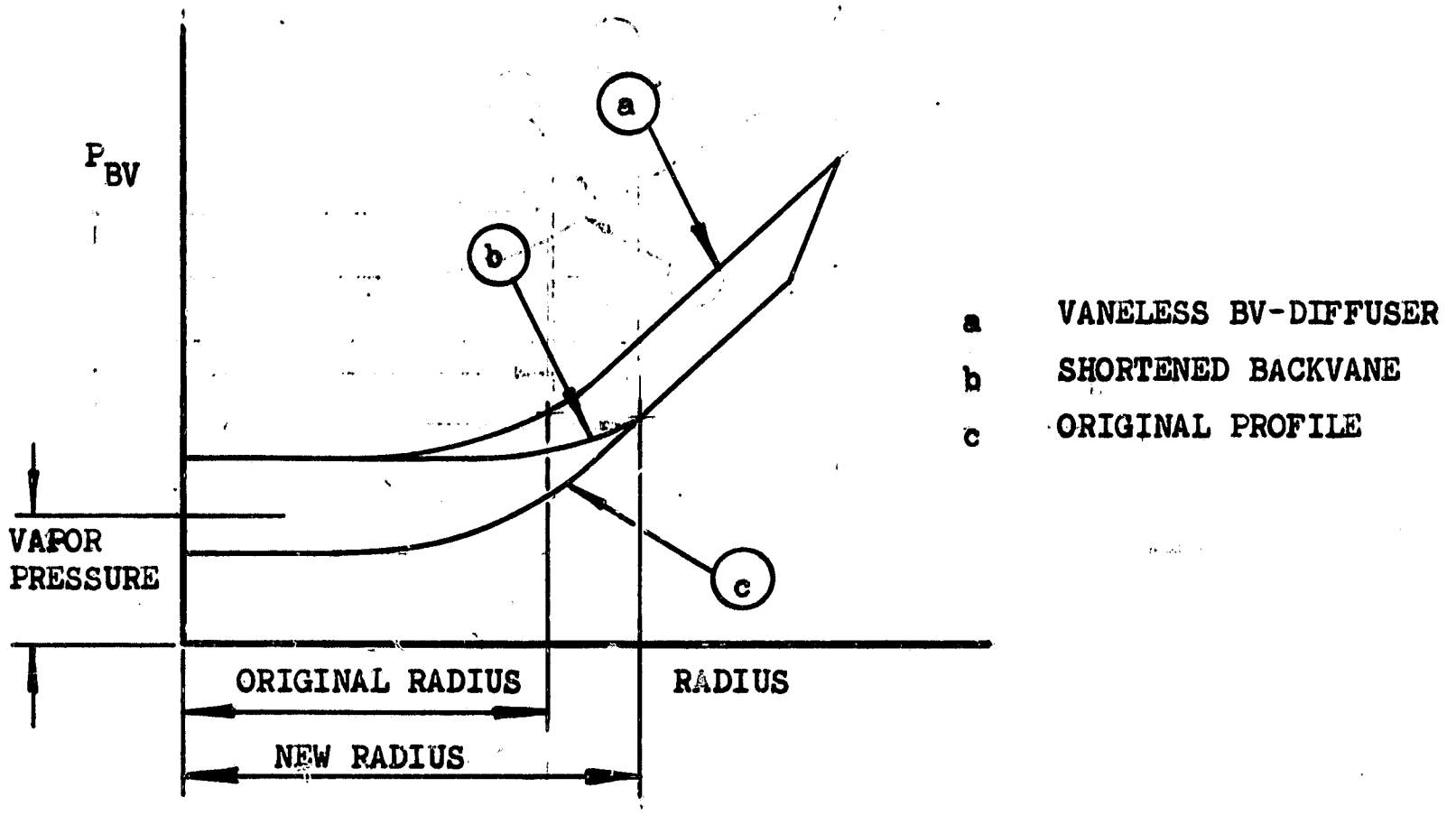

PUMPING FLUID LN_2

BACKVANE INLET RADIUS = 8.0 IN.

SUCTION PRESSURE = 120 PSIA

Q/N = NOMINAL

(A) - BACKVANES CAVITATING, CAVITY TEMPERATURE $f(\propto N^2)$

(B) - BACKVANES CAVITATING, CAVITY TEMPERATURE = CONSTANT

(C) - BACKVANES NON-CAVITATING

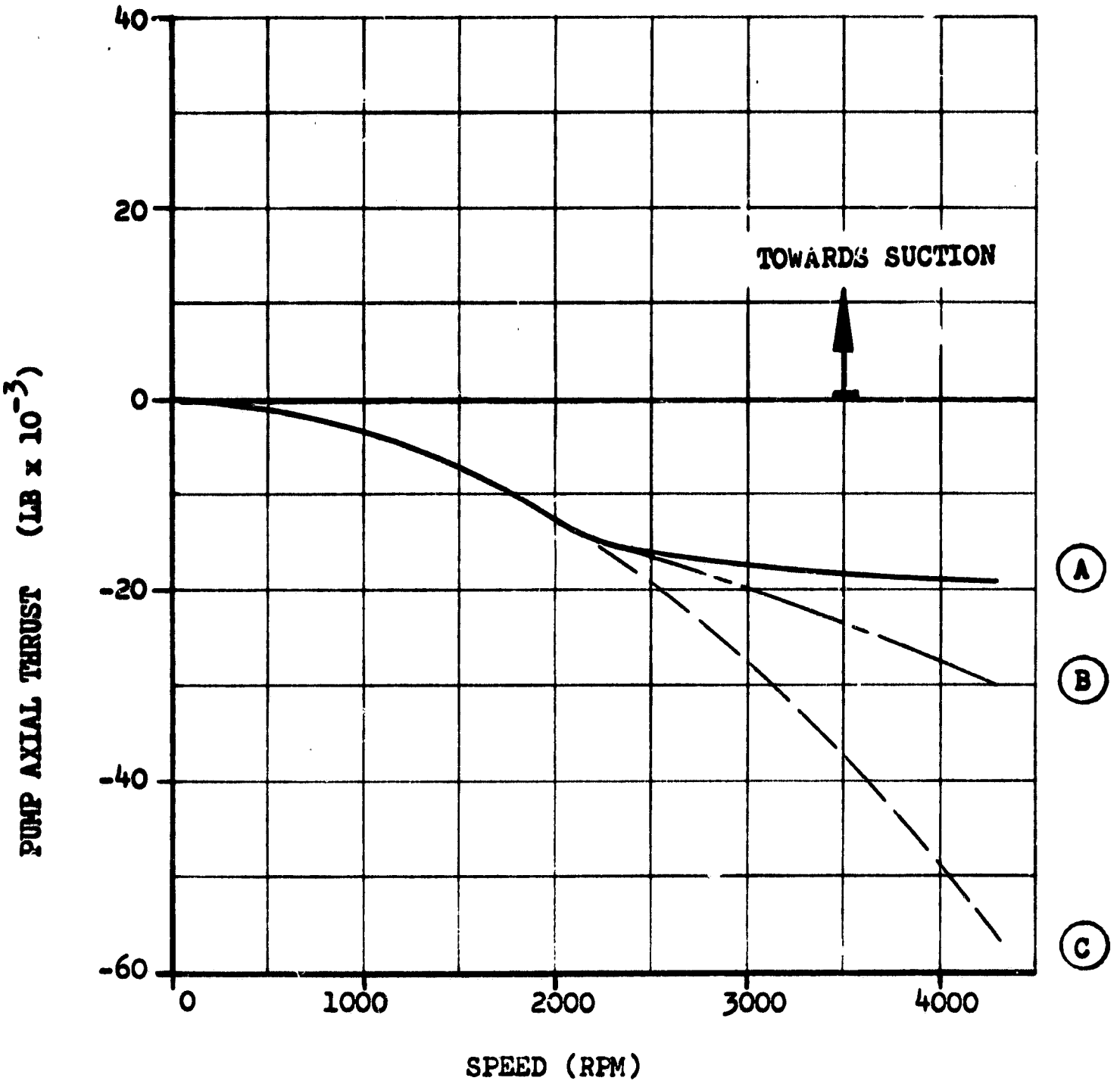

Figure 21

PREDICTED THRUST OF ORIGINAL IMPELLER WITH CAVITATING BACKVANES

The cavity pressure can be increased by either approach but the pressure force resulting from Method (a) will be considerably greater because of the upward shift of the backvane pressure profile. Approach (b) was selected for eliminating cavitation because of its lesser effect upon axial thrust.

3. Determination of New Backvane Inlet Radius

The new backvane inlet radius was determined using the following assumptions. To eliminate cavitation, the minimum pressure in the rear cavity was not to be less than 50 psia at these conditions:

Maximum Operating Speed: $N = 4000$ rpm

Nominal Suction Pressure: $P_{OS} = 115$ psia

Minimum Static Head Coefficient at 100% of Design Q/N: $\psi_{FB} = 0.355$

The new static head coefficient was calculated from Equation (7).

$$\psi_{BV_{MAX}} = \psi_{FB} - \frac{144g}{u_2^2 \rho} (P_c - P_s) = 0.38$$

The obtained value was not to be exceeded and therefore, was considered a maximum. Regarding the data scatter of 18% obtained during the first test series, a minimum head coefficient $\psi_{BV_{MIN}}$ of 0.32 was predicted.

From these two coefficients, the new vane inlet radius was determined analytically and graphically as shown in the following plot, by assuming that the sections of the pressure profile defined by the static headrise coefficients between inlet radius and tip will remain unchanged. The part from which the vane was to be shortened was assumed to follow the same parabolic law as observed in the vaneless portion of the original impeller. Based upon this assumption and on the resulting static headrise coefficient of 0.063 for the cavity, the backvane inlet radius was 9.6-in. This radius was later increased to 10-in. as a result of thrust verification tests conducted with the subscale pump, which indicated a larger than predicted headrise coefficient of 0.125 for the cavity.

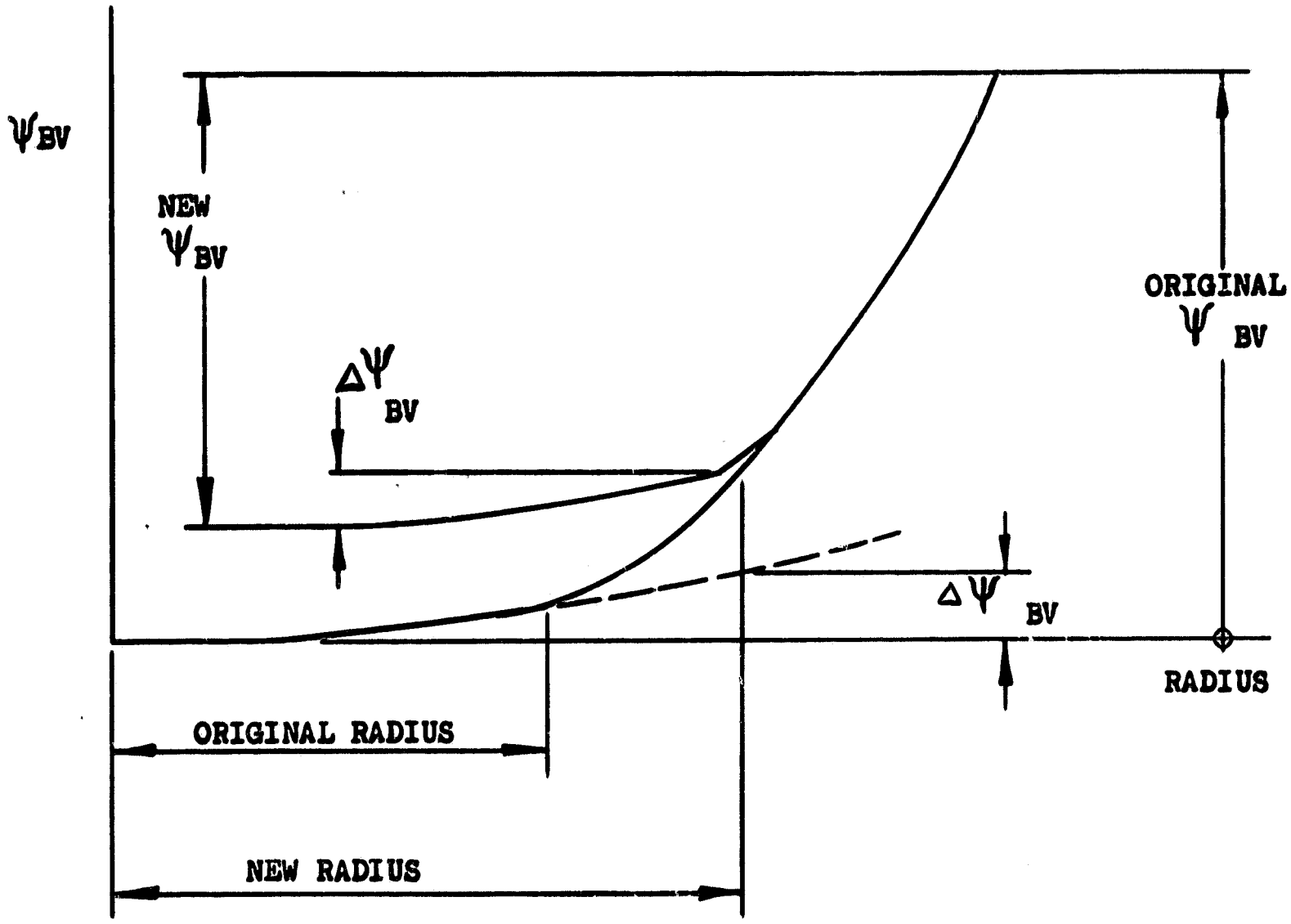

The new backvane profiles for $\psi_{BV_{MAX}}$ and $\psi_{BV_{MIN}}$ in coefficient form are shown in Figure 22. The thrust change resulting from the modification was calculated by graphical integration of the differential area described by old and new pressure profiles. Thrust predictions were determined by adding the computed thrust change to the hypothetical noncavitating thrust extrapolated from test results. Figure 23 depicts the new thrust predictions for liquid nitrogen at nominal Q/N. Results of these calculations are summarized in Table VI.

4. Effects of Backvane Modification Upon Subscale Pump Tests

Subscale pump tests were conducted to verify the method of predicting pressure and thrust changes as a result of backvane modifications.

a. The Subscale Pump

The subscale pump was a three-eights scale model of the full size pump. Impeller vanes and backvanes, diffusers, and inlet configuration were hydraulically similar. For simplicity, the collector was a torus of constant cross-sectional area. Power was provided by a synchronous motor driving a gearbox through an Eddy current-type clutch. All tests were conducted in the closed-loop pump test facility in Test Area D with water as the test fluid.

TABLE VI

SUMMARY OF RESULTS OF BACKVANE INLET RADIUS CALCULATIONS AND PREDICTED PUMP THRUST

Parameter	Initial Configuration	Modified Configuration
Backvane Inlet Radius (in.)	8	10
Propellant	LN_2	LN_2
Speed (rpm)	2400	4000
Suction Pressure (psia)	115	115
Backvane Static Head Coefficient		
$\psi_{B_{MAX}}$	0.44	0.38
$\psi_{B_{MIN}}$	0.38	0.32
Rear Cavity Pressure		
$P_{C_{MAX}}$ (psia)**	Vapor Pressure	50
$P_{C_{MIN}}$ (psia)***	Vapor Pressure	170
Thrust Change (ΔFAX_{pump} lb)	0	37,000
Net Pump Thrust		
$FAX_{pump_{MAX}}$ (lb)*		40,000
$FAX_{pump_{MIN}}$ (lb)*		-10,000

* Thrust directed towards suction is considered positive.
** At ψ_B minimum.
*** At ψ_B maximum.

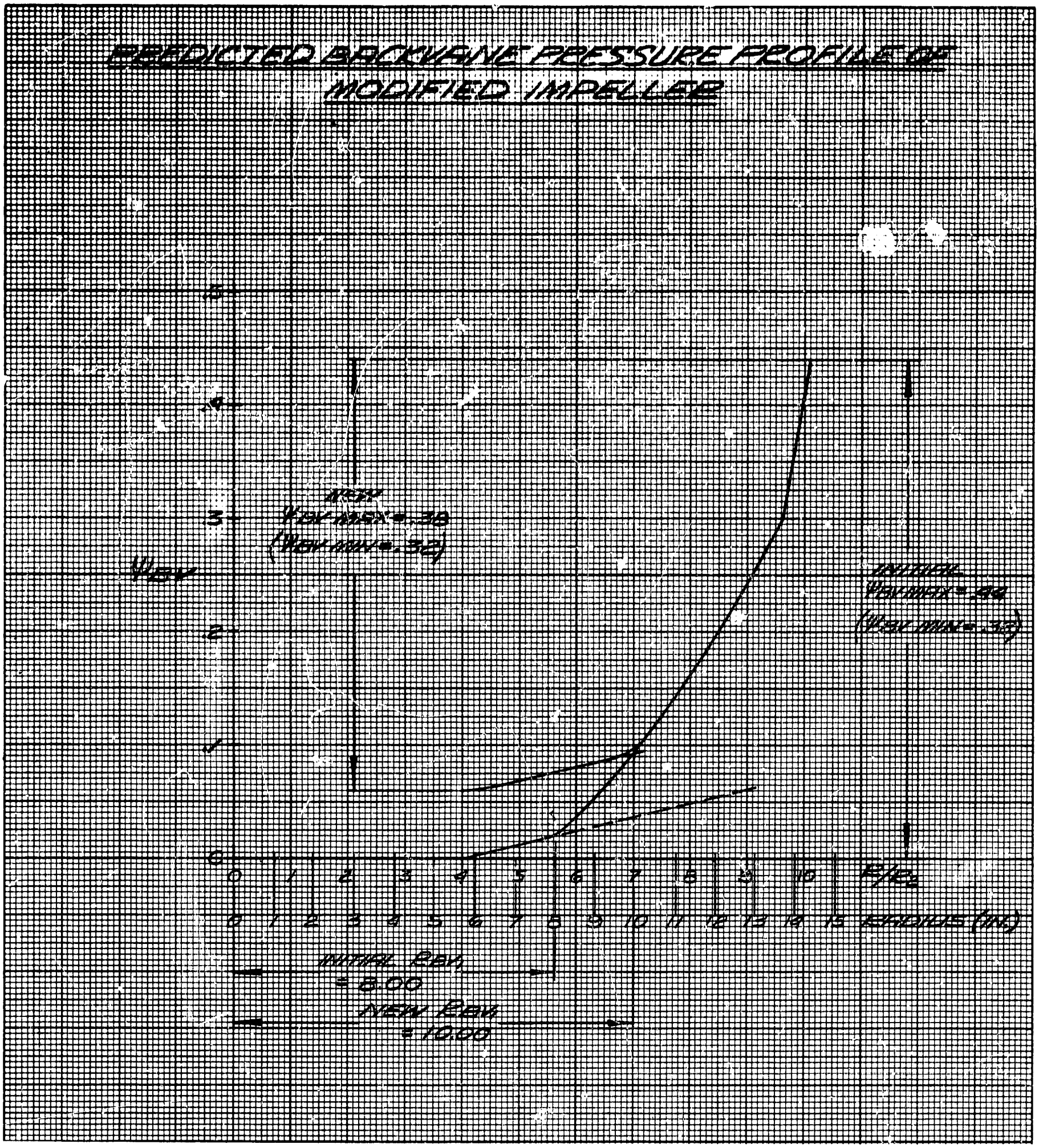

Figure 22

PREDICTED BACKVANE PRESSURE PROFILE OF MODIFIED IMPELLER

PUMPING FLUID LN_2

BACKVANE INLET RADIUS R_{BV1} = 10.0 IN.

SUCTION PRESSURE 120 PSIA

Q/N = NOMINAL

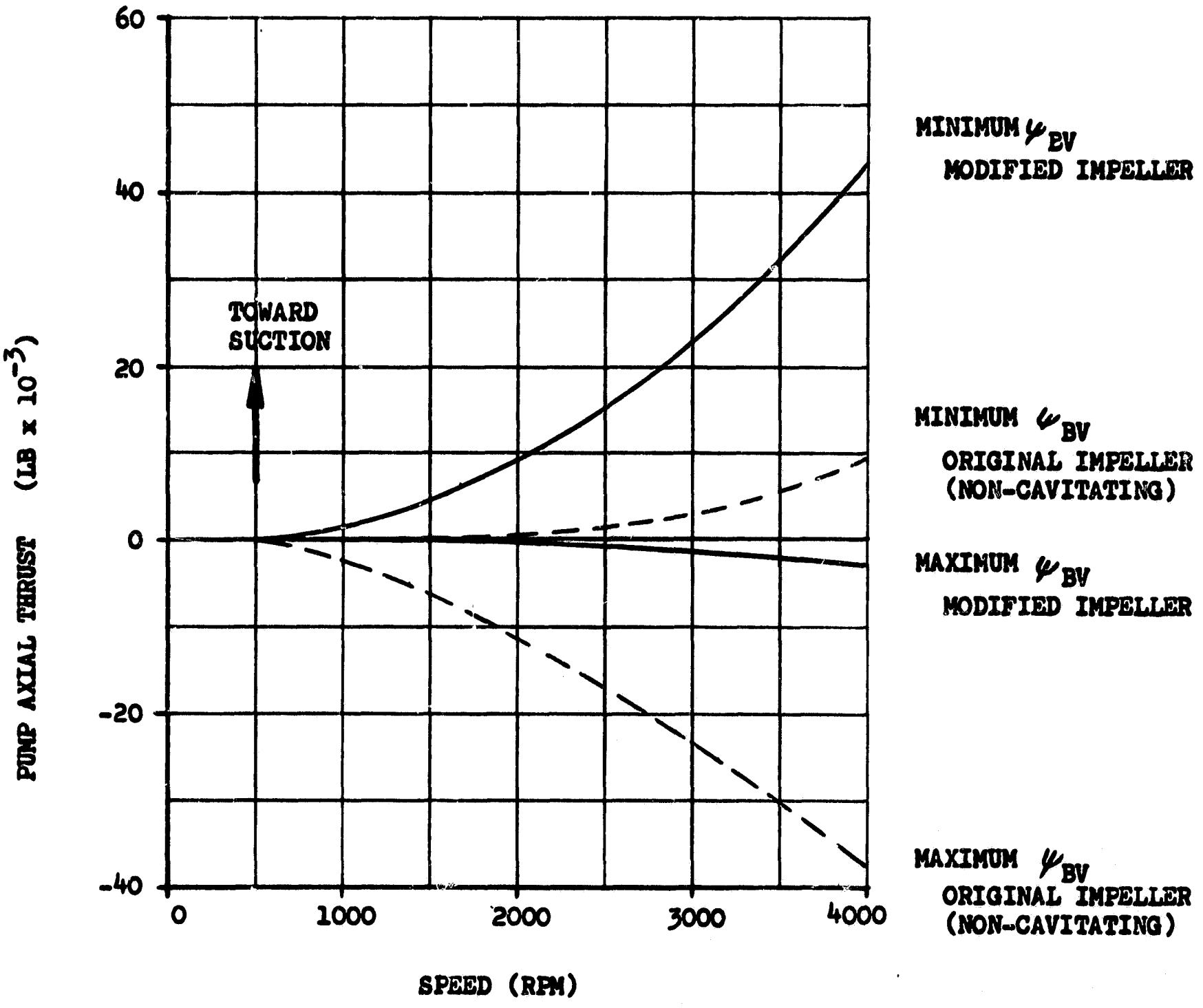

Figure 23

PREDICTED THRUST OF MODIFIED IMPELLER

b. Thrust Verification Tests

Two thrust change verification tests[2] were conducted with the subscale 24-vane initial design impeller. The test objectives were verification of backvane performance and thrust change predictions. The backvane inlet radius was increased from 3-in. to 3.6-in. ($R/R_2 = 0.675$). Thrust change predictions were established upon the same basis as those for the full size pump. Results of first tests are summarized in Table VII.

The backvane static head coefficient was approximately 5% higher than estimated. This difference was attributed to the unexpectedly high pressure generating ability of the enlarged cavity. In the predictions, the head coefficient was based upon the pressure rise in the irregularly shaped cavity and the vaneless parallel wall section. By trimming the backvanes to larger inlet diameters, the similarity of the whole vaneless area changed. Obviously, the vaneless parallel wall section performed better than the wider portion of the actual cavity. As a result of the more efficient backside pressure, the thrust was approximately 13.7% below predictions. To account for this deficiency, the backvanes of the subsequent impeller tested was trimmed to an inlet radius of 3.75 in. ($R/R_2 = 0.703$). Results of the second thrust verification test series are presented in Table VIII.

The second backvane trim of 0.15-in., performed on a different impeller with the same backside pressure had no measurable effect upon the static head coefficient.

In summary, the results of the scale tests demonstrated that predictions for thrust change and backvane performance can be verified with scale pump tests.

E. TEST RESULTS

The thrust characteristics discussed in this section are primarily those of Test Series 2, Buildup No. 2, incorporating the modified impeller with shortened backvanes. This unit was subjected to speed conditions up to design, at 85%, 100%, and 120% of design Q/N.

Results of the first low speed test series, including the flow excursions to 40% and 160% of the nominal capacity, are discussed in Section III.D. However, this data was not considered completely useful for evaluating thrust variables because of the rather low degree of accuracy at low thrust magnitudes.

All data plotted reflecting pump thrust was reduced by the computer data reduction program and therefore, is consistent and directly comparable.

The parameters affecting axial thrust are speed, pump flowrate, suction pressure, propellant density, turbine drive gas properties, turbine inlet pressure, pressure ratio, and turbine flowrate. The effects of each of these parameters upon calculated pump or turbine thrust are discussed for both transient and steady-state operation.

---

(2) ibid.

TABLE VII

RESULTS OF THE FIRST THRUST VERIFICATION TESTS

Parameter	Symbol	Unit	Original Configuration	Predicted Performance of Modified Configuration	Actual Performance of Modified Configuration
Backvane Inlet					
Radius	R_{1BV}	in.	3.0	3.6	3.6
Suction Press.	P_S	psia	87	90	88.3
Speed	N	rpm	7500	6500	6522
Backvane Flow Coefficient	ϕ_{BV}	----	0.066	0.066	0.066
Static Head Coefficient	ψ_{BV}	----	0.342	0.288	0.302
Net Pump Thrust Towards Suction	F_{AX}	lb	2960	5400	4660

TABLE VIII

RESULTS OF THE SECOND THRUST VERIFICATION TESTS

Parameter	Symbol	Unit	Predicted Performance of Modified Configuration	Actual Performance
Backvane Inlet Radius	R_{1BV}	in.	3.75	---
Speed	N	rpm	6500	6500
Backvane Flow Coefficient	BV	--	0.065	0.066
Static Head Coefficient	BV	--	0.288	0.302

1. Pump Thrust

a. Speed Effect

Design operating speeds (3635 rpm) were attained with Buildup No. 2 operating with gas generator (hydrogen-oxygen) turbine drive (see Figure 24).

A typical full-speed, full-duration test was conducted in accordance with the following speed-time diagram.

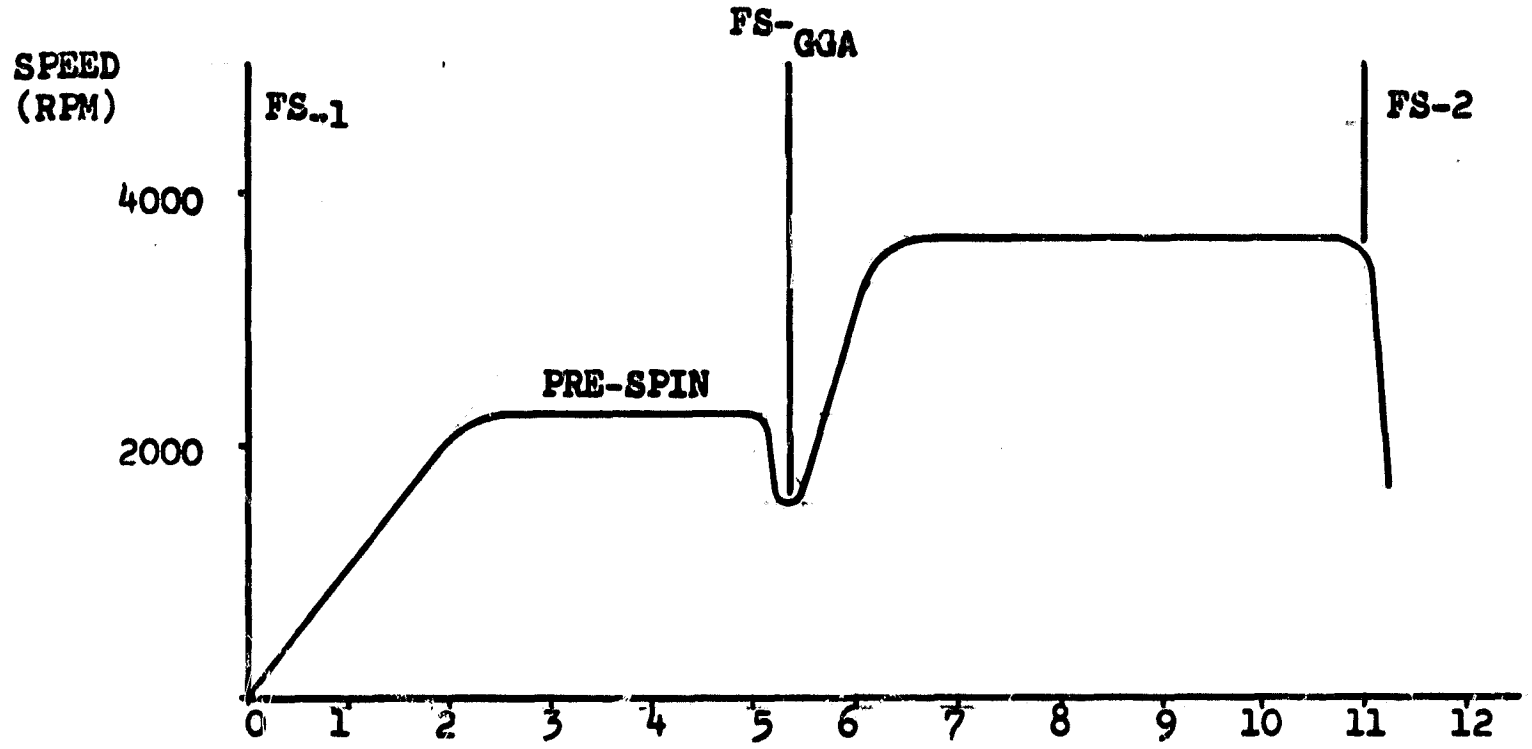

At Fire Switch One the operation of the turbopump assembly was initiated with gaseous nitrogen turbine drive to a prespin speed of 2100 rpm. This speed was maintained until gas generator assembly ignition at 5.5 sec after FS_1. At termination of the gaseous nitrogen drive phase, a usual speed drop of approximately 700 rpm occurred because of the timing of the gaseous nitrogen drive valve. Acceleration to full speed was very rapid and varied between 7000 and 12,000 rpm/sec depending upon the terminal speed and power balance. The steady-state, full speed duration of approximately 5 sec was limited by the capacity of the on-stand pump fluid tankage. Steady-state data was determined at two speeds in each test (i.e., during the latter portion of both the gaseous nitrogen and gas generator drive phases).

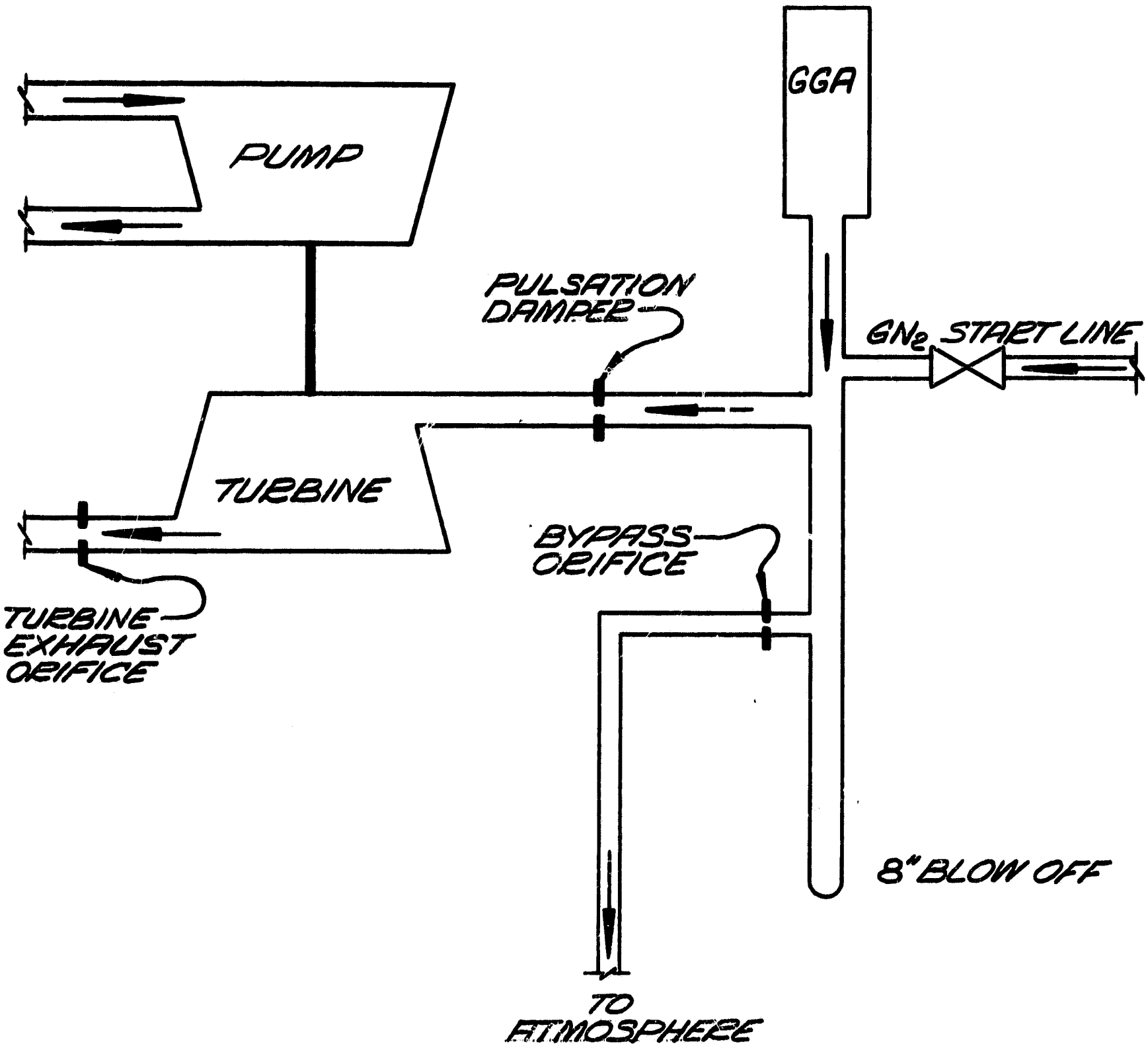

Figure 24

TURBINE DRIVE SYSTEM

The effect of speed upon pump thrust is illustrated in Figure 25. Lines of constant flow-speed ratios (Q/N) are presented for 85%, 100%, and 120% of design Q/N. All thrust values plotted are computed from steady-state data. The scale factors relating thrust at full speed to thrust during prespin with regard to speed are as follows:

$$F_{AX2} \text{ at } 85\% \text{ Design } Q/N = F_{AX1} \times \left[\frac{N_2}{N_1}\right]^{2.5}$$

$$F_{AX2} \text{ at } 100\% \text{ Design } Q/N = F_{AX1} \times \left[\frac{N_2}{N_1}\right]^{2.61}$$

$$F_{AX2} \text{ at } 120\% \text{ Design } Q/N = F_{AX1} \times \left[\frac{N_2}{N_1}\right]^{2.81}$$

The exponents of the speed ratios are considerably greater than those determined for the ideal thrust, which for 85%, 100%, and 120% of design Q/N amounted to only 2.135, 2.17, and 2.22. A comparison of actual and ideal thrust is shown in Figure 26 and thrust values extrapolated for design speed (3635 rpm) are presented in Table IX.

Although slightly higher than predicted thrust values were expected, the difference between actual and ideal thrust was considerably larger than anticipated. To obtain an explanation for the rather large discrepancies, a logical approach was to compare pressure profiles, because thrust was directly computed from pressure forces. The normalized pressure profiles for impeller frontside and backside at equal flow-speed ratios and different speeds are shown in Figures 27 through 29. All plots indicate decreasing pressure gradients on the impeller backside with increasing speed (Figures 27 and 29). The pressure profiles of the frontside for 85% and 100% of design Q/N normalized well while those for the higher flowrates (120% of design Q/N) shifted slightly upwards near the impeller discharge. An attempt was made to relate the decrease in the pressure gradient on the impeller backside and increasing speed with a temperature increase as a result of fluid heating in the backvanes. The cavity temperature TOBV-1, which was the only temperature measured on the backside, did not reflect the temperature rise of the fluid through the backvane system; it only measured the temperature of the flow entering the cavity. The temperature of this flow increased because the bearings developed more heat as speed and loads increased. Heat was dissipated by the coolant flow which increased the temperature of the fluid entering the cavity. The increase in temperature, or respectively the decrease in density of the fluid in the cavity, based upon cavity temperature, was not significant. However, the relationship of speed and fluid density in the cavity agreed with that of speed and measured pressure differentials when $\Delta P_{BV}/\rho =$ constant at all the speeds investigated. The fact that unequal temperature gradients were prevailing on impeller frontside and backside can be demonstrated by

Heat = Energy Loss

TABLE IX

COMPARISON OF ACTUAL AND IDEAL PUMP THRUST
AT FULL SPEED (3635 rpm)

% Design Q/N	Ideal Thrust (lb) (1)	Actual Thrust (lb) (1)	% Difference Exceeding Ideal Thrust
85	55,000	69,500	26.3
100	46,500	59,700	28.4
120	40,000	57,000	42.5

(1) Positive thrust directed towards suction.

M-1 - OTPA B/U 2

STEADY STATE PUMP THRUST

AXIAL THRUST VS SPEED AT NOMINAL SUCTION PRESSURE

TEST SERIES 1.2.08-EHP

SYMBOL	RUN	TIME (SEC)	% DES Q/N	P_{OS} (PSIA)
□	001	15.276 - 15.776	97.3	112
○	002	12.288 - 12.788	98	110
◇	003	8.854 - 9.354	99	110
◇	004	12.218 - 12.718	99.5	110
▽	006	4.805	99	111
△	006	10.233 - 10.733	85.5	110
◇	007	4.500 - 5.000	99	111
○	008	4.500 - 5.000	120	112.4
○	009	4.500 - 5.000	119	110
■	009	10.430 - 10.930	120.6	102.5
■	010	4.500 - 5.000	99.8	112.5
■	010	10.400 - 10.900	100.5	105
◇	011	8.950 - 9.450	99.4	110.4
◇	012	6.501 - 7.525	122.8	108.6
◇	012	13.521 - 14.494	101.5	109
◇	012	19.342 - 19.842	81	110.5
▽	013	4.500 - 5.000	119.6	111
▽	013	10.433 - 10.933	120.5	99
▷	014	4.500 - 5.000	85.2	116
▷	014	6.356	85	111.5

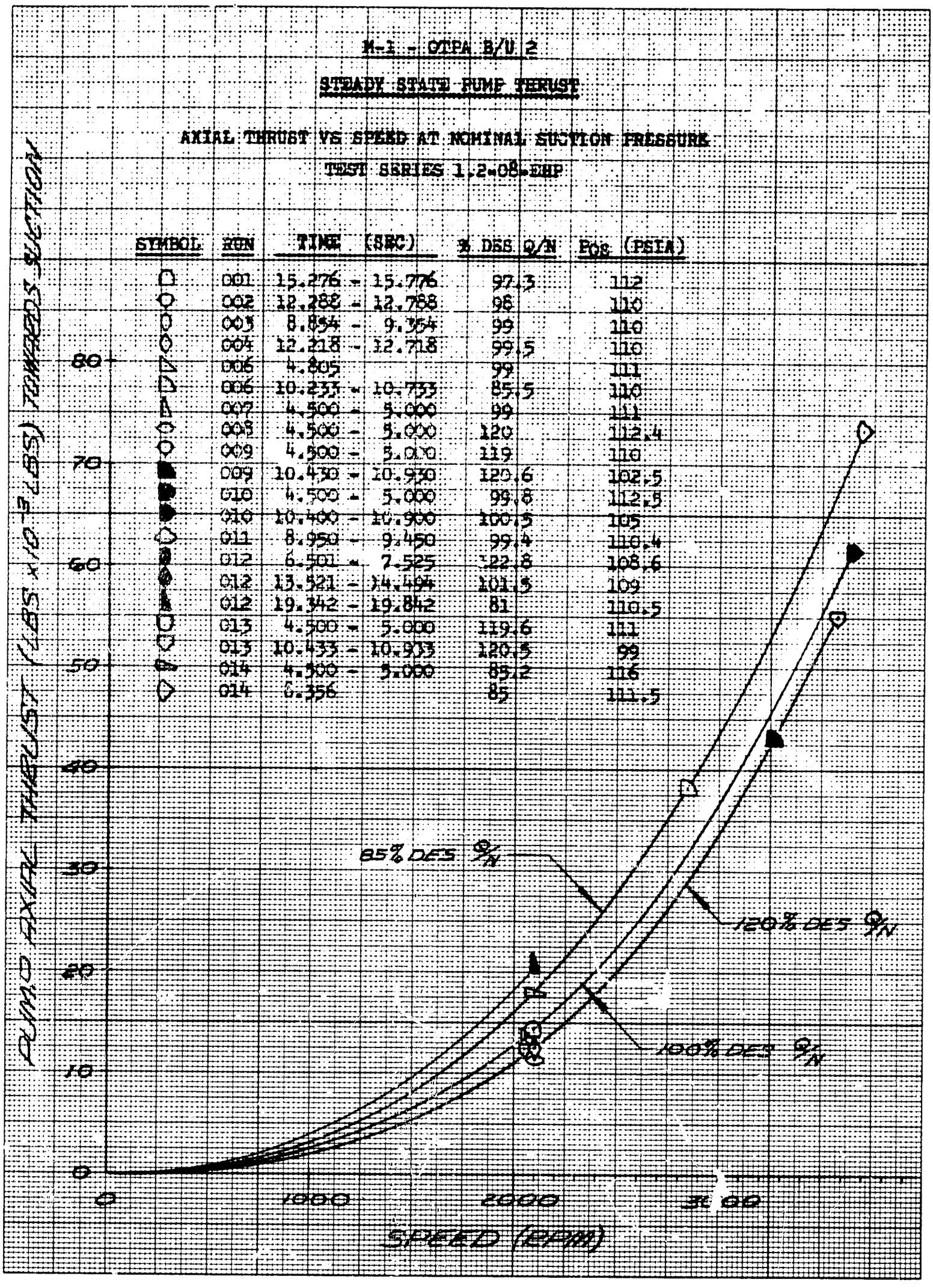

Figure 25

M-1 OTPA, B/U 2, STEADY-STATE PUMP THRUST

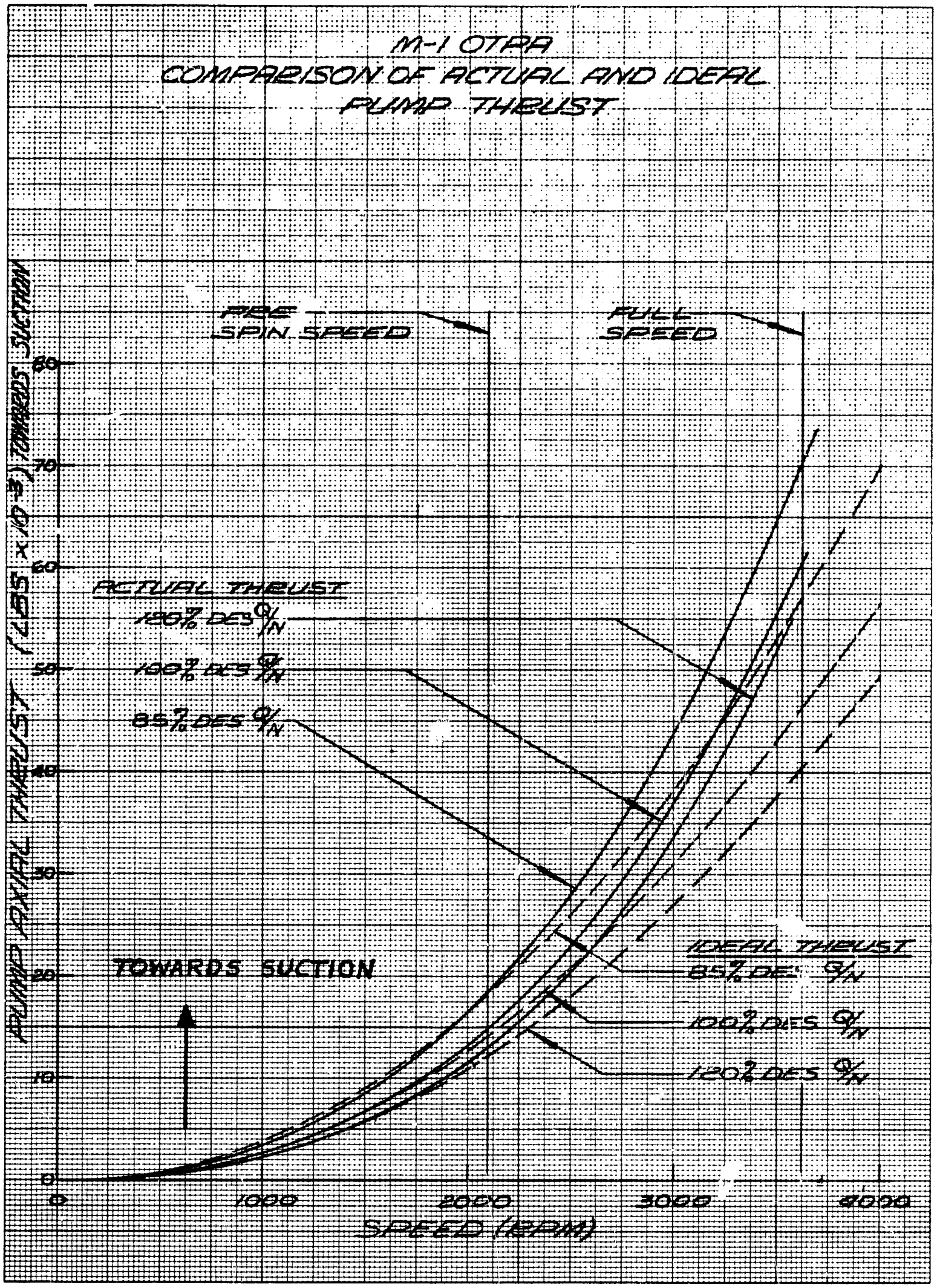

Figure 26

M-1 OTPA COMPARISON OF ACTUAL AND IDEAL PUMP THRUST

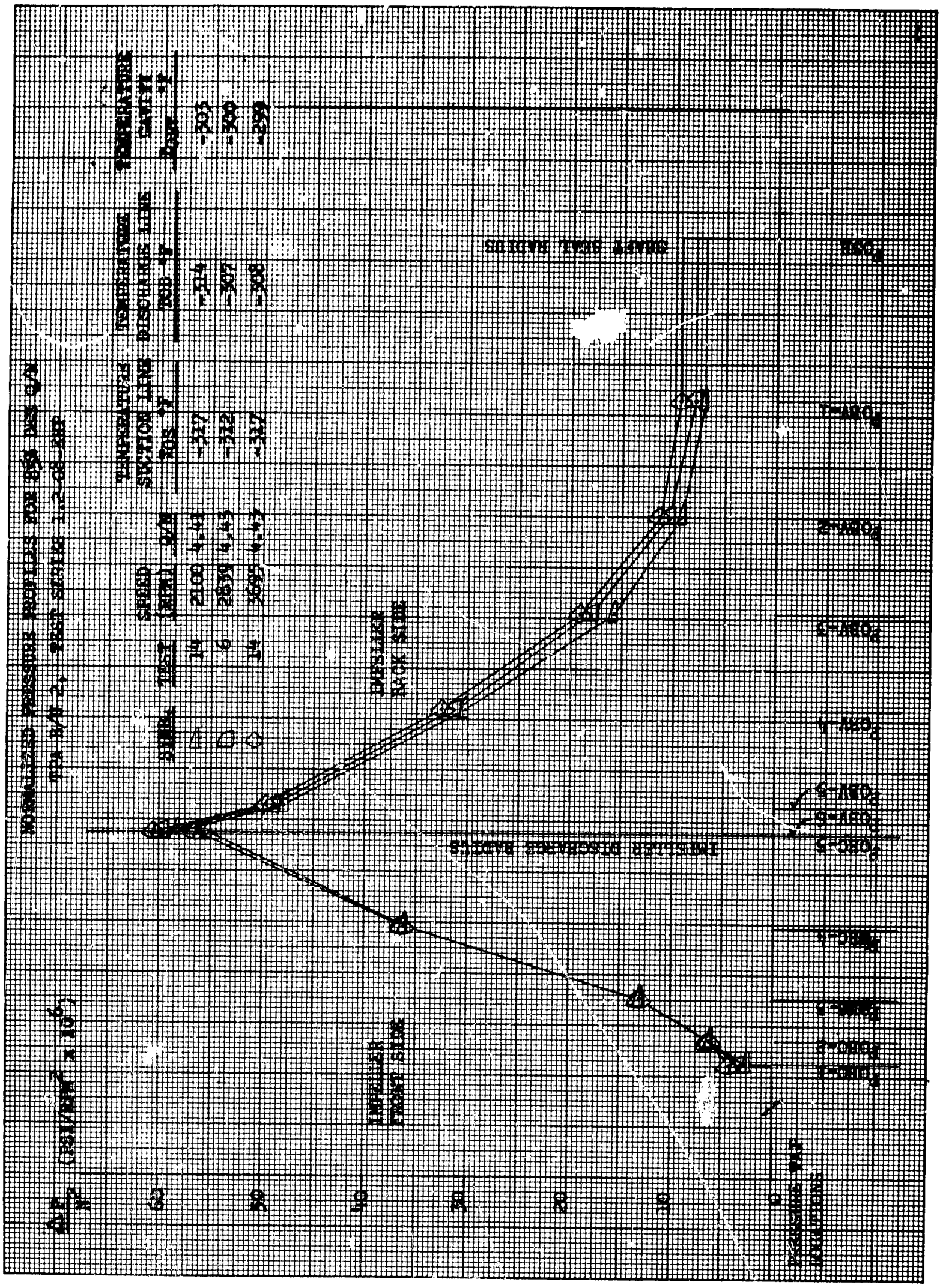
Figure 27
NORMAL PRESSURE PROFILES FOR 85% OF DESIGN Q/N OTPA B/U 2
Page 60

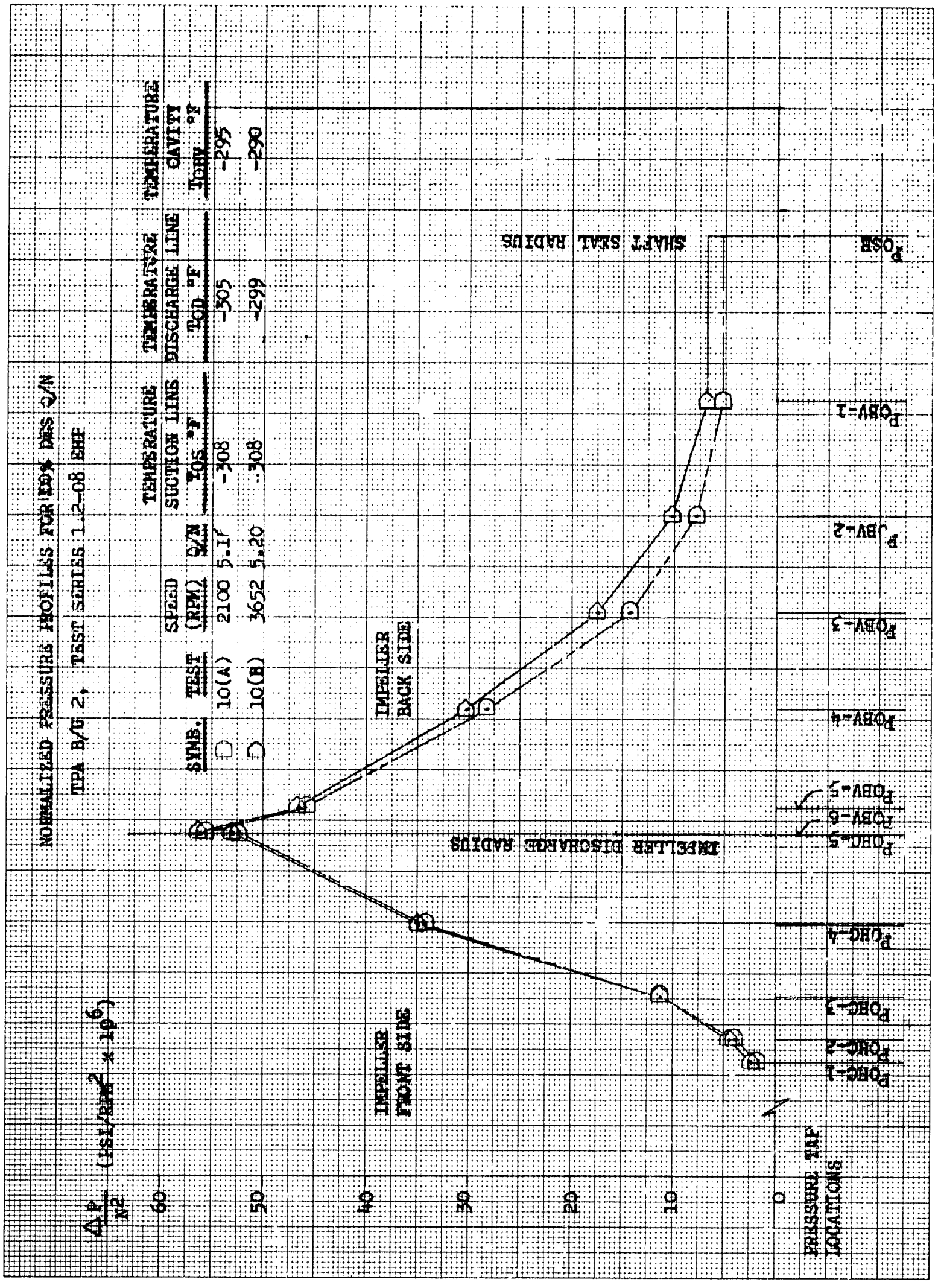

Figure 28

NORMAL PRESSURE PROFILES FOR 100%
OF DESIGN Q/N OTPA B/U 2

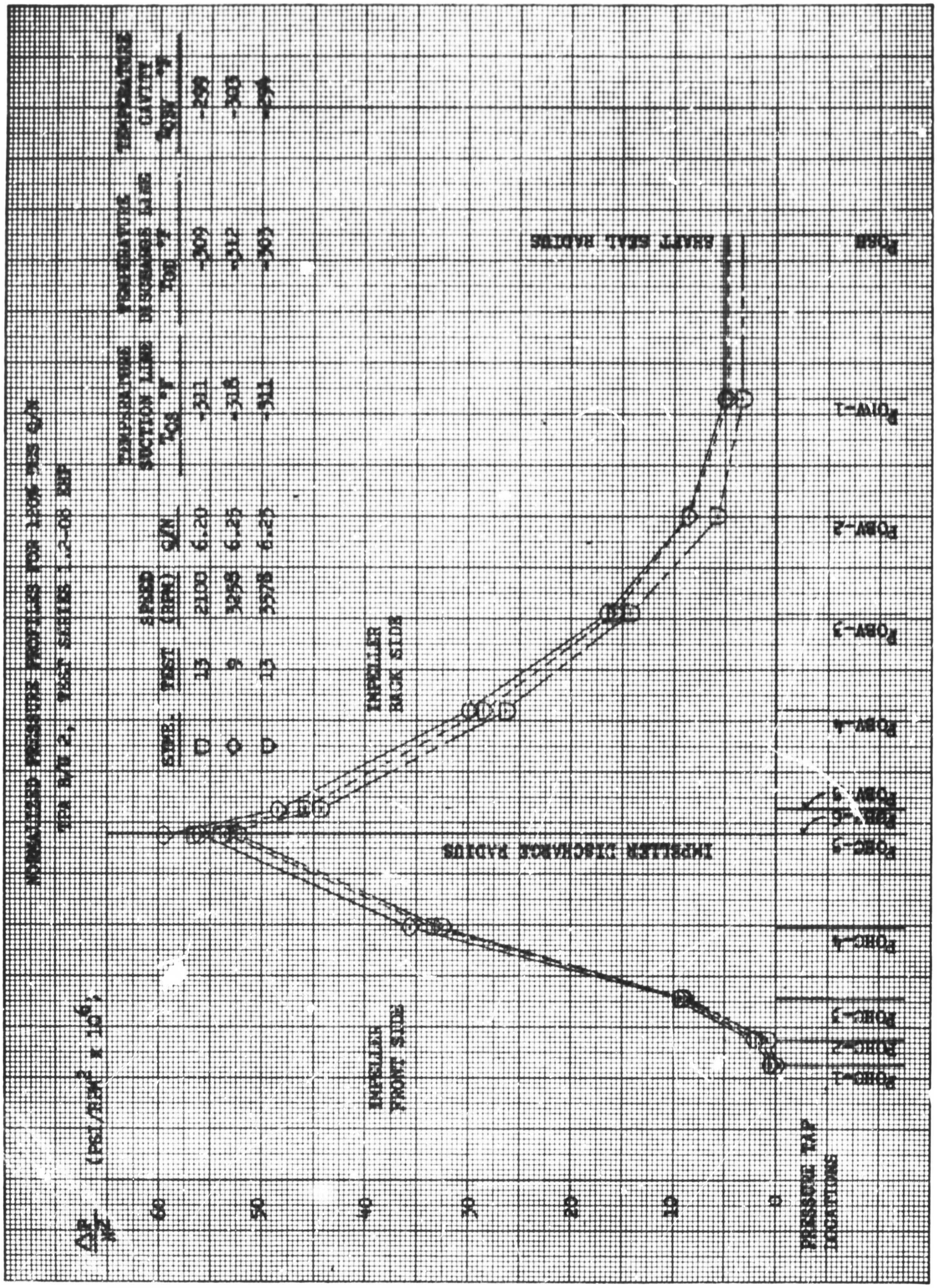

Figure 29

NORMAL PRESSURE PROFILES
FOR 120% OF DESIGN Q/N

or:

$$\dot{w}\, c_p\, \Delta T = \rho Q H\, (1 - \eta_h)$$

$$\dot{w}\, c_p\, \Delta T = \dot{w}\, \frac{\Delta P}{\rho}\, (1 = \eta_h)$$

substituting $K_p\, \rho\, \psi\, N^2$ for ΔP:

$$\Delta T = \frac{K_p \psi}{c_p}\, N^2\, (1 - \eta_h)$$

Applying this to impeller frontside and backside, the ratio of the temperature gradients is:

$$\frac{\Delta T_B}{\Delta T_F} = \frac{K_{p,B}\, c_{p,F}\, \psi_B}{K_{p,F}\, c_{p,B}\, \psi_F} \qquad \frac{(1 - \eta_{h,B})}{(1 - \eta_{h,F})}$$

This expression can be simplified by neglecting the nearly equal factors C_{pF} and C_{pB}, ψ_B and ψ_F and the constants $K_{p,B}$ and $K_{p,F}$.

Thus:

$$\frac{\Delta T_B}{\Delta T_F} \approx \frac{1 - \eta_{h,B}}{1 - \eta_{n,F}}$$

To be compared are hydraulic efficiencies expressed in terms of power:

$$\eta_h = \frac{Q \rho H}{Q \rho H + (Q \rho h_l)/\eta_{VOL}} = \frac{H}{H + h_l/\eta_{VOL}}$$

Estimated values for $\eta_{h,F}$ and $\eta_{h,B}$ are:

$$\eta_{h,F} = 0.85$$

$$\eta_{h,B} = 0.15$$

Hence:

$$\frac{\Delta T_B}{\Delta T_F} \approx \frac{1 - 0.15}{1 - 0.85} = 5.67$$

Temperature differentials of 3°F to 5°F across the backvanes were measured on the three-eights scale pump operating with cold water. The temperature rise of the frontside of the scale impeller estimated from temperature measurements taken at the suction and discharge line amounted to approximately 1/2°F. As a result, the ratio of temperature rise of backside and frontside varied between six and 10 and thus, exceeded the value estimated for the full size pump.

b. Conclusion

Based upon the above considerations, the temperature rise on the impeller backside was at least five times higher than on the frontside of the impeller. Because the backvanes operated near the shut-off point, it is concluded that a considerably higher backvane flow would have been required to obtain any significant increase in backvane efficiency to balance the temperature rise of the impeller frontside and backside.

c. Verification of Effect of Change in Temperature Rise Upon Backvane Pressures

A change in temperature rise of 7°F between the pump suction and discharge was measured in Test No. 10 from prespin to full speed. Assuming that losses in collector and impeller were almost equally divided, the change in temperature rise on the impeller frontside can be estimated at 3.5°F and that of the backside according to the proceeding conclusion at 5.67 x 3.5 = 20°F. Because of the measured temperature increase in the cavity of 5°F, the discharge temperature of the backvane system increased by a total of 25°F. If the mean temperature for the vaned section rises by 18°F, the following densities can be assumed:

Speed (rpm)	Mean Density* (lb/ft^3)	Backvane Pressure Gradient (Vaned Section) P_{BV6-3}/N^2 (psi/rpm^2)
2100	45.5	4.13×10^{-5}
3650	43.5	3.91×10^{-5}

* Pressure effect upon fluid density considered for mean pressure level.

The temperature effect decreases the pressure gradient at full speed by the ratio of densities:

$$\Delta P_{BV}/N^2 \text{ full speed} \approx \frac{\rho \text{ free spin}}{\rho \text{ full speed}} \times \frac{\Delta P_{BV}}{N^2}_{\text{free spin}}$$

or: $$4.13 \times 10^{-5} \approx \frac{45.5}{43.5} \times 3.91 \times 10^{-5} = 4.09 \times 10^{-5}$$

It is concluded that the decrease in backvane pressure gradients with increasing speeds was the result of the decrease in fluid density caused by the combined effect of additional inefficiency heating in the backvanes and added bearing heat input. An increase in by-pass flow of 200% to 300% would mainly limit the temperature rise in the seal cavity and therefore, have little effect upon the temperature unbalance of impeller frontside and backside.

Minor profile shifts, as shown in Figure 29 were also the result of small variations in the difference of tip pressures between frontside and backside housing walls. The term $(P_{BV6} - P_{HC5})/N^2$, which relates the frontside to the backside pressure profile, was investigated together with the circumferential pressure distributions (Figures 17, 18, and 19) for stability at different speeds and flowrates. The results revealed no significant profile deviations. Differences in profile levels at constant Q/N were caused by temperature and compressibility effects on fluid density. Evidence of scale effects (departure from affinity laws) was not discounted but could not be determined from the limited number of full speed tests and available instrumentation.

d. Flowrate

The effect of pump flowrate upon axial thrust is presented in Figure 30, which shows thrust over speed squared as a function of the discharge flow coefficient ϕ_2'. As thrust does not scale with N^2, two characteristics were obtained; one for prespin and one for full speed. Both curves reflect the nonsymmetrical variation of off-design thrust as indicated by the change in slopes of the two curves near the design flow coefficient. Thrust characteristics of the scale pump confirmed this trend (see Figure 31).

At constant speeds and suction pressure, thrust increases with decreasing flow according to the head-flow characteristic of the pump. However, as the pressure rise of the frontside varies with flow, the pressure gradient of the impeller backside remains constant. Discounting temperature effects, the rear cavity pressure and all backvane pressures vary directly with the impeller discharge pressure. Thus, the pressure force of the impeller backside is proportional to the impeller discharge pressure, whereas the frontside pressure force, which is dependent upon the fixed suction pressure as well as on the varying discharge pressure, changes at a lesser rate than the backside pressure force. As a result, thrust directed towards suction increases as flow decreases.

The thrust-flow characteristics of Buildup No. 1 and 2 are compared in Figure 32. Both curves indicate the same trend at capacities below that indicated by the design flow coefficient. Pump thrust at the minimum and maximum test flowrate (40% and 160% of design Q/N) was of low magnitude and accuracy level. The general thrust trend over an extended flow range can best be demonstrated by the thrust-flow relationship obtained with the scale pump impeller. Based upon all of the characteristics evaluated, it can be concluded that the backvanes trimmed to the optimum inlet diameter for nominal flowrates could also balance axial thrust at pump shutoff within structurally acceptable magnitudes. The desired optimum thrust-flow characteristic is denoted by the dotted line in Figure 32.

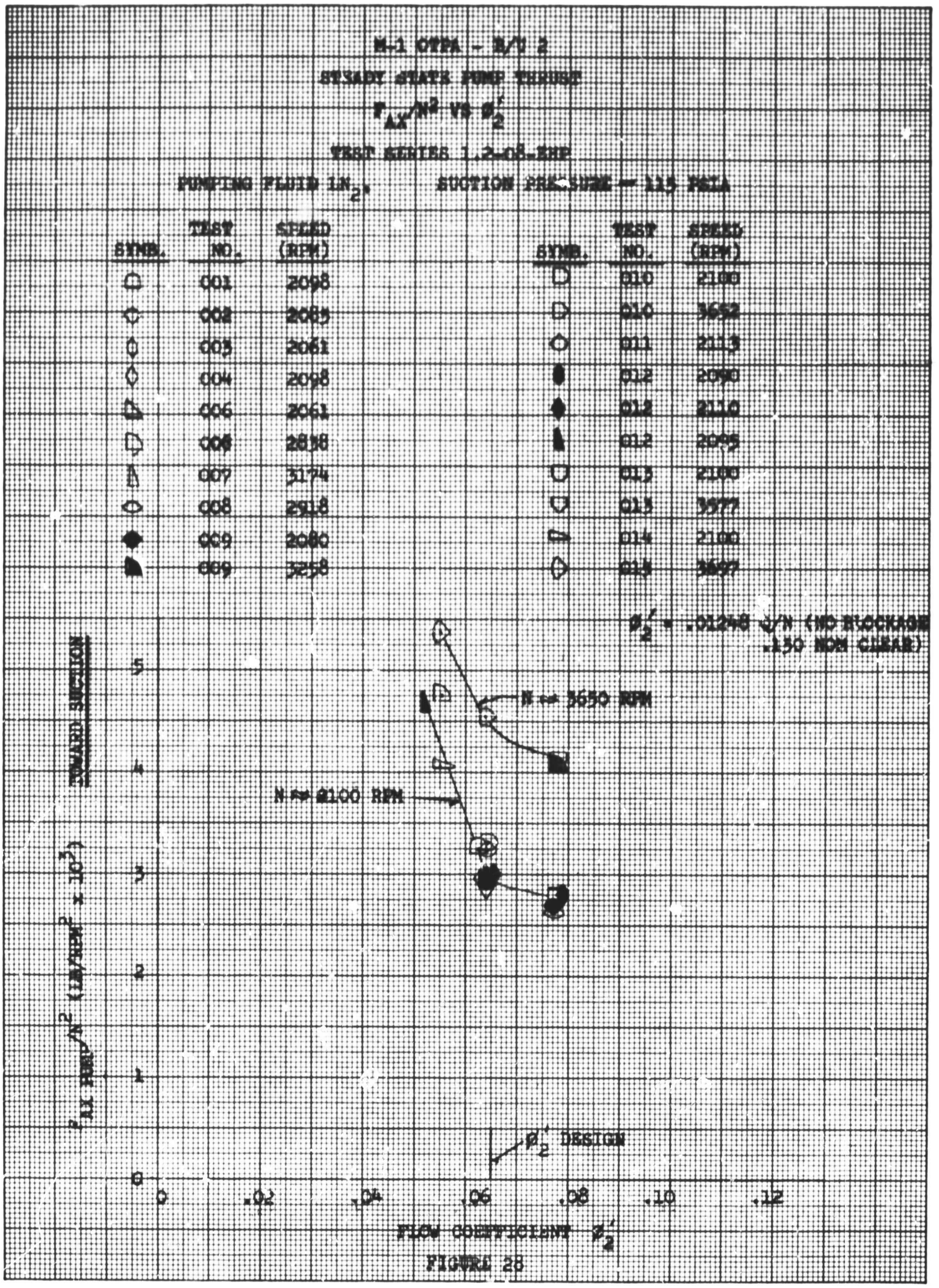

Figure 30

M-1 OTPA, B/U 2, STEADY-STATE PUMP THRUST

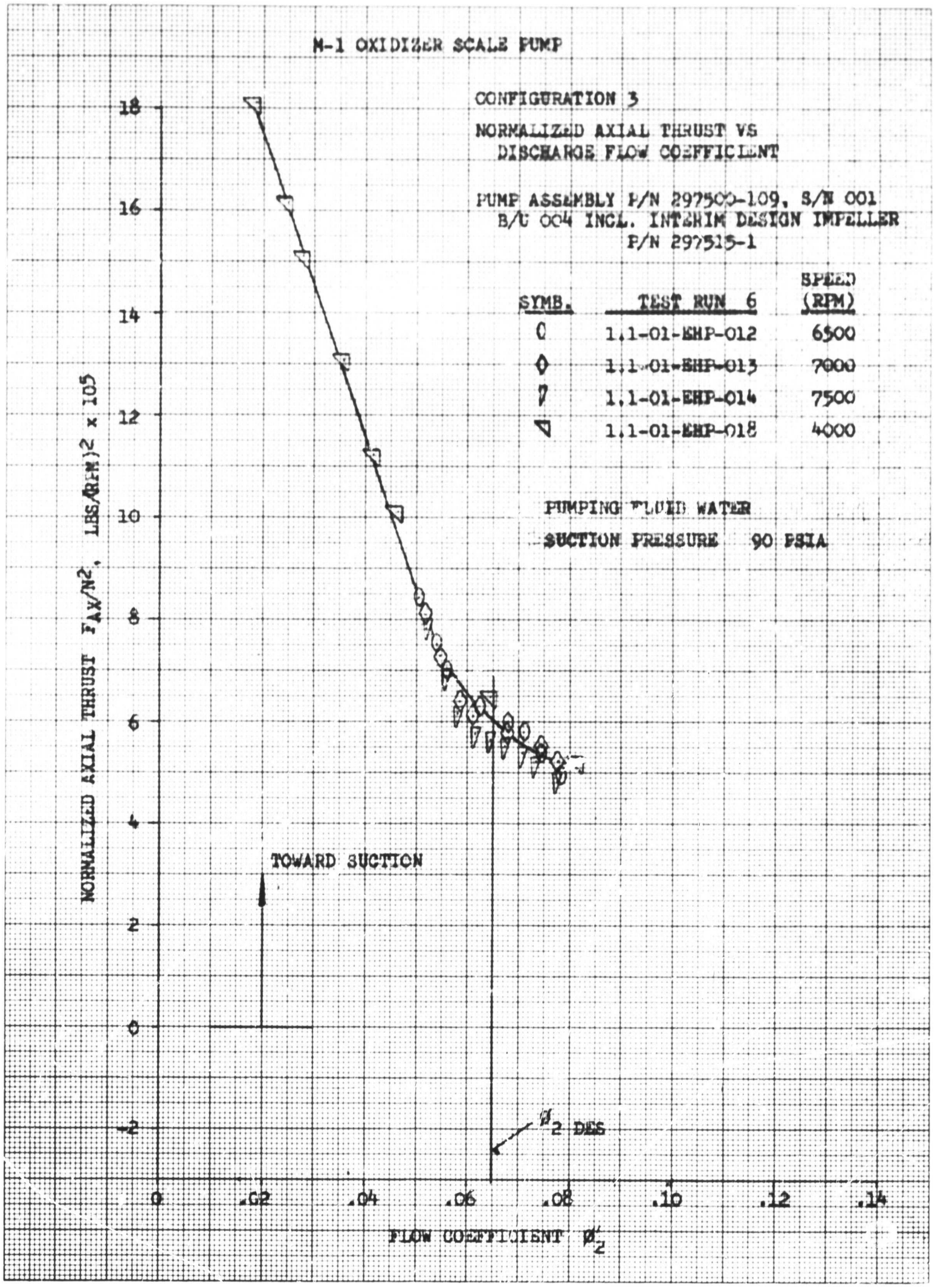

Figure 31

M-1 OXIDIZER SCALE PUMP

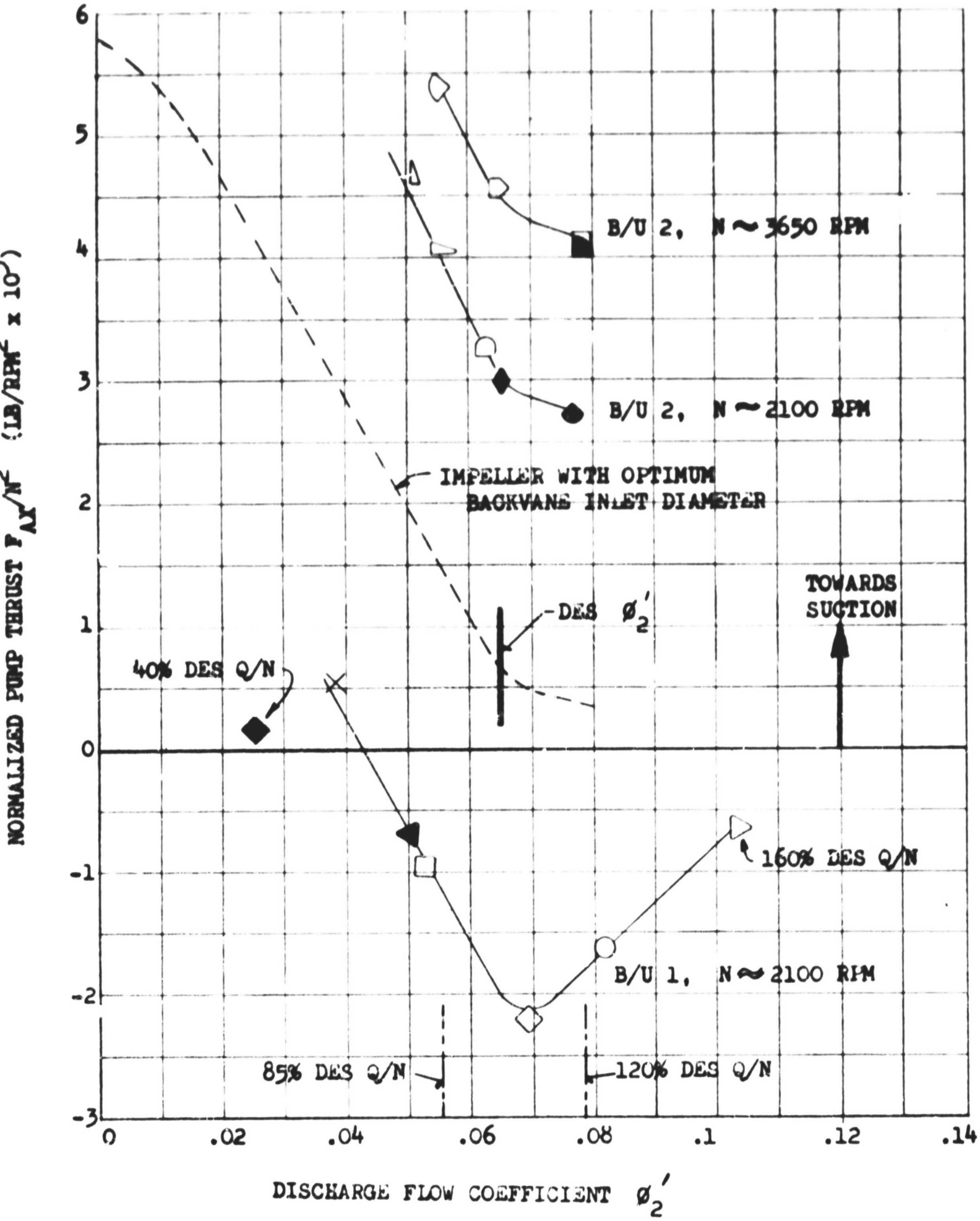

Figure 32

COMPARISON OF THRUST-FLOW RELATIONSHIP
OF PUMP BUILDUP 1 AND 2

e. Suction Pressure

No attempts were made during the second test series to intentionally vary suction pressure. However, during rapid accelerations to full speed a decrease in suction pressure of approximately 10 psi was not unusual. As explained in Section III.C. such a pressure loss affects only the thrust component caused by suction pressure: $F_S = P_S A_{SH}$. A 10 psi drop in suction pressure would decrease the end thrust by approximately 200 lb, a negligible magnitude in the calculation of axial thrust.

f. Fluid Density

The density of liquid nitrogen decreases with increasing temperature and also to a minor extent with decreasing pressure (see Figure 33). The decrease in fluid density caused by the increase in fluid temperature from pump suction to pump discharge was virtually offset by the decrease in density resulting from the increase in fluid pressure. Therefore, the fluid inlet density was approximately equal to the pump discharge density. The effect of fluid density upon pump thrust as a result of temperature changes is discussed in Section III.E.

As thrust is directly proportional to density, the thrust magnitudes for liquid oxygen operation can be estimated by scaling the thrust values for liquid nitrogen by the ratio of the densities $\rho LO_2/\rho LN_2 = 1.5$. By applying this factor to the thrust values obtained from the liquid nitrogen tests, the resulting thrust loads will undoubtedly exceed the load carrying capability of the bearings. Thus, for liquid oxygen operation, a new impeller will have to be provided with a somewhat smaller backvane inlet diameter.

g. Conclusions From Pump Thrust Evaluation

Pump thrust at full speed was 26% to 42% higher, depending on Q/N, than the predicted ideal thrust based upon determined thrust values at gaseous nitrogen drive speeds. This deficiency was attributed to a substantial temperature rise of the backvane flow because of the inefficiency of the backvane system. The static head coefficient of the impeller backside agreed with the predicted minimum value of 0.32. This minimum value resulted from a 32% reduction in backvane diffuser performance. This was caused by an increase in axial clearance between impeller disc and backvane diffuser blades on Buildup No. 2 when compared with Buildup No. 1. Because of this, pump thrust was significantly higher than that predicted for the modified impeller (see Figure 23).

2. Turbine Thrust

Normalized turbine thrust is plotted against turbine inlet pressure in Figure 34. The data can be divided into four different groups, depending upon the drive gas and turbine exhaust orifice. Each group falls on a curve that varies with turbine inlet pressure P_{OTTIC}. The four groups of data are summarized in Table X.

TABLE X

COMPARISON OF TURBINE THRUST DATA

Test No.	Gas	Pressure Ratio $PR=P_{OTTIC}/P_{OTRE}$	Exhaust Orifice ($in.^2$)	Thrust Direction	Relative Thrust Magnitude***
1 through 4*	GN_2	3.1	314	Downstream	Highest
5, 11, 12**	GN_2	2.3	240	Downstream	Moderate to High
6 through 10	H_2O_2	2.4	240	Upstream	Low
13, 14	H_2O_2	3.5	314	Downstream	Moderate

* Also prespin state of Test No. 13 and 14.
** Also prespin state of Test No. 6 through 10.
*** Based upon a common inlet pressure.

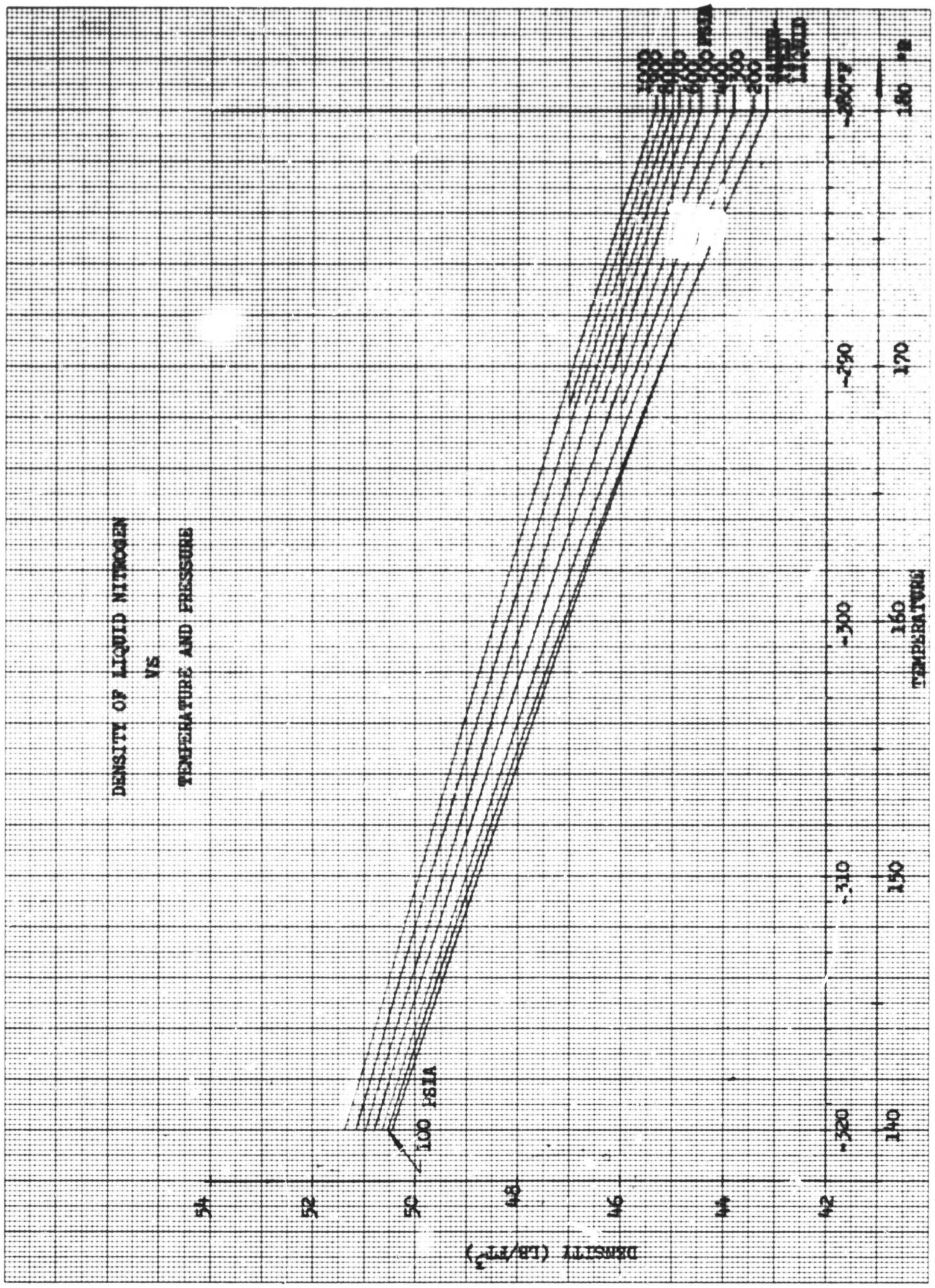

Figure 33

DENSITY OF LIQUID NITROGEN
VS TEMPERATURE AND PRESSURE

SYMB.	TEST NO.	SPEED (RPM)	EXHAUST ORIFICE (SQ.IN.)	SYMB.	TEST NO.	SPEED (RPM)	EXHAUST ORIFICE (SQ.IN.)
	001	2098	314		009A	2080	240
	002	2085	314		009B	3259	240
	003	2062	314		010A	2102	240
	004	2099	314		010B	3653	240
	005	2382	240		011	2110	240
	006A	2061	240		012A	2101	240
	006B	2839	240		012B	2103	240
	007A	2063	240		012C	2100	240
	007B	3176	240		013A	2100	314
	008A	2089	240		013B	3577	314
	008B	2580	240		014	3697	314

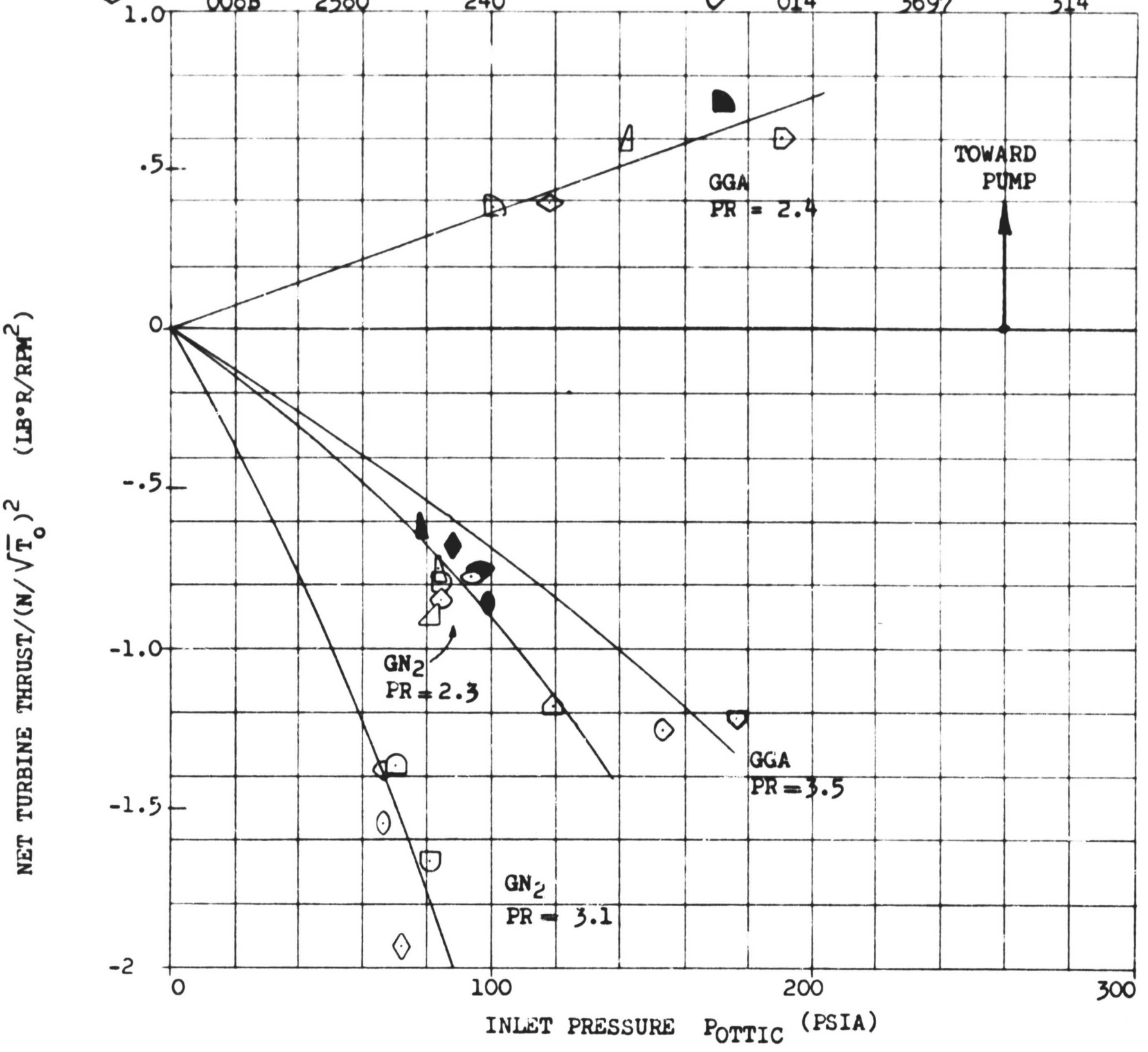

Figure 34

AXIAL THRUST OF MODEL I TURBINE

The larger exhaust orifice was selected for the last two tests to obtain some reaction in the rotor and thereby use the turbine to assist the backvanes in balancing the net thrust. Turbine thrust was significant at off-design conditions of the gaseous nitrogen drive. At prespin (2100 rpm, gaseous nitrogen), reaction in the turbine rotor resulted in a pressure differential across the blade of approximately 8 to 10 psi with the 240-in.^{2} orifice installed in the exhaust line. This pressure differential causes a significant downstream thrust, which grows larger with increasing inlet pressure and/or pressure ratio. Calculated thrust values are summarized in Table XI.

Impulse conditions were obtained during Test No. 6 through 10 with gas generator (hydrogen-oxygen) turbine drive. Thrust towards the pump under these conditions was appreciable because of radial equilibrium assumed at the rotor inlet which resulted in a large radial pressure gradient. Thus, the axial thrust of a large turbine rotor can be significant even under impulse conditions.

3. Comparison of Calculated and Measured Thrust

A comparison of calculated pump and turbine thrust with measured thrust is presented in Table XI for the second test series. Typical agreement obtained was within 10% for magnitudes in excess of 15,000 lb. This was satisfactory when considering the inconsistencies of the measuring system and the effects of small variation in pressure forces as discussed in Section III.C.

Data from the Bentley distance detectors installed on the impeller backside for clearance monitoring during testing showed good agreement in trends; however, magnitudes cannot yet be determined because of unresolved calibration problems.

4. Transient Thrust

Pump and turbine thrust as well as measured and calculated net thrust are plotted versus time on Figures 35 through 37 to represent the start transients of Test No. 1, 4, and 6.

Inconsistencies, such as flow and pressure lags, resulting in thrust peaks were observed during these tests. Such occurrences were reduced or eliminated after the proper adjustments were made to control transient excursions of Q/N. Some major problems encountered and their effects upon axial thrust are presented in the following discussion.

a. Unstable Q/N

Difficulties with the Q/N control during Test No. 1, Series 2, (Figure 35) resulted in a thrust spike exceeding thrust magnitudes at steady-state operation by 50%. The cause was attributed to a lag in flowrate at a relatively high speed, which resulted in a lower than desired flow-speed ratio. All housing contours and backvane pressures followed the trend of the measured thrust. This effect emphasizes the importance of maintaining constant Q/N ratios during start transients to eliminate large thrust fluctuations.

TABLE XI

OTPA AXIAL THRUST SUMMARY
TPA B/U 2 SECOND TEST SERIES

Comparison of calculated steady-state pump turbine thrust with measured thrust.

Run No.	Speed	Q/N (1)	F_{AX}-Pump Computer (lb) (4)	F_{AX}-Pump Calculated(2) (lb) (4)	F_{AX} - Turbine (lb) (4)	F_{AX}-Net(3) (lb) (4)	F_{AX} - Measured (lb) (4)
1	2098	5.04	14,290	16,480	-13,060	1230	-5500
2	2085	5.07	12,900	11,000	-12,300	600	-5000
3	2061	5.12	12,500	10,600	-13,420	-920	-5000
4	2098	5.15	12,560	10,500	-17,330	-4770	-9000
6	2838	4.43	38,200	35,200	2300	40,500	41,000
9	3258	6.25	43,300	41,500	6300	49,600	40,000
10	3652	5.2	61,650	59,700	6300	67,950	65,000
11	2113	5.15	14,450	N/A	-7300	7150	-2500
12	2095	4.20	20,420		-7100	13,320	3500
13	3577	6.25	55,050	52,700	-13,550	41,500	32,000
14	3697	4.43	73,400	70,370	-13,000	60,400	62,000

---

(1) Design Q/N = 5.18.

(2) Based upon straight line pressure profiles.

(3) F_{AX} - Net = F_{AX} - Pump Computer + F_{AX} - Turbine.

(4) Thrust directed towards suction is considered positive.

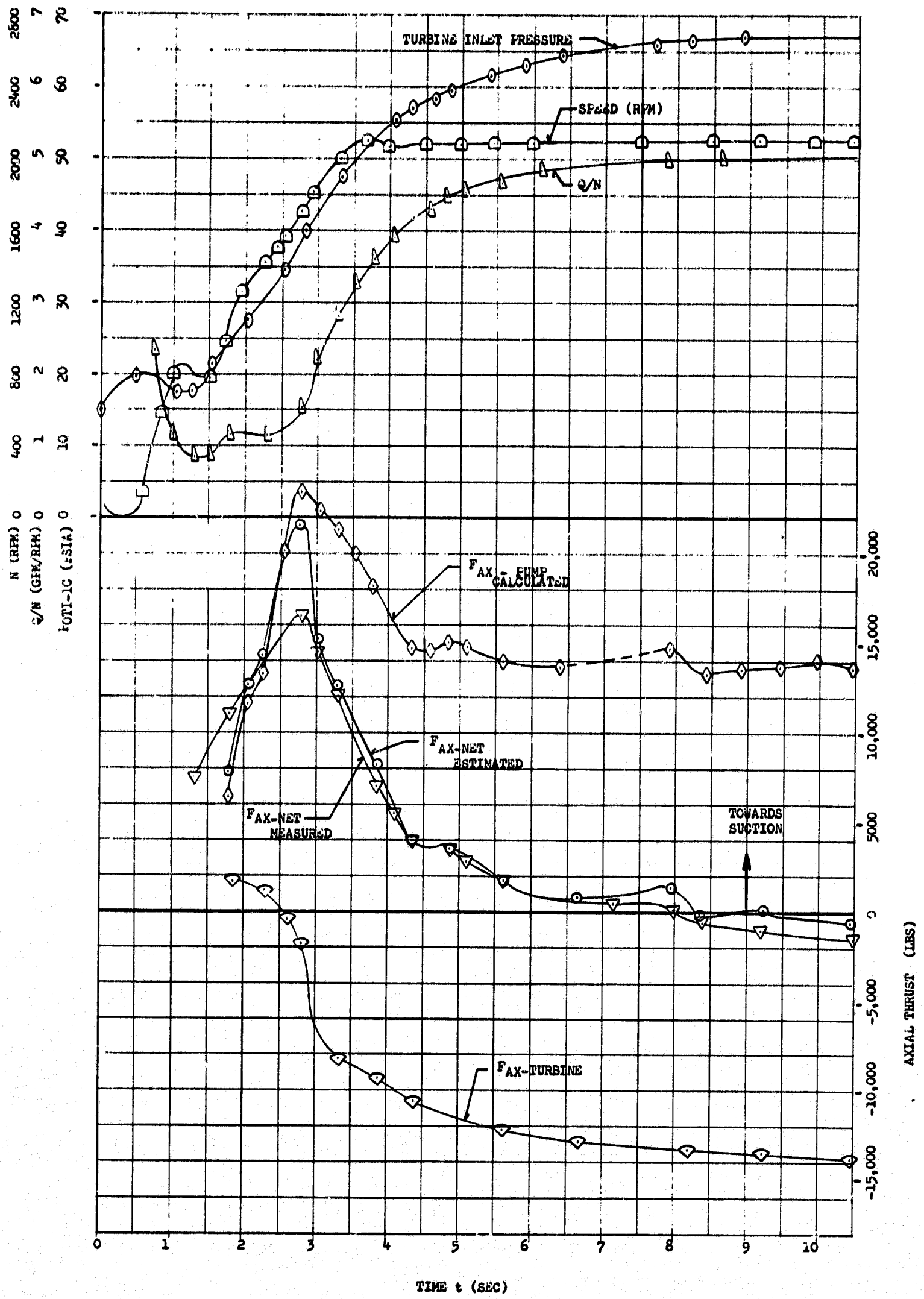

Figure 35

AXIAL THRUST AT START TRANSIENT TEST NO.-001

AXIAL THRUST AT START TRANSIENT
OTPA S/U 2, TEST 1.2-08-EHP-4

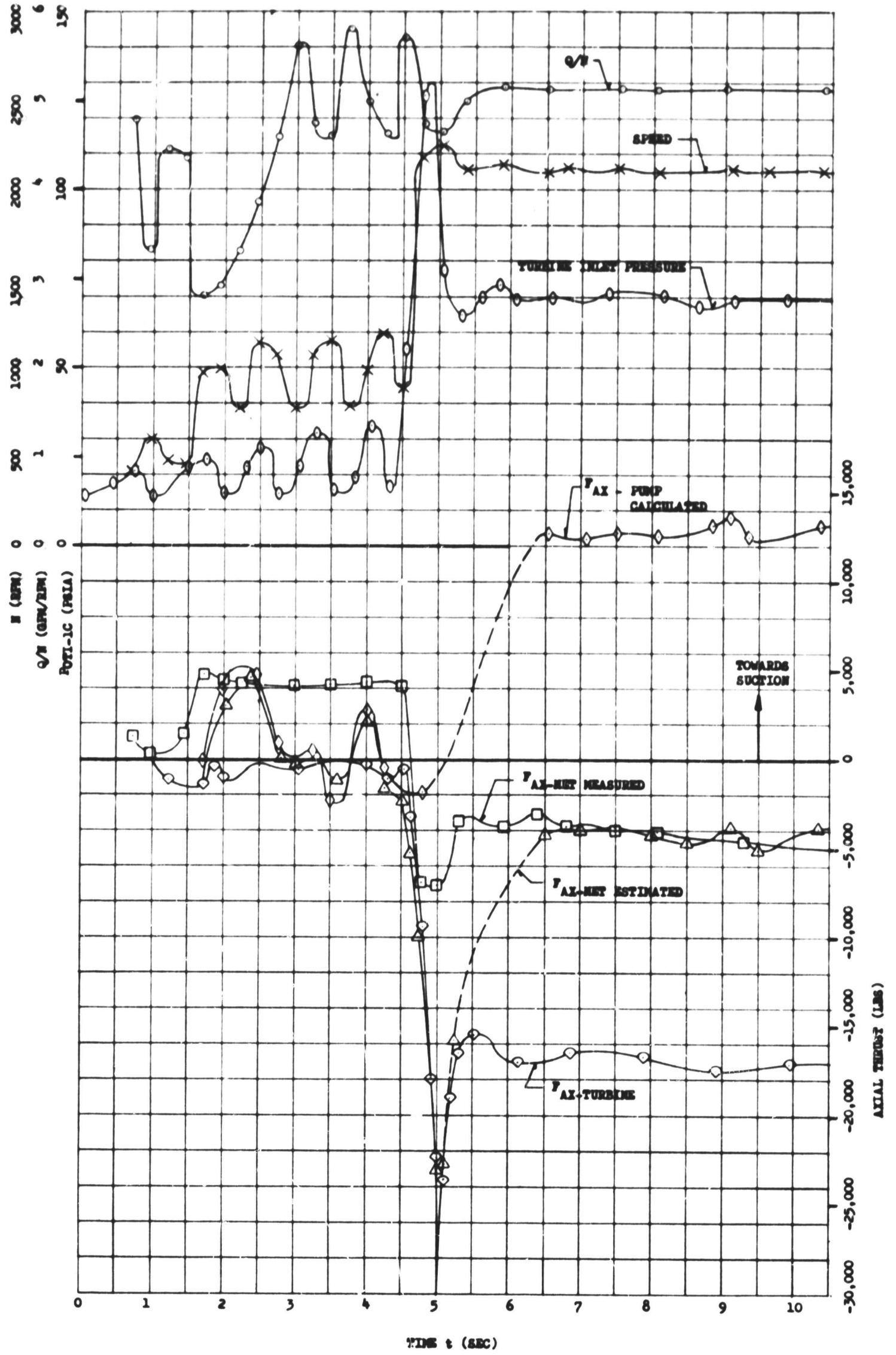

Figure 36

AXIAL THRUST AT START TRANSIENT TEST NO.-004

AXIAL THRUST AT START TRANSIENT

OTPA B/U 2, TEST 1.2-08-SHP-8

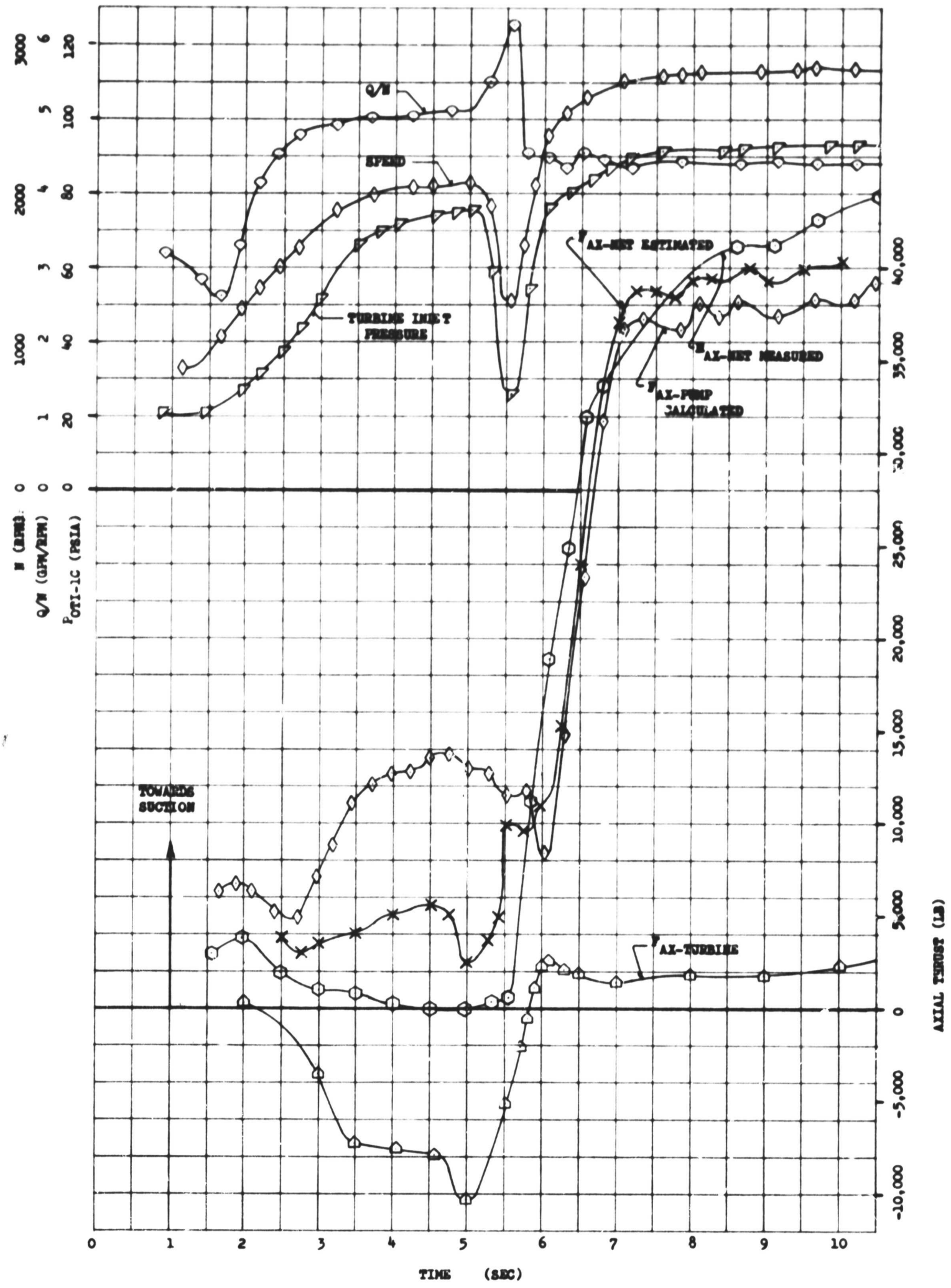

Figure 37

AXIAL THRUST AT START TRANSIENT TEST NO.-006

b. Effects of Lagging Backvane Pressures

Lagging backvane pressures observed during rapid accelerations resulted in a momentary decrease in pump thrust. This is discernible from Figure 37. The downward thrust peak occurred at the time when speed exceeded prespin. At this instant, the normally higher discharge pressure of the impeller backside was equal or less than the discharge pressure of the impeller frontside ($P_{OBV-6} \geq P_{OHC-5}$). The backvane pressure lag was apparent in all subsequent tests as well but caused no particular problems because the resulting effects upon thrust were relatively small.

c. Agreement of Measured and Calculated Net Thrust During Start Transient

A significant pressure wave was measured at the inlet to the turbine manifold during Test No. 4. Later investigations revealed that the wave originated in the valve system upstream of the gas generator and was responsible for causing a gas generator assembly failure during subsequent gas generator assembly tests. The effect of the pressure wave upon calculated and measured thrust is shown in Figure 36. The resulting downward thrust peak calculated from pressure forces was only partly registered by the measuring system, although both measured and calculated net thrust were time correlated. It appears that because of the inertia of the large rotor, the calculated magnitude was not truly representative; however, it was also evident that the measuring system was not sufficiently sensitive to measure the actual magnitudes of thrust spikes.

The amplitude accuracy of the measuring system at low and unstable thrust values is rather low because of hysteresis effects in the measuring system and power transmission assembly.

IV. CONCLUSIONS AND RECOMMENDATIONS

Thrust balance was obtained at full operating speeds and over a range of flowrates from 85% to 120% of design flow with liquid nitrogen as the pumping fluid. The highest net thrust estimated from pressure profiles was directed towards suction and amounted to 67,000 lb, or 3000 lb below the anticipated maximum safe short duration operating load of 70,000 lb. Measured thrust values were lower but agreed in most cases within 10% at magnitudes in excess of 15,000 lb.

Pump thrust was 26% to 42% higher, depending upon Q/N, than the predicted ideal thrust because of a decrease in fluid density caused by fluid heating on the backside of the impeller resulting from the inefficiency of the backvanes. The decrease in fluid density was caused by the combined effect of additional inefficiency heating in the backvanes (compared to the impeller) and added bearing heat input. A reasonable increase in by-pass flow would have primarily limited the temperature rise in the seal cavity and therefore, had little effect upon the temperature unbalance between the impeller frontside and backside. Because the backvane operated at near shutoff conditions, a considerably higher backvane flow would have been required to obtain any significant increase in backvane efficiency to balance temperatures and densities on both sides of the impeller.

The static head coefficient for the backside of the modified impeller agreed with the predicted minimum value of 0.32. The minimum value was obtained because of a 32% drop-off in backvane diffuser performance as a result of an increase in axial clearance between impeller disc and backvane diffuser.

Results of the first full speed tests provide a means for determining the optimum backvane inlet radius for liquid oxygen operation. To operate with the design fluid, the backvane inlet radius must be decreased, which can be done without any danger of obtaining cavitation in the rear impeller cavity.

Turbine thrust was significant (up to 19,000 lb towards exhaust) under the off-design condition of the gaseous nitrogen drive. Thrust estimates for impulse conditions yielded appreciable magnitudes (up to 7000 lb toward the pump) because of an estimated radial pressure gradient resulting from radial equilibrium assumed on the upstream side of the turbine disc.

Small variations caused by circumferential unbalance in pressure forces in the 200,000 to 300,000 lb range have a significant effect upon thrust. Therefore, for large pumps it is important that more than one pressure tap be provided per radial location to improve the accuracy of thrust estimates based upon pressure forces.

For large pumps, where the margin percentages are lower between nominal and maximum safe operating thrust loads than on smaller size pumps, it is always recommended that either a subscale pump test or a partial speed test be conducted to verify estimates before attempting full speed operation.

APPENDIX A

NOMENCLATURE

NOMENCLATURE

I. SYMBOLS AND ABBREVIATIONS

A	Area, $in.^2$
c_p	Specific heat at constant pressure, BTU
D	Diameter, in.
F	Force, lb
F_{AX}	Axial thrust, lb
F_{Mt}	Momentum force, lb
g	Acceleration caused by gravity, 32.17 ft/sec^2
GGA	Gas generator assembly
GN_2	Gaseous nitrogen
H	Total head, ft
H_{St}	Static head, ft
h	Blade length, turbine, in.
h_l	Total hydraulic head loss, ft
HP_{hyd}	Hydraulic horsepower, ft lb/sec 550
K_p	Dimensional constant relative to pressure
K_f	Dimensional constant relative to force
N	Speed, rpm
OTPA	Oxidizer turbopump assembly
P	Static pressure, $lb/in.^2$
Ps	Suction pressure, $lb/in.^2$
Pc	Cavity pressure, impeller, $lb/in.^2$
P_{vap}	Vapor pressure, $lb/in.^2$
PTA	Power transmission assembly

Q	Pump flow, gal/min
R, r	Radius, in.
T	Temperature, °R
TPA	Turbopump assembly
u	Tip speed, ft/sec
V	Fluid velocity, ft/sec
$\dot{w}$	Weight flow, lb/sec
η	Efficiency
ρ	Weight density of fluid, lb/ft^3
ϕ	Flow coefficient
ψ	Static headrise coefficient
ω	Angular velocity, rad/sec

II. SUBSCRIPTS

B	Backside (impeller)
BV	Backvanes
F	Frontside (impeller)
m	Meridial or mean
SH	Shaft seal diameter
1	Relative to speed at free spin or to measuring station
2	Relative to full speed or measuring station

III. SUPERSCRIPTS

'	Relates to no blockage, includes nominal clearance

IV. EQUATIONS

Static headrise coefficient for a given vane section defined by R_1 and R_2

$$\psi_{(1-2)} = 20{,}736 \frac{g}{\rho\omega^2} \frac{(P_2 - P_1)}{(R_2^2 - R_1^2)} \qquad \text{Equation (1)}$$

Backvane diffuser efficiency:

$$\eta_{BV} = \frac{288g \quad \Delta P_{BV}}{\rho(V_{2BV}^2 - V_{4BV}^2)} \qquad \text{Equation (2)}$$

Backvane static heat coefficient, (D_2 = 28.5 in.)

$$\psi_{BV} = \frac{\Delta H_{St,\ BV}}{u_2{}^2/g} = 3\,(10^5) \frac{\Delta P_{BV}}{\rho BV \quad N^2} \qquad \text{Equation (3)}$$

Momentum force on impeller frontside

$$F_{MT} = \frac{\dot{w}}{g} V_{m,1} = \rho Q V_{m,1} \qquad \text{Equation (4)}$$

Ideal pump thrust:

$$F_{AX} = P_S (A_B - A_F) + N^2 \left[A_B (K_{p,F} \psi_F + K_{p,TIP} \psi_{TIP} - K_{p,B} \psi_B) \right.$$

$$\left. + K_{f,B} \int_{R_{SH}}^{R_2} \psi_B (r)\, r\, dr - K_{f,F} \int_0^{R_2} \psi_F^2 (r)\, r\, dr \right]$$

Equation (5)

Ideal thrust - speed relationship

$$\frac{F_{AX,2} + P_S A_{SH}}{F_{AX,1} + P_S A_{SH}} = \left[\frac{N_2}{N_1}\right]^2$$

or:

$$F_{AX,2} = \left[\frac{N_2}{N_1}\right]^2 (F_{AX,1} + P_S A_{SH}) - P_S A_{SH} \qquad \text{Equation (6)}$$

Cavity pressure P_c cavitating

$$P_c = P_s + \frac{u^2 \rho}{144g} (\psi_{FB} - \psi_B) = P_{vapor} \qquad \text{Equation (7)}$$

Flow coefficient, front vanes (D_2 = 28.5-in.)

$$\phi_F' = \frac{V_{m,2,F}}{u_2} = 0.01248\ Q/N \qquad \text{(No blockage, nominal clearance)}$$

Flow coefficient, backvanes ($D_{2,BV}$ = 27.41)

$$\phi_{BV}' = \frac{V_{m,2,BV}}{D_{2,BV}} = 0.0483\ Q_{BV}/N \qquad \text{(No blockage, nominal clearance)}$$